Nadeem Jelani

# Investigating the Role of Active Loads in the Future Electrical Grid Dominated by Power Electronics

Thesis for the degree of Philosophiae Doctor

Trondheim, May 2014

Norwegian University of Science and Technology
Faculty of Information Technology,
Mathematics and Electrical Engineering
Department of Electric Power Engineering

**NTNU – Trondheim**
Norwegian University of
Science and Technology

**NTNU**
Norwegian University of Science and Technology

Thesis for the degree of Philosophiae Doctor

Faculty of Information Technology, Mathematics and Electrical Engineering
Department of Electric Power Engineering



ISBN 978-82-326-0270-4 (printed ver.)
ISBN 978-82-326-0271-1 (electronic ver.)
ISSN 1503-8181

Doctoral theses at NTNU, 2014:174

Printed by NTNU-trykk

# Acknowledgements

This thesis summarizes the results of the research work I have been doing as PhD student during last 3 years from October 2010 to August 2013 at Norwegian University of Science and Technology (NTNU), Department of Electric Power Engineering. The financial support for this project was provided by *Higher Education Commission of Pakistan* and *Norwegian Centre for International Cooperation in Higher Education* and is gratefully acknowledged.

First and foremost, I would like to record deep and sincere gratitude to Professor Marta Molinas for her supervision, continuous support, encouragement and guidance during this research as well as giving me the chance to pursue my postgraduate studies.

Special thanks are due to Professor Olav Fosso for his consistent support, suggestions and guidance during my 5 years stay at NTNU. Thanks to all the other professors of the department. I appreciate their contributions of time and intriguing ideas to make my study experience productive and stimulating. I convey special thanks to Inger, Åshild, Eva, Kurt and Anders for their help in administrative matters. At ENO group, thanks to all my fellow PhD candidates for their assistance and support. All of you greatly enriched this work in one way or another and specially my stay in this beautiful country. I would like to thank Mohammad Jafar and Jon Are Suul for their invaluable suggestions and ideas. I would like to thank all my friends who filled my life with joy during my stay in Trondheim.

I thank my mother and my siblings who accepted me going so far away from them for so long and always prayed for my success. I would not have finished this work without their continuous support and encouragement. For my mother Khadija, my brothers Naveed, Tauqeer and Naeem, thank you!

# Abstract

The advancements in power electronics in the past decade have resulted in a wide spread use of power electronically interfaced generation units and loads in both AC and DC distribution systems. Power electronics plays an important role in the modern automotive, sea and under sea and aircraft industry. Moreover, the use of power electronics based motor drives in industrial application has been growing very fast. Depending on the type of regulation, many of these PE interfaces behave as constant power loads (CPLs) for the utility. These power electronic (PE) interfaces can be optimally controlled to provide the bidirectional power flow and can therefore emerge as strong candidates to replace many dedicated devices being utilized for specific grid services.

CPLs are important part of modern power distribution networks and their number will increase in the foreseeable future. In this research program, main focus has been put to use CPLs for transient stability enhancement and fault ride through (FRT) under balanced/unbalanced grid voltage dips instead of employing a dedicated compensating device for such ancillary grid services. Alleviation of harmonics and current distortions caused by the non-linear loads under both ideal and non-ideal voltage conditions has also been investigated in this work using CPLs as active power filters (APF). Simulations are carried out in PSCAD/EMTDC and different models of AC distribution systems with different shares of loads are considered in accordance with specific study.

Transient stability study of the AC distribution system demonstrates that the CPLs can effectively replace the existing compensating devices and provide many ancillary grid services. A large increase in transient stability margins has been observed under balanced grid voltage sags when CPLs provide the ancillary reactive power during the fault and avoid a possible voltage collapse due to excessive reactive power consumption. The ancillary reactive power provision increases the current rating of the CPL converters. However, the increase in the current rating of the distributed CPLs is always less compared to the current rating of a dedicated STATCOM when providing the reactive power during the voltage sag. It has been concluded that the reactive injection by the CPLs improves the terminal voltage by a small amount and hence decreases the total branch current. Therefore, an optimal operating point for a CPL can be established depending on the load power, network impedance and the severity of the grid fault.

FRT enhancement under asymmetrical grid faults using CPLs has been carried out and a modification in the CPL control structure is proposed incorporating the positive and negative sequence voltage extraction. The positive sequence voltage compensation avoids the possible voltage collapse and the rotor does not accelerate beyond the electro-mechanical stability. The negative sequence voltage control removes the torque

and power oscillations during the asymmetrical grid fault and improves the life time of the generation system. FRT enhancement by the CPLs increases the current rating of the devices. However, each distributed CPL requires lower current rating compared to one centralized STATCOM when providing FRT enhancement services.

Power quality issues have been addressed in a distribution system under ideal/non-ideal voltage conditions. CPL is used as APF and time domain *IRP p-q* and frequency domain *CPC* approach is used to extract the compensating current references in order to eliminate the harmonics in the source current. A positive sequence voltage detector is employed in the CPL control structure under non-ideal voltage conditions. Simulation results for both ideal and non-ideal source voltage conditions indicate that the harmonics in the source currents are removed using both the time and frequency domain approaches. *CPC* based control algorithm, however, provides slightly better results due to the sequence separation of the compensating current. The natural CPL action further decreases the THD in source current because it adds a fundamental current component in the total source current.

# Contents

# List of Figures

# List of Tables

# List of Notations

| | |
|---|---|
| AC | Alternating Current |
| APF | Active Power Filter |
| CPL | Constant Power Load |
| CPS | Controllable Power Source |
| DC | Direct Current |
| DG | Distributed Generation |
| DER | Distributed Energy Resource |
| DFIG | Doubly Fed Induction Generator |
| DSOGI | Dual Second Order Generalized Integrator |
| FRT | Fault Ride Through |
| IGBT | Insulated Gate Bipolar Transistor |
| LVRT | Low Voltage Ride Through |
| PLL | Phase Locked Loop |
| PWM | Pulse Width Modulation |
| PNSC | Positive-Negative-Sequence Compensation |
| PE | Power Electronic |
| SOGI | Second Order Generalized Integrator |
| QSG | Quadrature Signal Generator |
| SCIG | Squirrel Cage Induction Generator |
| THD | Total Harmonic Distortion |
| VSC | Voltage Source Converter |

# 1 Introduction

*This chapter briefly discusses the CPLs as elements of the future electrical grid and the state of the art research being carried out in CPL area. It presents an overview of the modern AC distribution system and the ancillary grid services being provided by some of its components. It also provides a short overview of the thesis and presents the objectives, scope and major contributions.*

The existing electrical grid, being unidirectional in nature, converts only one-third of fuel energy into electrical energy. The losses along the transmission lines are almost 8% while 20% of its generation capacity is kept active for only 5% of the time to meet the peak load demand, making the system inherently inefficient [1, 2]. We need better grid reliability while dealing with aging power system infrastructure. The future electrical grid known as smart grid is supposed to address the shortcomings of the existing grid. The smart grid is expected to achieve the environmental targets and to support the distributed generation and storage capabilities. The move towards the smart grid has to start from the distribution system as nearly 90% of the power outages and disturbances have their roots in the distribution system.

Generally, smart grid is comprised of number of distributed energy resources (DERs) and power electronic (PE) interfaces, which must be properly exploited to address the power quality issues and increase the distribution system stability and efficiency. The existing power system is based on the assumption of few power sources with large capacity and sinusoidal supply. The smart grid paradigm is different from traditional grid. The future smart microgrids are low voltage grids with small distributed energy sources of few megawatts range, where the possibility of supply voltages being asymmetrical and distorted is very high [3]. On the other hand, distributed generation (DG) feeding a microgrid offers many advantages. Having the DG close to the point of power consumption reduces the transmission and distribution losses and prevents network congestion. Moreover, the chances of having the blackout are also reduced because many of these microgrids may be able to operate in islanded or standalone mode while being disconnected from the high or medium voltage transmission networks under abnormal grid conditions and contingencies [4]. System reliability is also improved because the smart grid consists of small generation units and the chance of losing big amounts of generation at a time is much reduced.

DERs based on wind, solar, geothermal, micro gas turbines, micro hydro turbines, engines and many energy storage devices have to be integrated into the Smart Grids [5]. Among them, wind has emerged as the fastest growing source of renewable energy and it will continue to grow in near future. Solar generation is lagging behind, but new advances in technology exhibit great promise for solar generation. Depending on the grid handling capacity, new wind or solar power generation can be installed, interconnected and commissioned in a short span of time. The economics of these resources are improving every year, reaching a close parity with conventional fossil fuel generations. However, intermittent nature of wind and solar generation poses many operational challenges for the transmission grid, including additional ramping and regulation requirements. In case of standalone microgrids, such as island power system, intermittency of these renewable sources might lead to instability, low operational efficiency and poor power quality, demanding different compensation strategies [2, 6]. Therefore, interconnection standards have to be further explored and broadened to address the power factor controllability and low voltage ride through (LVRT) needed to mitigate any transient stability issues in such power systems.

There are many methods employed to address the stability related issues in a smart electrical network. One of them is the use of a centralized shunt connected static synchronous compensator (STATCOM) in grid-connected mircogrids to improve the voltage sags/swells and unbalances. The use of grid-connected converters of distributed energy resources for voltage support under grid faults is also very common. In doubly fed induction generator (DFIG)-based wind farms, either rotor or grid side converters can be used to address the power quality issues and provide the necessary voltage support. Another compensation solution that has been selected as the main area of research in this thesis is the use of tightly regulated PE load interfaces called constant power loads (CPLs) for stability enhancement in a microgrid scenario. This demands an optimal and robust control of PE converters serving as load interfaces in a distribution system. In this case, CPLs will be providing ancillary grid services such as reactive power and voltage support for transient stability, fault ride through and harmonic mitigation.

## 1.1 Scope of Work

The work carried out during the course of this research is focused mainly on the use of CPLs in AC distribution systems. In the past decade, the advancements in the power electronics have lead to a greater use of voltage source converters using IGBT switches in many applications. The persistent technology being used within CPLs has been mainly based on power diodes and thyristors in most of the applications. In spite of having advantages like higher power ratings, robustness and simplicity in control, they have the limitation of being unidirectional and hence cannot be easily used as active front end converters. Due to the lack of control flexibility, they are not able to provide any extra functions and just act as load interfaces. CPLs considered in this research are based on the VSC technology and are controlled to provide many ancillary grid services.

The desired features that should be fulfilled for control and operation of a VSC based CPL providing ancillary grid services in this thesis can be summarized by the following points:

- The converter control system should be able to respond to the drop in voltage under different grid fault conditions. The voltage sag becomes critical in the presence of CPLs in distribution system as they try to draw more current to ensure the constant active power demanded by the load. The provision of reactive current during the fault will ensure the system stability and avoid a possible disconnection of the distribution system fed by a wind source.
- CPLs as provider of ancillary reactive power can only be employed if they emerge as cost effective solution compared to already established reactive power compensation solutions. Therefore, the current rating of the CPLs has to be investigated when they are used to provide the extra services. The operation of a CPL demands to establish an optimal operating point where the CPL current remains at the lowest value.
- The converter control system should be able to control both active and reactive power flow as well as the double frequency oscillating components of the active and reactive powers during asymmetrical grid faults. The control strategy should be generally valid for both balanced and unbalanced conditions, and it should be possible to respond quickly to asymmetrical grid faults in order to avoid the system disconnection and overheating in the generation drive train.
- The converter control scheme should have the flexibility of adapting to the role of a shunt active filter in the presence of harmonic generating loads in the distribution system. It should be simple to accommodate the present reference current generation schemes into the converter control structure. It should be able to provide the power quality improvement as an ancillary service while being operating as a CPL.

The focus of this thesis will therefore be limited to the use of CPLs as ancillary grid services providers in AC distribution system under both balanced and unbalanced grid voltage conditions and in the presence of harmonic generating loads within the power network.

## 1.2 State of the Art Research in CPL Area

PE load interfaces and motor drives when tightly regulated behave as CPLs which exhibit negative impedance characteristics at the input terminals. This might lead to voltage collapse, system oscillations and power quality issues. The stability of CPLs has been extensively addressed in DC distribution systems and several stability criteria have been investigated in specific applications. Power electronics based DC power distribution systems are becoming increasingly common, particularly for applications such as aircrafts, vehicles, future ships, the International Space Station and satellite power systems [7-13]. AC distribution system comprising of CPLs, on the other hand, have not been given the same share of research consideration. In the following

paragraphs, we will discuss some of the research efforts that have been made in the past few years to investigate the stability related issues of the power system having CPLs as resources.

The large-signal analysis of a buck DC/DC converter operating with a CPL and using a PI controller has been carried out by C. Rivetta in [14]. This type of configuration is present as part of the integrated power systems in sea and undersea naval vessels. Similar work has previously been carried out in [15, 16] to buck and boost DC/DC converters with CPLs. An interesting digital control technique named pulse adjustment is introduced by A. Khaligh in [17-21], applied to a DC/DC buck–boost and flyback converter driving CPLs. The technique enables the power converters to operate in fixed switching frequency. The proposed method does not require a detailed small or large signal model of the power converter. In spite of its simplicity, it offers a fast dynamic response, and it is robust against the variations of the parameters of the power converter. In [22], A. Khaligh studied the effects of loss components in the stability of DC/DC converters loaded by CPLs and traditional loads in both continuous and discontinuous conduction modes and necessary conditions for small-signal stability have been suggested.

The stability characteristics of a DC power distribution system comprising of CPLs have been analyzed by W. Jiabin in [23]. It has been emphasised that in the presence of a CPL it will be very difficult to maintain stability with a conventional voltage and current control structure, mainly when resistive loads are not present. It has also been shown that the stability margin reduces as the nominal output voltage decreases and the power demand increases. In [24], A. Rahimi proposes an active damping method to stabilize the DC/DC converters loaded by CPLs. It has been reported that by following a similar procedure, this technique can be applied to isolated converters. The operation and stability of basic buck and boost converters in discontinuous conduction modes loaded by CPLs have been investigated in [25] by A. Rahimi. Using time domain analysis, it has been shown that the open loop buck and boost converters are stable when they are loaded by CPLs. A. Rahimi in [26], introduces a novel nonlinear feedback, which is called the loop-cancellation technique, to cancel the destabilizing effect of the CPLs. Theoretically, any amount of CPLs can be compensated by this method. Another advantage of this technique is that its implementation is identical for different kinds of converters such as buck, boost and buck-boost converters.

CPL connected to a DC power supply may lead to instability problems on the DC-link variables. In [27], local stability of the DC-link variables has been analyzed using Nyquist stability criteria. An oscillation compensation technique is proposed to improve the system stability margin driving a CPL. Reference [28] investigates start-up process and step response of average current-controlled buck cascading converters loaded with CPLs. The design criteria have been proposed to achieve system stability during dynamics, such as start-up and load transient processes. In [29], a boundary control operation of a buck converter with a CPL has been discussed. Boundary control is used to overcome the destabilizing effects introduced by the CPL and to drive the two-state buck converter system to a desired operating point. Current mode control has been examined in [30] for the boost converters with CPLs. By small signal modelling it has been shown how peak current mode control provides active damping.

Stability issues present in DC microgrids comprising of CPLs have been extensively addressed in recent research. CPLs introduce a destabilizing effect in DC microgrids that may cause their main bus voltages to show significant oscillations or to collapse. Reference [31] proposes techniques to achieve a stable DC voltage at the microgrid main buses by compensating the oscillatory action of CPLs both through hardware dependant techniques and through control related strategies. In [32], amplitude death methods are employed to solve the issue of unwanted oscillations appearing due to the presence of CPLs in DC microgrids.

The growing number of electric vehicles and aircrafts utilizing CPLs demands the designers to minimize the size and the weight of power systems. DC-link capacitors are part of the first elements that should be reduced. Magne and Marx in [33, 34] propose a stabilization technique to reduce the DC-link capacitance supplying a CPL. Moreover, it is shown that the DC-bus voltage transient response can be shaped by the virtual capacitor. It has been investigated how a large signal stability analysis gives useful hints on the design of the system to optimize the stability criteria for constant and variable power loads. Another such study has been carried out in [35] based on the small signal model of the CPL. The implemented technique for damping DC-link oscillations and instability in brushless DC-drive systems results in a small DC-link capacitor and will make many passive damping networks undesirable.

For distributed AC and hybrid AC/DC systems with CPLs, the very first design-oriented stability criteria have been developed by M. Belkhayat in [36, 37]. In this work, the stability criteria for a CPL to choose proper components of a single-stage *LC* filter based on the Brayton-Moser mixed potential theory has been derived. Moreover, AC stability criterion has been introduced based on the generalized Nyquist criterion and reference frame theory. A. Emadi in [38, 39] proposes a generalized state-space averaging method to investigate the negative impedance instability in hybrid AC/DC distribution systems. A stable region for a typical system has been presented. Some recommendations have been suggested to avoid negative impedance instability when designing AC power systems. In [40], CPL stability criteria has been developed based on the Brayton-Moser mixed potential theory to choose the appropriate parameters of multistage *LC* filters for an ideal CPL. The proposed criteria utilize the negative incremental impedance of the CPL to constrain the filter parameters and can be extended to actual CPLs. In [41], an analytical technique based on Brayton-Moser mixed potential for predicting the large-signal stability behaviour of a hybrid AC/DC power system with CPLs has been established. The proposed technique provides a computationally efficient tool for protection sizing and filter design optimisation. An interesting research has been carried out to stabilize the hybrid AC/DC power system with CPLs in hybrid electric vehicles in [42]. To improve system stability, model predictive control (MPC) is applied to minimize the change of DC-link voltage and the change of complex input impedance seen at the point of common coupling (PCC) during transients and faults. MPC provides an optimal trade-off between modification of load impedance, variation of DC-link voltage and battery current ripples.

## 1.3 Composition of Modern Distribution System

Due to the recent growing emphasis on environmental issues in many countries, modern distribution networks are rapidly evolving toward the new concept of smart grid with an increasing level of penetration of distributed generation (DG) units, storage systems and information and communication technologies [43-46]. Depending on the characteristic of the grid supply voltage, the current distribution systems can be classified as hybrid AC/DC system. DG incorporates a wide range of prime mover technologies, such as internal combustion (IC) engines, gas turbines, micro turbines, photovoltaic (PV) systems, fuel cells, wind power and AC storage. Most emerging technologies such as micro turbines, photovoltaic systems, fuel cells and AC storage have an inverter to interface with the electrical distribution system. These emerging technologies have lower emissions and are becoming cost effective with the passage of time [44]. Using DG in the distribution system reduces the physical and electrical distance between generation and load. By bringing the sources closer to loads contributes to the enhancement of the voltage profile, reduction of distribution and transmission losses, and postpones the investments in new transmission and large scale generation systems. The main changes in the modern distribution network due to the inclusion of DG technologies are the bidirectional power flow, the uncertainty in bus voltage profiles and the uncertainties in short-circuit power [47]. Basic configuration of a modern hybrid AC/DC distribution network connected to a medium voltage bus has been presented in Figure 1.1.

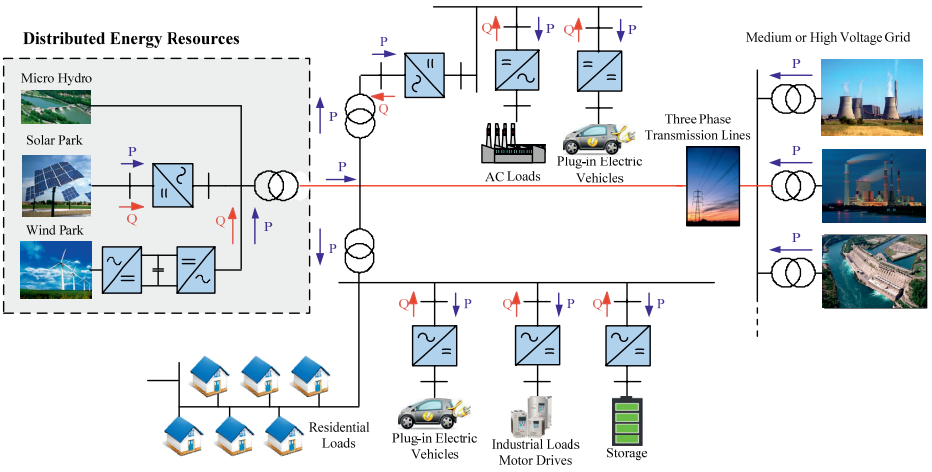


Figure 1.1: Basic configuration of hybrid AC/DC distribution system

The loads present in a distribution system can be classified as passive or active. Passive loads consume power from the utility without taking into consideration the stability and efficiency of the overall system. However, an active load can be used to enhance the system efficiency and stability under grid contingencies. Plug-in electric vehicle, motor drives and many other home appliances requiring DC are some of the examples of active loads. Depending on the type of regulation many of these loads behave as CPLs.

Due to the growing use of power electronics to interface the loads, the total low voltage distribution network could become a CPL in future electrical grid.

CPLs interfaced to the grid by PE converters are the most destabilizing loads under abnormal voltage conditions due to inherent negative resistance instability characteristics. Most of the research efforts focusing CPLs have been focussed on the instability effects of the constant power characteristic as mentioned in section 1.2. On the other side, when operated efficiently these loads can be used to improve the stability and operation of the electrical system they are part of and provide many additional services, otherwise, requiring dedicated compensating devices.

### 1.3.1 Ancillary Services in Distribution System

In order to maintain the balance in supply and demand and grid reliability ancillary services are necessary in the power system. Ancillary services provided by DG systems interconnected to the electric power systems are defined by the IEEE standards [48]. Issues addressed in the standard include load regulation, energy losses, spinning, and non-spinning reserve reactive supply. Future ancillary services may also include power quality enhancement [49]. Ancillary services contribute to an efficient approach for management of the new power system characterized by several DG units. In fact, they are based on the specific characteristic of power electronically interfaced DG systems that can be used to inject active power, reactive power, and harmonics. The reactive power and harmonic mitigation is provided even if the energy source is not available. In this case, dedicated compensators are installed at the distribution level. Ancillary services provided by different types of DG units are briefly discussed as follows:

- Ultracapacitors (UCs) are emerging storage devices characterized by high power density and high cycling capability. The combination of a fuel cell and an ultracapacitor, when interconnected to the distribution network through PE interfaces, allows performing ancillary services such as power quality improvement and the load regulation [50, 51]. This hybrid system with an efficient converter control structure is able to provide a fast and reliable response under several conditions. Fuel cell alone being not able to comply with the fast dynamics of the electrical system is not suitable for providing such ancillary services.
- PV generation units are being used extensively in order to have a local production resulting in cutting down the use of conventional fuels and improving the reliability of the supply at the distribution level [52]. Such grid-connected systems fix mandatory constraints to PE converters to meet power quality specifications and draw the maximum power conversion from renewable sources. Grid-connected PV units as reactive power compensators have been studied in the recent research and advanced control schemes have been developed in order to regulate active and reactive power injection into the grid [53].
- Wind power plants nowadays are able to partly participate in provision of ancillary grid services through different sets of control possibilities. Reactive

power/voltage control can be obtained from wind systems without significant investment and cost of equipment [54]. Generally, with tendency of increasing reactive power control capabilities, wind farms can significantly contribute to voltage regulation and act as reliable grid ancillary service provider. In the last decade, more advanced back-to-back (BTB) PE converters have been introduced in large scale which started to regulate the generated power from the wind turbines. The partial-scale power capacity for the DFIG and the full-scale power capacity for the asynchronous/synchronous generator (A/SG) are two most widely used configurations these days [55-57]. By introducing the BTB PE converters, it is possible to fully control the extracted power from the wind turbines, and also provide ancillary services to the grid. The advancement in power electronics has significantly improved the performance of the wind power plants. It resulted in the reduction of mechanical stress and increase in power production.

- Plug-in vehicles can both behave as loads or as distributed energy and power resources in a concept known as vehicle-to-grid (V2G) connection [58]. The efficiency, stability, and reliability of the renewable electricity system can be enhanced with the vast untapped storage of plug-in vehicles when connected to the grid. Because of the bidirectional power transfer capability, the transmission system operator can request for a power transfer through an aggregator fleet of vehicles through control signals thus providing services like power system regulation [59]. Moreover, V2G-capable vehicles can offer reactive power support, peak shaving, tracking of variable renewable energy sources and current harmonic filtering. These technologies may provide ancillary services, such as voltage and frequency control and spinning reserve [58, 60]. The plug-in vehicles behave as CPLs when their PE converter is tightly regulated. In this work, CPLs have been introduced to provide some of the ancillary services mentioned in this section. The power rating of the converters used in a single plug-in vehicle is not sufficient enough to provide all the demanded ancillary services. However, when used as dispersed resources at different locations, better results can the achieved.

## 1.4 Reactive Power Compensation Technologies

Reactive power compensation is defined as the management of reactive power to improve the efficiency and stability of AC power systems [61]. The reactive power compensation issue is generally focused on two aspects; load compensation and voltage support. The main objectives of the load compensation is to improve the system power factor, to filter the active power drawn from the AC supply and to eliminate current harmonic components produced by large and fluctuating non-linear industrial loads. Voltage support is generally performed to reduce voltage fluctuation at a given terminal of a transmission or distribution line. There are many cost effective and easiest methods of reactive power provision in AC distributed systems and are explained as follows:

- In distributed power systems based on squirrel cage induction generators, capacitor banks are installed at the generator terminal to achieve the reactive power requirements [62, 63]. Capacitor banks are either connected in parallel at the generator terminals all the times or multiple capacitor banks are switched in and out based on the requirements at particular instant of time.
- An alternative approach to parallel reactive power compensation is the use of static Var compensator (SVC), which consists of a thyristor controlled reactor (TCR) connected in parallel with a thyristor controlled capacitor. SVC serves as a shunt-connected adjustable capacitive or inductive reactance, which supplies or absorbs reactive power in order to regulate the voltage magnitude at the point of connection to the distribution line [63].
- Another very effective shunt reactive power compensation scheme is VSC based STATCOM, which is composed of a PE converter with a capacitor or a DC voltage source on its DC side, a coupling transformer, and a control block [63]. STATCOM is a controlled reactive power source/sink that delivers or consumes the desired amount of reactive power entirely by means of electronic processing of voltage and current waveforms in a VSC [64].
- In wind energy conversion systems (WECS), series capacitive compensation is the most cost effective method of improving voltage profile. Typical series compensation systems employ capacitors to decrease the equivalent reactance of a power line at rated frequency [62]. Variable series capacitance is usually implemented by using thyristor control series capacitor (TCSC).
- Application of unified power flow controllers (UPFC) is a combination of both series and shunt compensation of reactive power. The UPFC consists of two PE converters operated from a common DC link. One is connected in series with the line, and the other in parallel [61]. This arrangement functions as an ideal AC to AC power converter in which the real power can freely flow in either direction between the AC terminals of the two inverters and each inverter can independently sink/source reactive power.

The reactive power supply from the network resources like CPLs could greatly improve the performance and stability of the power network. It could also prove to be the cost effective solution as it can replace the existing reactive power providers mentioned in this section. The work carried out in this thesis presents the application of CPLs to achieve the reactive power compensation targets as ancillary service for the grid in addition to feeding a load demanding constant power all the time.

## 1.5 Main contributions of the thesis

Following are the main contributions of this thesis:

- CPLs providing ancillary reactive power: Most of the recent research work regarding the provision of reactive power in AC distribution system for voltage support considers a dedicated centralized STATCOM as a compensating device.

The use of DG inverters for voltage support is also common. This thesis presents CPLs as built in distribution system resources providing transient stability improvement through reactive power compensation. CPL works on voltage source principle and it inherits negative resistance instability, thereby, requiring a robust control. An optimal CPL control strategy has been developed in this work. A comprehensive investigation considering the current rating of the devices due to reactive injection is carried out. It confirms the advantages of using distributed CPLs over a centralized STATCOM.

- Optimal operating point for a CPL: The reactive injection results in a small decrease in total CPL current as the voltage improves by a small amount. An analytical study aiming to find optimal operating point for the CPL has been performed. This can serve as a base to develop the loss minimization algorithms in a microgrid using distributed CPLs [65-68]. The amount of reactive injection by CPL increases with the increase in load power, grid impedance and grid voltage drop and optimal operating point varies with the varying network parameters.
- CPLs providing unbalance fault ride through: The stability of the wind farm supplying a local microgrid under asymmetrical grid faults is very critical, specially, in the absence of any compensating devices. Unbalanced fault ride through has been achieved in DFIG-based wind farms using rotor and grid side converters. In case of absence of a PE interface for the DER, this service has been provided by a STATCOM. This work introduces the application of CPLs for fault ride through services under asymmetrical grid faults. The obvious advantage in this case is that a dedicated compensating device is not required and a CPL being a part of electrical network can be utilized, providing a cost effective solution. This requires a modification in the CPL control structure and it must be able to extract an incorporate the positive and negative sequence of the voltage to be compensated [69, 70].
- Active power filtering with CPL: Active power filtering and power quality improvement is one of the most interesting research topics these days. Traditionally, harmonics in the source currents are removed using a shunt compensating device. Likewise, harmonics in the source voltage can be effectively removed by using series compensator injecting the negative harmonic voltages into the network. This work investigates the use of CPL to address the power quality issues in the AC distribution system comprising a microgrid. The alleviation of current harmonics has been achieved with a modified CPL control structure under ideal and non-ideal source voltage conditions. This is an extra grid service that a CPL provides in addition to acting as an interface for a load requiring constant power. An interesting feature of the study is that CPL is naturally suited for source current harmonics alleviation as it adds a perfect sinusoidal term in it [71-74].

## 1.6 Scientific Publications

The results of this research work have been published in various renowned peer-reviewed conferences and journals. One journal paper is under review at the time of thesis submission.

### 1.6.1 Journal Papers

1. **N. Jelani**, M. Molinas, and S. Bolognani, "Reactive Power Ancillary Service by Constant Power Loads in Distributed AC Systems," *IEEE Transactions on Power Delivery*, vol. 28, pp. 920-927, 2013. Reference [65]
2. **N. Jelani** and M. Molinas, "Mitigation of Asymmetrical Grid Faults in Induction Generator-Based Wind Turbines Using Constant Power Load," *Energies, MDPI*, vol. 6, pp. 1700-1717, 2013. Reference [69]
3. **N. Jelani** and M. Molinas, "Asymmetrical Fault Ride Through as Ancillary Service by Constant Power Loads in Grid-Connected Wind Farm," *IEEE Transactions on Power Electronics,* vol. PP, pp. 1-1, 2014**.** Reference [70]
4. **N. Jelani** and M. Molinas, "Reactive Power Ancillary Service and Harmonic Alleviation with Constant Power Load under Non-Ideal Voltage Conditions in AC Distribution System," *IET, Power Electronics (Under Review).* Reference [71]

### 1.6.2 International Peer-Reviewed Conferences

1. **N. Jelani** and M. Molinas, "Optimal Use of Power Electronic Interfaces for Loads in Distributed Systems," *in IEEE International Symposium on Industrial Electronics (ISIE) 2010*, pp. 2449-2454. Reference [66]
2. **N. Jelani** and M. Molinas, "Loss Minimization in AC Distribution System with High Share of Power Electronic Loads Providing Ancillary Reactive Power," *in IEEE PowerTech, 2011 Trondheim*, pp. 1-6. Reference [67]
3. **N. Jelani** and M. Molinas, "Stability investigation of control system for power electronic converter acting as load interface in AC distribution system," *in IEEE International Symposium on Industrial Electronics (ISIE), 2011*, pp. 408-413. Reference [68]
4. **N. Jelani** and M. Molinas, "Shunt Active Filtering by Constant Power Load in Microgrid Based on IRP p-q and CPC Reference Signal Generation Schemes," *in IEEE International Conference on Power System Technology (POWERCON), 2012*, pp. 1-6. Reference [72]
5. M. Zadeh, **N. Jelani**, and M. Molinas, "Seamless Control of Distributed Multi-Converter System with High Power Quality," CIRED, *22nd International Conference on Electricity Distribution*, Stockholm, 2013. Reference [73]

6. M. Shahbaz, **N. Jelani**, and M. Molinas, "Alleviating Harmonic and Reactive Power Issues in Smart Grid Based on the Implementation of the Instantaneous p-q Power Theory under Unbalanced and Distorted Supply Voltages," *International Conference on Power Systems Transients*, IPST, Vancouver, Canada, 2013. Reference [74]

## 1.7 Layout of the Thesis

Chapter 1 of this thesis presented a brief introduction to the distribution system components focusing mainly on CPLs. It provides an overview of the past research done in this area. It also discusses briefly the provision of grid ancillary services by the DG units in a power network. It presents some of the technologies and configurations used to provide reactive power in a power system. This helped to identify the scope of work as presented in section 1.1.

In chapter 2, a discussion has been made on different types of loads and their characteristics. It provides a brief overview of the different PE device being used as front end converters for CPL in AC distribution system. Negative resistance instability associated with CPLs has been briefly discussed. CPL modeling approach has been presented and control structure is proposed.

Chapter 3 presents the impact of reactive injection on the terminal voltage of the CPL. It first present the AC distribution system and its different components under consideration. A transient stability investigation has been performed in AC distribution system and the stability margins for different shares of load under balanced grid faults have been identified. A comparison between the current ratings of distributed CPLs and centralized STATCOM has been made. An analytical study has been presented in this chapter to identify the minimum CPL current for different load powers and varying network parameters.

Chapter 4 studies the mitigation of asymmetrical grid faults in a wind farm using the CPLs. A control scheme has been presented to extract and incorporate the positive and negative sequence components of the voltage for asymmetrical fault ride through. It also presents a comparison between the current ratings of CPLs and a STATCOM under different values of asymmetrical grid faults.

Power quality issues have been presented in chapter 5 under both ideal and non-ideal voltage conditions in an AC distribution system. The time and frequency domain approaches have been considered. It has been discussed that a CPL can effectively acquire the functionality of a shunt active filter and it naturally suited for such an application as it draws sinusoidal current from utility.

Chapter 6 presents the summary of the thesis with concluding remarks and an outline of possible topics for further research based on the presented work.

Four appendices are included to complement the thesis work. Appendix A presents the per unit system and the parameters of the different components of the distributed AC

system. Appendix B discusses the time and frequency domain results under low system voltage to assist the analysis done in chapter 2. Appendix C presents some of the generation and grid quantities that were not shown in chapter 3 and chapter 4. In Appendix D, a simulation study is performed to present the role of generation PE interface as shunt active filter.

# 2 CPL: Modelling and Control

*This chapter presents a discussion about the existing CPL technologies. It first presents the characteristics of different types of electrical loads. It briefly discusses the negative resistance characteristic of a CPL. The control system for a CPL is developed and presented. It presents an analytical study for the derivation of transfer functions for different CPL controllers and suggests the tuning methods for finding the values of controller parameters.*

Proliferation of power electronics in the home appliances many years ago lead to the introduction of CPLs that now represent a significant part of modern power distribution networks. Many of the industrial application are using power electronics based motor drives that in some of the cases behave as CPLs. The number of this kind of loads has been rapidly growing and will continue increasing in the near future. A modification in their control structure can enable them to provide some of the services that were earlier provided by the dedicated compensating devices. A CPL can be either controlled or uncontrolled PE interface utilizing either diodes or thyristors for specific applications having higher power rating and better reliability and robustness. However, these PE devices provide limited control options and cannot be used to provide ancillary grid services. The constant power feature leads to negative resistance characteristics in CPLs. Due to negative resistance instability, it is very essential for the CPL control to be stable and robust [38, 39, 75]. For more flexibility in control, VSC based on IGBT switches are better option. Because of the unique characteristics, dynamics, and stability problems associated to constant power behaviour, conventional methods in AC power systems are not appropriate for investigating the role of these PE loads in AC distribution systems. In order to achieve the ancillary grid services from CPL, its control must be modified accordingly. This demands a basic robust control structure that can be easily made adaptive to the type of service required by the grid under different situations. This chapter presents the modelling, control and tuning techniques for the CPL to be further used in AC distribution system. A mathematical model of a VSC based PE load in synchronous reference frame (SRF) is considered with the implementation of vector control. The transfer functions for the voltage and current control loops have been derived and the tuning rules for the CPL controllers are proposed. A frequency domain analysis is carried out to see the effectiveness of the control scheme.

## 2.1 Types of Loads

Power system dynamic behaviour can be affected by the load characteristics as the loads change the system transfer impedance [76]. The importance of proper representation of loads in power system stability studies has long been recognized and many studies have been made. Load modelling is qualitatively different from generator modelling; it is relatively simple and straightforward to construct models of practically any of the typical load components. The exact composition of the load is often very difficult to evaluate because it changes persistently reflecting the customer's pattern of using various appliances and devices during different times of the day. The usage of appliances also depends on the customer's lifestyle, the weather conditions, the state of economy and many other factors. Therefore, it is essential to estimate the load composition at time of critical interest such as under a heavy or light load condition. Load models are usually classified into two broad categories; static models and dynamic models.

### 2.1.1 Static Characteristics

It is most common to represent the loads by constant impedance (resistance or reactance), constant current and constant power (active or reactive) elements by separately considering the active power $P$ and the reactive power $Q$. These types of loads are typically categorized as follows [76, 77]:

- Constant impedance load: It is also referred to as a constant admittance load. The active and reactive powers vary with the square of the load voltage magnitude. An incandescent lamp is an example of such kind of loads.
- Constant current load: The active and reactive powers are directly proportional to the load voltage magnitude.
- Constant power load: It is also referred as a constant MVA model.The active and reactive powers are independent of the load voltage magnitude. The common examples are the motors linked to the grid through front end PE regulating converters.

Static load characterization is implemented by the exponential model in which the powers are represented as an exponential expression of the load voltage magnitude as indicated by the following expressions [77, 78]:

$$P = P_o \cdot \left( \frac{V}{V_o} \right)^a$$
$$Q = Q_o \cdot \left( \frac{V}{V_o} \right)^b \qquad (2.1)$$

where $P_0$ and $Q_0$ stand for the active and reactive powers consumed at a reference voltage $V_0$. For a CPL model where real and reactive powers do not vary with changes

in load voltage (i.e. $a$ =0). In constant current load model, the power varies directly with the voltage magnitude (i.e. $a$= 1). For constant impedance load model, the power varies with the square of the voltage magnitude (i.e. $a$ = 2).

### 2.1.2 Dynamic Characteristics

Many components of power system respond to disturbances dynamically; i.e. responses to disturbances do not occur instantaneously but require some time. Depending on the nature of disturbances and also for the purpose of the study, the dynamics with a certain range of response times become more important. Therefore, a dynamic load model is a function of time and may be represented by differential equations. Spinning or dynamic loads are mainly induction motors [76, 78].

The dynamics associated with the motors are probably the only dynamic characteristics of the load that have been comprehensively studied. Various methods of analysis have been established to predict the dynamic behavior of a motor subjected to specific disturbances on the supply side. A large portion of the total load is comprised of motor load and exhibits the major dynamics during certain disturbances. In US only, more than 60% of the total electrical energy is consumed by motors. Aggregate motor load cannot be satisfactorily represented by single motor. Large induction motor loads can cause relatively severe instability conditions; the system is more stable with a dynamic representation of motor load at a remote generation than with a constant impedance representation of the same load. The total active power of the motor load depends not only on the system frequency, but also on the rate of the frequency change. For example, all the motors try to run faster when the system frequency is increasing, and consequently draw more active power to increase the kinetic energy associated with the inertia, as well as to compensate the increased losses and shaft loads [76]. Once the system frequency reaches a higher value, the motors need power only to compensate the increased losses and shaft loads. In this respect, small and medium induction motors can have substantial effects on stability. It might not be suitable to ignore inertia of small and medium motors when the disturbances are sufficiently abrupt and large and therefore, one can reasonably expect rapid changes in the motor speeds. There are many small and medium motors aggregating to a large portion of the total load with a substantial total inertia and a significant effect on damping.

There are other dynamic characteristics of the load which must be discussed. They include the characteristics associated to protective operations of thermal and over-current relays, such as one fitted on compressor motors, arc extinction and restart of various discharge lamps and thermostat control of space conditioning and refrigeration. The first two examples may be largely categorized as discrete-state characteristics. One can easily associate the characteristics with two distinctive states, on/off states for motor tripping and arc/no-arc states for discharge lamps. They are dynamic because it usually takes some time before motors are tripped or discharge lamp restarts.

## 2.2 CPLs in AC Distribution System

Figure 2.1 shows several loads connected to each bus in a distribution system. The responsibility of the source subsystem is to maintain the amplitude and frequency of the bus voltage at a fixed level. It has been assumed that some of the loads, which are supplied from source subsystem, are tightly regulated controlled or uncontrolled PE converters. Therefore, these PE loads, which may be voltage regulators or motor drives, behave as CPLs [38].

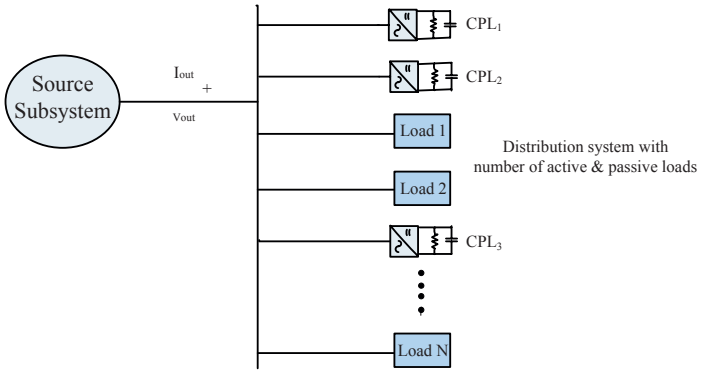


Figure 2.1: PE controlled CPLs and passive loads connected to a typical bus [38]

Figure 2.2 shows the CPL and conventional constant voltage load (CVL) connected to a typical bus. It also shows the equivalent circuit of the source subsystem at this typical bus with equivalent impedance [38]. Because $P$ and $R$ are equivalent constant power and constant voltage loads, respectively, they can change according to the number and power of the loads. It means that if a load is disconnected or a new load is added, $P$ and $R$ may change accordingly. However, $P$ and $R$ instantaneously show the equivalent power of CPLs and the equivalent resistance of CVLs, respectively. In order to determine the necessary conditions for stability of the circuit shown in Figure 2.2, CPL must be modelled.

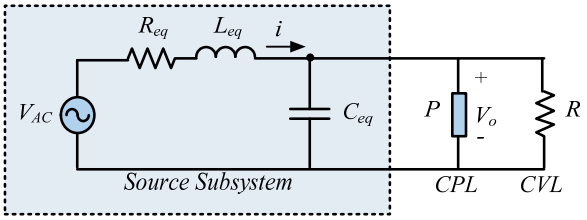


Figure 2.2: CPL and CVL connected to a typical bus [38]

## 2.3 Modelling of Diode/Thyristor-Based CPLs

Most of the PE loads have rectifiers at their front end. Therefore, generally, CPLs are connected to AC distribution systems via a controlled or uncontrolled rectifier. These loads consume constant active power from the generation system irrespective of any abnormalities in the system voltage. In a CPL, input current is inversely proportional to the input voltage, it decreases/increases when the input voltage increases/decreases. As a result, CPLs have negative impedance characteristics at the input terminals [9, 17, 18, 39, 79-81]. Figure 2.3 shows a thyristor rectifier connecting two AC and DC subsystems. The rectifier can be replaced by diodes as well. It has been assumed that the DC subsystem behaves as a DC CPL. The modeling and behavior of these loads has been presented from the AC subsystem point of view, considering small signal variations around the operating points [38]. The cases of diode and thyristor rectifiers driving a CPL have been discussed in the following subsection.

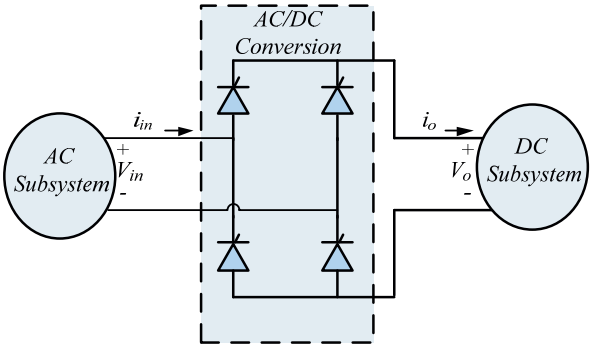


Figure 2.3: AC/DC rectifier connecting a DC subsystem with CPL to an AC subsystem

### 2.3.1 CPLs with Uncontrolled Diode Rectifiers at the Front End

In this case, the rectifier is using the diodes to drive the DC subsystem behaving as CPL. Figure 2.3 is considered utilizing diodes instead of thyristors for the front end conversion. It is assumed that the converter is in continuous conduction mode (CCM) of operation and the voltage of the CPL is assumed to be sinusoidal; however, the current is not sinusoidal [38]. By neglecting harmonics in this section, only the fundamental component of the current is considered. Therefore, voltage and current of the load can be written as:

$$\begin{aligned} v(t) &= V_{\max}.\cos(\omega t) \\ i(t) &= I_{\max}.\cos(\omega t - f) \end{aligned} \tag{2.2}$$

The average active power is presented by:

$$P = \frac{1}{2} V_{\max} I_{\max}.\cos\phi \tag{2.3}$$

For a diode rectifier, the voltage and fundamental component of the current are in phase assuming that the output current of the rectifier is constant. Therefore, the average power is expressed as:

$$P = \frac{1}{2} V_{\max} I_{\max} = \frac{1}{2} V_{rms} I_{rms} \tag{2.4}$$

For modeling this load, a small-signal perturbation in the voltage amplitude is considered. This will further lead to a small-signal perturbation in the load current amplitude:

$$\begin{aligned} v(t) &= \left(V_{\max} + V_{\max}{}^{*}\right).\cos(\omega t) \\ i(t) &= \left(I_{\max} + I_{\max}{}^{*}\right).\cos(\omega t) \end{aligned} \tag{2.5}$$

As the load power remains constant therefore:

$$P = \frac{1}{2}\left(V_{\max} + V_{\max}{}^{*}\right)\left(I_{\max} + I_{\max}{}^{*}\right) = \frac{1}{2} V_{\max}.I_{\max} \tag{2.6}$$

By neglecting the second order term [38], it is possible to obtain:

$$\frac{V_{\max}{}^{*}}{I_{\max}{}^{*}} = -\frac{V_{\max}}{I_{\max}} = -R_{CPL} \tag{2.7}$$

This relation describes the small-signal behavior of the load. $R_{CPL}$ is defined as:

$$R_{CPL} = \frac{V_{\max}}{I_{\max}} = \frac{V_{rms}^2}{P} \tag{2.8}$$

Therefore, the AC CPL considering small-signal variations behaves as a negative resistance. The absolute value of this resistance is equal to the impedance of the CPL at its operating point. Figure 2.4 shows the small-signal model of the load.

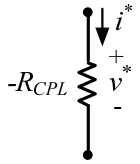


Figure 2.4: Small-signal model of AC CPLs with uncontrolled diode rectifier at the front end

This model is also valid for unity displacement which means that the voltage across the load and the fundamental component of the current through the load are in phase. Therefore, the same model of Figure 2.4 is used for this category of AC PE loads. Generally, these converters have a DC/DC boost converter after the diode rectifier. In this section, it has been assumed CCM of operation for the converters. However, some PE converters are working in discontinuous conduction mode or there is a buck converter after the rectifier. Therefore, the input current of the load is not continuous. If

the voltage and fundamental component of the current are in phase, the small-signal model given in Figure 2.4 is valid. However, if there is a phase difference, the small-signal behavior of the load becomes inductive.

### 2.3.2 CPLs with Controlled Thyristor Rectifiers at the Front End

Like the uncontrolled diode rectifier, the fundamental component of the current in CCM mode of operation is considered for the uncontrolled thyristor rectifier at the front end [38]. The voltage and the current of the load are therefore represented by:

$$\begin{aligned} v(t) &= V_{\max}.\cos(\omega t) \\ i(t) &= I_{\max}.\cos(\omega t - \alpha) \end{aligned} \tag{2.9}$$

where $\alpha$ is the firing angle of the rectifier. The average power can be expressed as:

$$P = \frac{1}{2} V_{\max} I_{\max}.\cos\alpha = V_{rms} I_{rms}.\cos\alpha \tag{2.10}$$

For small-signal modelling of the load, small-signal voltage and current perturbations have been considered. Since the average power of the load is constant, it is possible to write:

$$P = \frac{1}{2}\left(V_{\max} + V_{\max}^{*}\right)\left(I_{\max} + I_{\max}^{*}\right).\cos\alpha = \frac{1}{2} V_{\max}.I_{\max}.\cos\alpha \tag{2.11}$$

By neglecting the second-order term, it can be established:

$$\frac{V_{\max}^{*}}{I_{\max}^{*}} = -\frac{V_{\max}}{I_{\max}} = -Z_{CPL} \tag{2.12}$$

$Z_{CPL}$ is defined as:

$$Z_{CPL} = \frac{V_{\max}}{I_{\max}} = \frac{V_{rms}^2}{P}.\cos\alpha = R_{CPL}.\cos\alpha \tag{2.13}$$

Therefore, the AC CPL interfaced through controlled rectifiers considering small-signal variations behaves as negative impedance. The absolute value of this impedance is equal to the impedance of the CPL at its operating point. Furthermore, there is a phase difference between the current and the voltage. Therefore, the small-signal impedance of the CPL can be expressed as:

$$Z_{CPL}^{*} = R_{CPL}.e^{j\alpha} = -R_{CPL}.\cos\alpha - jR_{CPL}\sin\alpha \tag{2.14}$$

The small-signal resistance and inductance of the load can be represented as:

$$\begin{aligned} r_{CPL}^{*} &= -R_{CPL}.\cos\alpha \\ L_{CPL}^{*} &= -\frac{R_{CPL}}{\omega}.\sin\alpha \end{aligned} \tag{2.15}$$

The small-signal model of the load is illustrated in Figure 2.5.

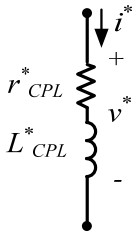


Figure 2.5: Small-signal model of AC CPLs with controlled thyristor rectifier at the front end

## 2.4 Case Study: CPL

In general, AC motor connected to the grid by a back to back converter can be considered as a CPL as shown in Figure 2.6. The intermediate phase is represented by the DC link which is usually modeled with a capacitance. Besides motor drives, other typical examples of CPLs in a modern grid are the battery chargers for electric vehicles and large rectifiers for DC loads.

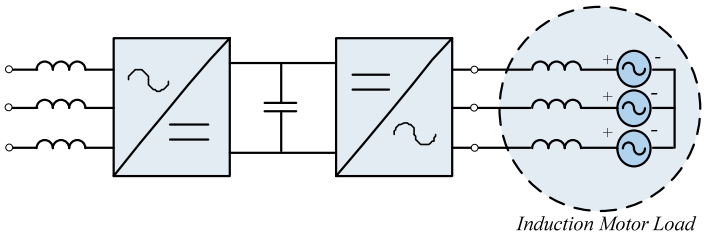


Figure 2.6: Induction motor load with back to back converters

In the system under investigation, for simplicity, the equivalent DC side load is considered as shown in the Figure 2.7.

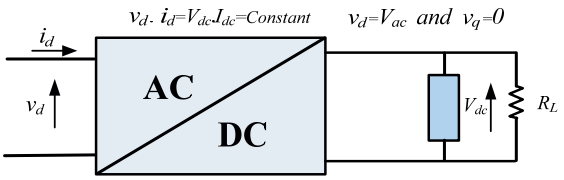


Figure 2.7: Simplified model of a CPL

In our case, CPL is an active rectifier such as three phase full bridge inverter with IGBTs or other similar switching semiconductor devices. An active rectifier provides more flexibility in operation, power factor controllability and reduced THD. A well-known application of an active rectifier is a VSC as it is naturally suited for controlling

active and reactive current in a decoupled manner [75]. In this way, the inverter can control the direct current component absorbed towards the load independently of the control of reactive current, which can be injected towards the grid, thus supporting the stability of the distribution system under abnormal grid voltage conditions. Figure 2.8 illustrates the VSC model of a CPL.

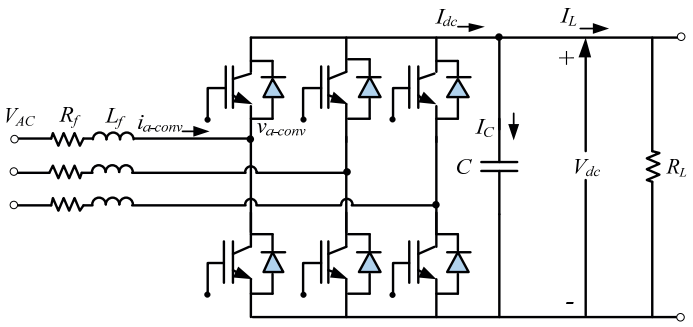


Figure 2.8: Three phase VSC based on IGBT switches

### 2.4.1 Negative Resistance Characteristic of a CPL

Like many other non-linear loads the resistance of the CPL depends on the applied voltage at its terminals. Many of the home appliances are loads with AC/DC converters inside, feeding an internal part that works on a constant DC voltage. The control system of these AC/DC converters controls the direct voltage $V_{dc}$ such that it becomes independent of the applied grid voltage $v_d$. This means that the AC power is independent of the value of grid voltage [82-84]. A lower AC side voltage from the rated value results in a drop in DC link voltage. However, the increase in AC side current neutralizes the drop in DC link voltage which remains constant under all the conditions. Under symmetrical grid voltage sags, with no negative sequence voltage, the operation of the internal controller demands the VSC to draw more/less grid current to maintain a constant active power at the converter input, such that:

$$v_d = \frac{P_{in}}{i_d} \tag{2.16}$$

where $P_{in}$ is the constant input active power and $i_d$ and $v_d$ are the active components of the AC side current and voltage respectively. Since the input active power to the converter remains constant in a wide range of operating conditions, provided that the controller works properly and instantly, the *vi* characteristic of the CPL is investigated by considering the incremental input resistance $R_{CPL}$ [79]. This value is given by the ratio of small signal changes in input voltage over small signal input current:

$$R_{CPL} \approx \frac{\Delta v_d}{\Delta i_d} \tag{2.17}$$

Differentiating (2.16) with respect to the current yields negative input resistance:

$$\frac{dv_d}{di_d} = -\left|\frac{P_{in}}{i_d^{\,2}}\right| = -\left|\frac{v_d^{\,2}}{P_{in}}\right| = -R_{CPL} \tag{2.18}$$

$R_{CPL}$ represents the negative resistance seen from the AC side. Figure 2.9 demonstrates the negative resistance characteristic of the CPL and confirms the inverse relationship that holds between voltage and active current under balanced voltage dips. It can also be seen that the destabilizing effects of the negative resistance can be minimized when the CPL is able to inject the reactive current $i_q$ into the power system. The reactive injection leads to a small increase in AC side voltage at the CPL terminal and the active component of the current decreases to keep the input power constant. The increase in voltage is dependent on the amount of reactive injection and the overall impedance of the power network. The higher the reactive injection and the network impedance the more the voltage support. This has been addressed in details in chapter 3.

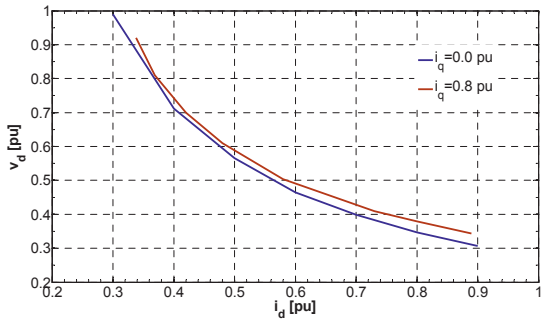


Figure 2.9: Negative resistance characteristics of a CPL and impact of reactive current injection [65]

## 2.5 CPL Control Structure

The control strategy implemented for CPL is based on vector control method in a synchronous reference frame (SRF) to achieve an independent control of active and reactive powers. Vector control method transforms the AC current and voltages into DC quantities, thereby, allowing the PI controllers to remove effectively the static errors in the control system. However, this is one possibility of the control scheme; many other control methods can also be employed.

Figure 2.10 illustrates the CPL control configuration. Clark and Inverse-Clark transformations convert the three phase voltages and currents into stationary $\alpha\beta$ complex reference frame and vice-versa. Similarly, Park and Inverse-Park transformations convert the voltage and current quantities from stationary $\alpha\beta$ reference frame to rotating SRF, and vice versa. Phase-locked loop (PLL) is a control system that generates a signal that has a fixed relation to the phase of a reference signal [85]. It is a closed loop control that controls the angle $\theta$. The overall control scheme is based on the cascade of two independent controllers, a DC link voltage controller to regulate the output DC voltage and the current controller to control the load current.

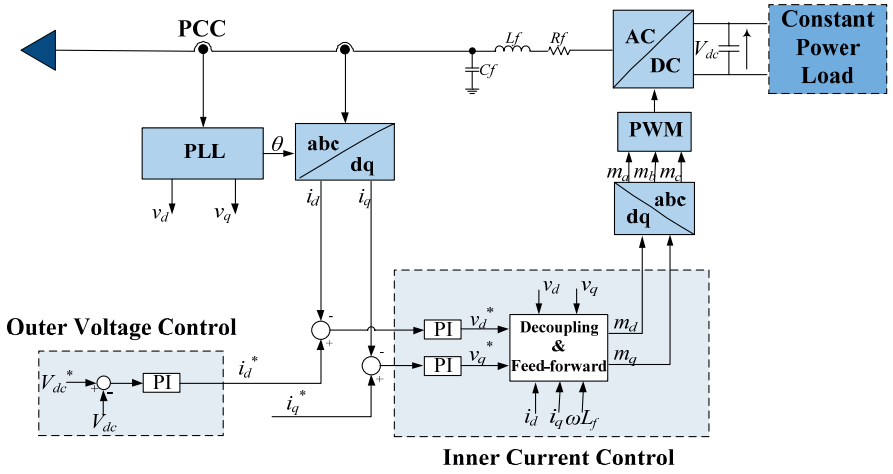


Figure 2.10: CPL control structure with independent control of active and reactive powers in SRF

### 2.5.1 Inner Current Controller

The inner current control consists of two PI regulators separately for active and reactive current control, decoupling factors and the feed-forward terms. It controls the current flowing through the load to define the voltage that it needs to generate. The basic structure of the current control is shown in Figure 2.11.

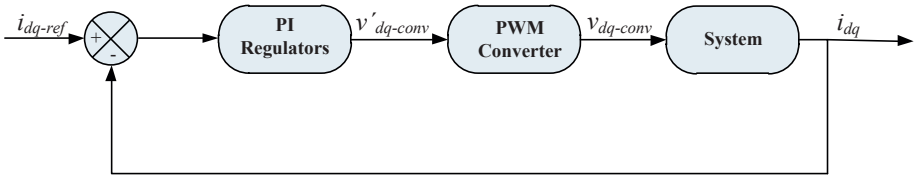


Figure 2.11: Block diagram of current controller

PI regulators transform the error between the active and reactive components of current into corresponding voltage signal. The general expression for the PI regulators is presented by:

$$P(s) = K_{pc} + \frac{K_{ic}}{s} = K_{pc} \cdot \left( \frac{1 + T_{ic} \cdot s}{T_{ic} \cdot s} \right) \tag{2.19}$$

where the subscript '*c*' represents the current regulator. *P(s)* is the transfer function of the PI regulator, $K_{pc}$ is the proportional gain and $T_{ic}$ is the integral time constant. The regulator block transfer function is then:

$$\left(i_{dq-ref}(s)-i_{dq}(s)\right).\left(K_{pc}+\frac{K_{ic}}{s}\right)=v'_{dq-conv}(s) \tag{2.20}$$

where $i_{dq}$ and $v'_{dq\text{-}conv}$ are the active and reactive components of measured current and PI output voltage.

PWM converter is an ideal power transformer with an average time delay equal to half of the IGBT switching cycle [86]. The transfer function of PWM converter is therefore presented by:

$$Q(s)=\left(\frac{1}{1+\frac{T_{switch}}{2}.s}\right)=\left(\frac{1}{1+T_a.s}\right) \tag{2.21}$$

where $T_{switch}$ is the switching time and $T_a$ is the average delay of the PWM converter. The converter block transfer function is given by:

$$v'_{dq-conv}(s).\left(\frac{1}{1+sT_a}\right)=v_{dq-conv}(s) \tag{2.22}$$

where $v_{dq\text{-}conv}$ is the output voltage of the PWM converter as shown in Figure 2.8. Combining the PI regulators and PWM converter transfer functions, we have:

$$\left(i_{dq-ref}(s)-i_{dq}(s)\right).\left(Kpc+\frac{Kic}{s}\right).\left(\frac{1}{1+sT_a}\right)=v'_{dq-conv}(s) \tag{2.23}$$

The reference voltage for PLL is $V_{AC}$ and current reference for the CPL control system is $i_{conv}$ as presented in Figure 2.8. The reference voltage is written as:

$$V_{AC}=v_{conv}+R_f\,i_{conv}+L_f\,\frac{di_{conv}}{dt} \tag{2.24}$$

In SRF, (2.24) can be expressed as:

$$\begin{aligned} v_d-v_{d-conv}&=R_f i_d+L_f\,\frac{di_d}{dt}-\omega L_f i_q \\ v_q-v_{q-conv}&=R_f i_q+L_f\,\frac{di_q}{dt}-\omega L_f i_d \end{aligned} \tag{2.25}$$

where $v_d$ and $v_q$ are the active and reactive components of the AC side reference voltage. The frequency terms in (2.25) provide cross coupling between the two axis. The cross coupling terms are compensated by the feed-forward terms in the controller. The system input from converter is defined as:

$$v'_{d-conv} = -\left(i_{d-ref} - i_d\right).\left(Kpc + \frac{Kic}{s}\right) + \omega L_f i_q + v_d$$
$$v'_{q-conv} = -\left(i_{q-ref} - i_q\right).\left(Kpc + \frac{Kic}{s}\right) + \omega L_f i_d + v_q \tag{2.26}$$

Substituting (2.26) into (2.22) and equating with (2.25), we have:

$$R_f i_d + L_f \frac{di_d}{dt} = v_{d-conv}$$
$$R_f i_q + L_f \frac{di_q}{dt} = v_{q-conv} \tag{2.27}$$

The cross coupling terms are thus cancelled out and independent control of active and reactive current is achieved, which is one of the important features of vector control [87]. Thus current controllers of each axis operate independently. The frequency domain representation of the active component of current is therefore:

$$i_d(s) = \left(\frac{1}{R_f + sL_f}\right).v_{d-conv}(s) \tag{2.28}$$

The transfer function of the system is:

$$H(s) = \frac{1}{R_f}.\left(\frac{1}{1 + \frac{L_f}{\omega_b R_f}\cdot s}\right) = \frac{1}{R_f}.\left(\frac{1}{1 + s.\tau}\right) \tag{2.29}$$

where $\tau$ is the time constant of the distribution line. Complete block diagrams of active and reactive current component controllers are presented in Figure 2.12.

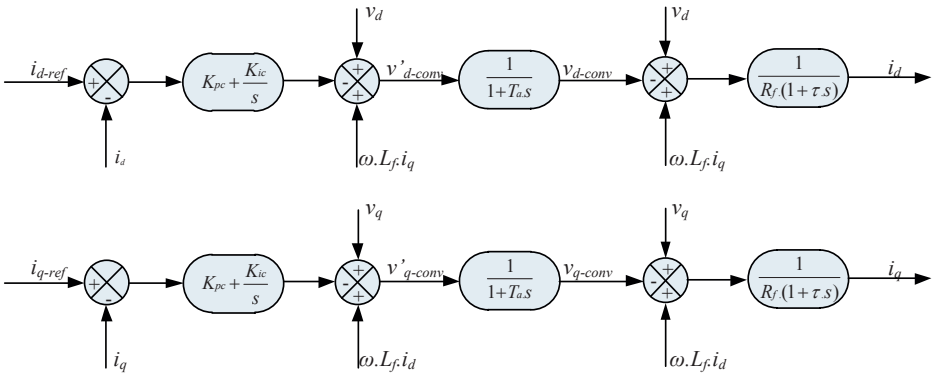


Figure 2.12: Complete block diagram of active and reactive current controllers

However, as the cross coupling terms are cancelled out by the feed forward terms, therefore, the block diagram reduces to two separate loops in the *d* and *q* axis as shown in Figure 2.13. All the values are referred in per unit (pu).

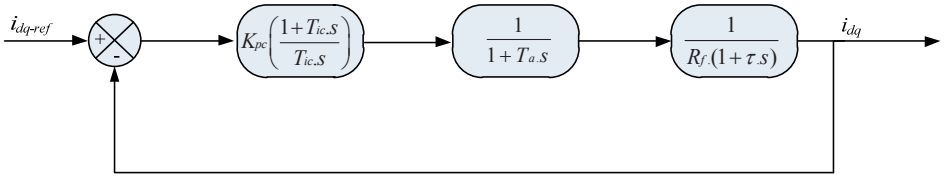


Figure 2.13: Reduced block diagram for inner current control

The reference of the inner current controller comes from outer controller. The outer controller consists of DC voltage controller or active power controller. Active current $i_d$ is used to control either of active power or DC voltage level. Similarly, the reactive current $i_q$ is used to control either of reactive power flow into stiff grid connection or AC voltage support in weak grid connection or during faults on the transmission lines.

## 2.5.2 Outer Voltage Controller

The outer voltage controller maintains the DC link voltage to a specified level. The basic components of the voltage controller are the same as in the case of current controllers. The measured voltage is compared with the specified value and the error is fed to the PI regulators. The general block diagram of the outer voltage controller is given in Figure 2.14.

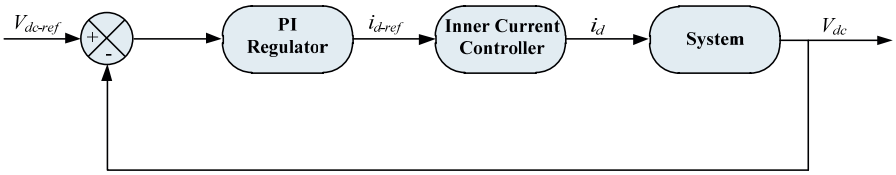


Figure 2.14: Block diagram of DC link voltage controller

PI regulator converts the DC link voltage error signals into corresponding active current signal that acts as input for the inner active current controller. Fluctuations in the DC link voltage caused by the variations in the AC side voltage are translated by the increase/decrease of the active current component. The regulator block is represented by the following expression:

$$\left(V_{dc-ref}(s)-V_{dc}(s)\right).\left(K_{pv}+\frac{K_{iv}}{s}\right)=i_{d-ref}(s) \tag{2.30}$$

where $K_{pv}$ is the proportional gain and $T_{iv}$ is the integral time constant. The subscript *'v'* represents the voltage regulator.

For the design of outer voltage controller, the inner active current controller is generally assumed as ideal and represented by unity [87]. In this case, a simplified representation of the second order closed loop transfer function of the inner active current controller by the equivalent first order approximation is assumed, such that:

$$Q(s) = \left( \frac{1}{1 + 2T_a.s} \right) = \left( \frac{1}{1 + T_{eq}.s} \right) \tag{2.31}$$

As the active power drawn by the CPL is constant, the power balance relationship between the input and output of the converter is given as,

$$\begin{aligned} P &= \frac{3}{2}\left( v_d.i_d + v_q.i_q \right) = V_{dc}.I_{dc} = Constant \\ Q &= \frac{3}{2}\left( v_d.i_q - v_q.i_d \right) \end{aligned} \tag{2.32}$$

where $V_{dc}$ and $I_{dc}$ are the voltage and current respectively on the DC output side. The DC side current is represented by:

$$I_{dc} = C\frac{dV_{dc}}{dt} + I_L \tag{2.33}$$

where $I_L$ is the load current. As *d*-axis is always synchronized with the grid voltage vector, therefore, $v_q=0$. Therefore, (2.32) is reduced to:

$$\begin{aligned} P &= \frac{3}{2}v_d.i_d = V_{dc}.I_{dc} = Constant \\ Q &= \frac{3}{2}v_d.i_q \end{aligned} \tag{2.34}$$

The active current component corresponds to the active power absorbed by the load while the reactive current component represents the injected or absorbed reactive power. The relation between the active component of AC current and the DC side current is represented by:

$$I_{dc} = \frac{3}{2}.\frac{v_d}{V_{dc}}.i_d \tag{2.35}$$

Inserting (2.35) into (2.33), we get:

$$C\frac{dV_{dc}}{dt} = \left( \frac{3}{2}.\frac{v_d}{V_{dc}}.i_d \right) - I_L \tag{2.36}$$

The DC link current equation is non-linear equation. The linearization of (2.36) is done based on Taylor series expansion and it is observed that $I_L$ acts as a disturbance and only significant input is the active component of AC current $i_d$. After linearization (2.36) is represented in frequency domain such that:

$$\frac{\Delta V_{dc}(s)}{\Delta i_d(s)} = \frac{3}{2}.\frac{v_{d,0}}{V_{dc,ref}}.\frac{1}{s.C} \tag{2.37}$$

In pu the final system transfer function of (2.37) reduces to:

$$\frac{\Delta V_{dc}(s)}{\Delta i_d(s)} = \frac{v_{d,0}}{V_{dc,ref}}.\frac{\omega_b.C}{s} \tag{2.38}$$

To maintain the power balance, the DC link voltage controller controls the capacitor so that $I_c$=0 and, therefore, $I_{dc}$=$I_L$. Using this value of $I_{dc}$ in (2.35) and representing in pu, we have:

$$i_d = \frac{V_{dc}}{v_d}.I_L \tag{2.39}$$

This is the feed forward term used to minimize the slow dynamic response of the controller and to compensate for the variation in the load. The complete block diagram of the outer voltage controller with the derived transfer functions is shown in Figure 2.15.

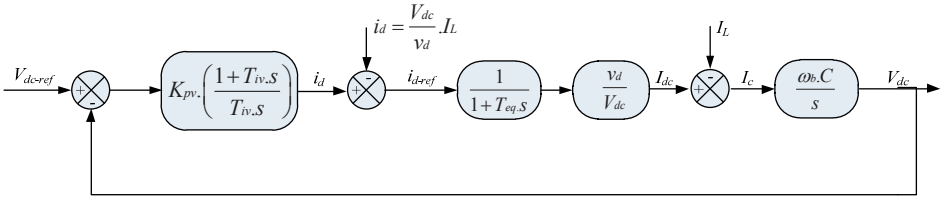


Figure 2.15: Complete block diagram of outer voltage controller

In the case of CPL, the outer voltage controller ensures a constant active power to the load under most the operating conditions. It has to adjust the level of the active component of the current in response to the changes in DC link voltage under grid side faults. The outer voltage controller has to be tuned to optimize the system behaviour and to show robustness in response to a disturbance.

## 2.6 Controller Tuning

Optimal performance of the inner and outer controllers can only be achieved when controllers are tuned properly. The optimal controller operation requires lowest possible overshoot and fast response which can be achieved by keeping the cutoff frequency higher. To obtain the described objectives *modulus optimum* and *symmetrical optimum* tuning methods have been implemented to select the parameters for inner current controller and outer voltage controller respectively.

### 2.6.1 Tuning of Inner Current Controllers

Modulus optimum technique is used for the plants with low order transfer functions and makes the cutoff frequency as high as possible. When the system has one dominant and another minor pole in the transfer function, the integral time constant of the PI controller is selected to cancel out the dominant pole.

From the Figure 2.13 the open loop transfer function of the inner current controller is represented as:

$$H_{C,OL}(s) = K_{pc}.\left(\frac{1+T_{ic}.s}{T_{ic}.s}\right).\left(\frac{1}{1+T_a.s}\right).\left(\frac{1}{R_f.(1+s.\tau)}\right) \tag{2.40}$$

The zero of the PI controller is cancelled out by defining $T_{ic}=\tau$. The open loop transfer function hence reduces to:

$$H_{C,OL}(s) = \frac{K_{pc}}{\tau.R_f}.\frac{1}{s.(1+T_a.s)} \tag{2.41}$$

The close loop transfer function can be presented as:

$$H_{C,CL}(s) = \frac{K_{pc}}{\tau.R_f.T_a.s^2+\tau.R_f.s+1} \tag{2.42}$$

The controller gain is calculated from the unity gain condition at cutoff frequency such that:

$$\left|H_{C,CL}(j\omega)\right| = \left|\frac{K_{pc}}{\tau.R_f.T_a.(j\omega)^2+\tau.R_f.(j\omega)+1}\right| = 1 \tag{2.43}$$

The evaluation of (2.43) provides the value of inner current controller proportional gain $K_{pc}$, such that:

$$K_{pc} = \frac{\tau R_f}{2T_a} \tag{2.44}$$

where $T_a=T_{sw}/2$. The parameters of the inner current controller are summarized in Table 2.1. The values of filter inductance $L_f$ and filter resistance $R_f$ are chosen to be 5 % and 1% of the base impedance respectively [88].

Table 2.1: Parameters of the inner current controller

| Parameter | Value |
|---|---|
| Filter inductance $L_f$ | 0.05 pu |
| Filter resistance $R_f$ | 0.01 pu |
| DC link capacitor $C$ | 1.34 pu |
| Base frequency $f$ | 50 Hz |
| Switching frequency $f_{sw}$ | 5 kHz |
| Average time delay $T_a$ | 100 µs |
| Integral time constant $T_{ic}$ | 0.016 s |
| Proportional gain $K_{pc}$ | 0.8 |
| Integral gain $K_{ic}$ | 50 |

Using the calculated current controller parameters in (2.41), we get the open loop transfer function:

$$H_{C,OL}(s) = \frac{5000}{100 \times 10^{-6} s^2 + s} \tag{2.45}$$

The modulus optimum method offers a relatively non-oscillatory closed loop tracking response. A faster response and simplicity is required for the inner control loop of the CPL. Bode plot for the second order open loop transfer function is shown in Figure 2.16. The gain margin is infinite and the phase margin is 65˚. Therefore, from the frequency domain stability criteria stated in [89], the bode plot suggests the closed loop system to be stable and robust.

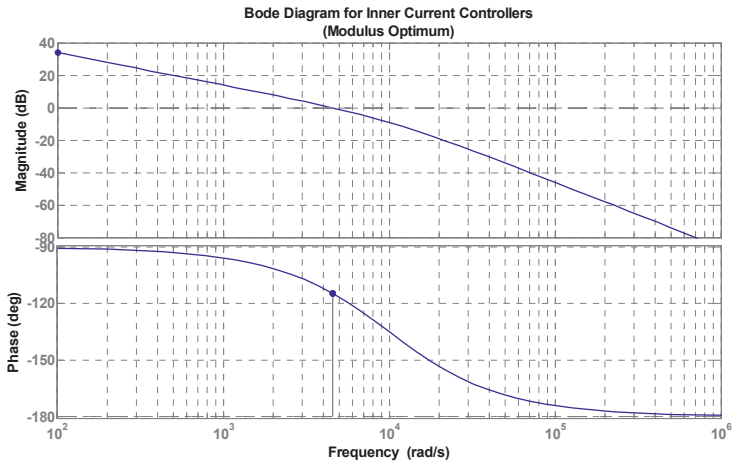


Figure 2.16: Bode plot for open loop transfer function of current controllers

### 2.6.2 Tuning of Outer Voltage Controller

Modulus optimum criterion is not a good choice in a case where one pole of the open loop transfer function is close to or at the origin. Instead, symmetrical optimum tuning technique is used to select the PI controller parameters [87]. The main advantage of the tuning schemes is that it maximizes the phase margin and optimizes the control system behavior with respect to disturbance input.

From the Figure 2.15, open loop transfer function can be represented as:

$$H_{V,OL}(s) = K_{pv}.\left(\frac{1+T_{iv}.s}{T_{iv}.s}\right).\left(\frac{1}{1+T_{eq}.s}\right).\left(\frac{v_d}{V_{dc}}.\frac{\omega_b.C}{s}\right) \tag{2.46}$$

(2.46) is simplified by defining the $T_c=1/\omega_b.C$ and $K=v_d/V_{dc}$, such that:

$$H_{V,OL}(s) = K_{pv}.\left(\frac{1+T_{iv}.s}{T_{iv}.s}\right).\left(\frac{K}{1+T_{eq}.s}\right).\left(\frac{1}{s.T_c}\right) \tag{2.47}$$

According to the tuning criteria based on Nyquist stability, the parameters of the outer DC link voltage controller are found as:

$$\begin{aligned} &K_{pv} = \frac{T_c}{a.K.T_{eq}} \quad \text{and} \quad T_{iv} = a^2 T_{eq} \\ &\text{where, } a = \sqrt{\frac{1+sin\Phi_M}{1-sin\Phi_M}} \\ &\text{Phase Margin, } \Phi_M = tan^{-1}\sqrt{\frac{T_{iv}}{T_{eq}}} - tan^{-1}\sqrt{\frac{T_{eq}}{T_{iv}}} \end{aligned} \tag{2.48}$$

where $a$ is a constant number and its recommended value is between 2 and 4 [87]. With the new defined controller parameters, (2.47) becomes:

$$H_{V,OL}(s) = \frac{1}{a^3.T_{eq}{}^2.s^2}.\left(\frac{1+a^2.T_{eq}.s}{1+T_{eq}.s}\right) \tag{2.49}$$

The outer voltage controller parameters are selected using (2.48) and are presented in Table 2.2.

Table 2.2: Parameters of the outer voltage controller

| Parameter | Value |
|---|---|
| Equivalent time delay $T_{eq}$ | 200 µs |
| Integral time constant $T_{iv}$ | 0.0018 s |
| Capacitor time constant $T_c$ | 0.0024 s |
| Proportional gain $K_{pv}$ | 4 |
| Integral gain $K_{iv}$ | 2222.22 |
| Steady state voltage ratio $K$ | 1 |

The open loop transfer function, therefore, becomes:

$$H_{V,OL}(s) = \frac{0.0018s + 1}{0.216 \times 10^{-9} s^3 + 1.08 \times 10^{-6} s^2} \tag{2.50}$$

The role of CPLs under abnormal grid side conditions is the main focus of this work. DC link voltage controller of the CPL must show robustness under distorted voltage and current conditions and must provide a constant active power to the load by adjusting the active current component. Figure 2.17 presents the open loop bode plot for the DC link voltage controller. The phase margin is 53˚ and it occurs at a frequency of 1.69e+3 rad/s. The gain margin is infinite. Therefore, the margins to instability are sufficiently high. This ensures the stable operating limits of the system. The phase margin is maximum at the cross over frequency. Bode plot shows that the response of the transfer function is similar to a band pass filter. Therefore, the tuning of the outer voltage controller by symmetrical optimum method appears to be effective.

Appendix B presents the detailed frequency domain analysis under low voltage conditions and impact of AC voltage drop on controller stability is discussed. It also presents the detailed simulation results confirming the results from analytical study.

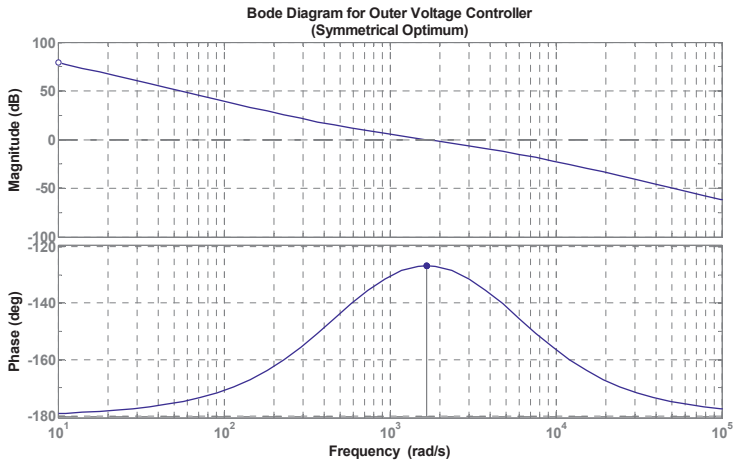


Figure 2.17: Bode plot for DC link voltage controller

## 2.7 Summary

This chapter first presents the different types of loads and their behaviour. Different schematic arrangements of the CPLs in AC systems have been presented and discussed. A brief discussion on the modelling of controlled and uncontrolled CPLs in AC subsystems have been made. A model of the CPL based on VSC has been presented as a case studied in this work. A brief discussion highlights the negative resistance instability effects of the CPL. It has been discussed that the reactive injection by the CPL can decrease the negative resistance instability by supporting the terminal voltage

and decreasing the active component of the CPL current. A mathematical model of the CPL control system in SRF is described and the tuning rules for the PI regulators of the converter controllers are established. For inner current controllers, modulus optimum tuning method is used to derive the parameters. DC link voltage controller parameters are derived by using the symmetrical optimum tuning technique. The stability of the CPL control system is analyzed in frequency domain to see its effectiveness under abnormal grid voltage conditions. Bode plots for both inner current and outer DC link voltage controller suggest a robust control with reasonably high phase and gain margins.

# 3 Role of CPLs in Transient Stability Enhancement and Loss Minimization

*This chapter investigates the role of CPLs on the transient stability margins and loss minimization in AC distribution system. The critical clearing time of the system is selected as a measure of the transient stability limit for investigating and comparing the cases of CPLs with and without reactive current control. The increment in the current rating of the converter due to the reactive injection is investigated. Centralized reactive compensation by a STATCOM is used as reference to compare with distributed compensation by the CPLs. Finally, the influence of reactive compensation on the total attainable CPL current is investigated analytically as well as through simulations and a loss minimization methodology is introduced.*

Reactive power is one of the power system ancillary services and can be supplied from either static or dynamic VAR sources. Provision of reactive power in the proximity of load is clearly beneficial for the stability and efficiency of the overall system. The stability of PE loads compared to traditional passive loads has been a subject of research in DC distribution systems for a long time and several stability criteria have been investigated. However, the role of controlled CPLs in AC distribution systems from the system stability point of view has not been yet extensively investigated [38, 39, 75]. Reactive power provision as an ancillary service by the load itself could greatly increase the margin to voltage collapse in certain types of systems and, therefore, influence the stability of the overall system.

This chapter investigates the role of the CPLs and their control in the transient stability and loss minimization of AC distribution systems. Other sources of instability in an AC power system, such as rotating machine parameters and overall system inductance, have also been taken into account. A typical AC distribution feeder with CPLs and other types of loads is modeled in PSCAD/EMTDC to investigate and compare the behavior during different levels of voltage sags. The impact of reactive current control by CPLs on the transient stability margins of the power system has been studied. Fast reactive power compensation will increase the power transfer capability of the power system and can, in this sense, help increase the robustness and stability margins of the power system. This will increase the capability to tolerate higher shares of CPLs in the system during steady-state operation and transient conditions. The additional functionality of

reactive current control by the loads is investigated on the assumption that all CPLs in the system are based on VSC as described in chapter 2, with force-commutated semiconductors and PWM techniques. Finally, loss minimization is discussed based on optimal reactive current injection by CPLs.

## 3.1 Case Study: AC Distribution System

The basic schematic diagram of the AC distribution system is shown in Figure 3.1. This basic system will be further extended to a larger system with multiple CPLs, depending on the type of analysis. The AC distribution system is composed of a squirrel cage induction generator (SCIG), a medium voltage grid, two transformers with voltage levels at 690 V and 22 kV, a CPL and electrical lines to connect the components together. The generation and the load are operating at 690 V and are connected to the distribution grid through two transformers. The main grid is a three phase AC source with impedance. The SCIG represents a wind turbine. Induction machines are most commonly used as wind turbine generators and small hydro applications due to their ruggedness, low cost and the need for little maintenance. However, under grid contingencies SCIG based DG need a dedicated compensating device to avoid possible disconnection. This system has been chosen because CPL will be used as a compensating device in addition to operating as a regulated load interface.

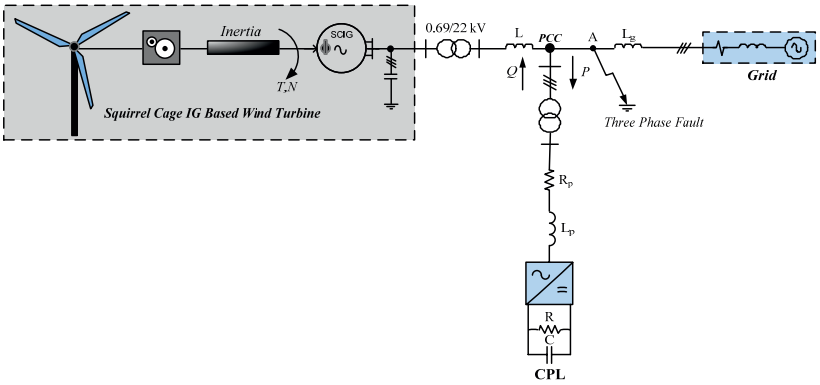


Figure 3.1: Basic AC distribution system under investigation

## 3.2 Impact of Reactive Injection on Voltage

The relationship between converter terminal voltage and the active component of the CPL current can be understood by injecting the reactive current component $i_q$ under abnormal voltage conditions. The distribution system of Figure 3.1 has been considered and a resistive three phase to ground fault is simulated in the grid between the CPL and transmission line inductance $L_g$ for a period of 0.5 sec as shown in Figure 3.1. By decreasing the value of the fault resistance, reduced values of the converter terminal

voltage can be obtained. In this simulation model, the CPL is consuming 30% of power generated by the generation system.

Figure 3.2 shows the values of active and reactive components of current and active component of terminal voltage on the AC side of the converter when a voltage drop of 20% compared to nominal voltage is simulated with no injection of the reactive current. When the voltage drop occurs, the active component of the current representing the load power also increases to keep the power input to the load constant in accordance with (2.16) and illustrated by the Figure 3.3.

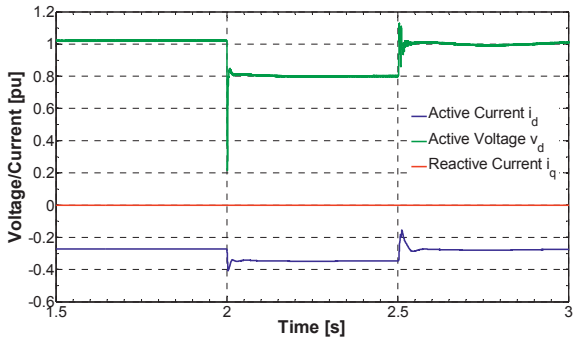


Figure 3.2: Voltage dip under no reactive current injection

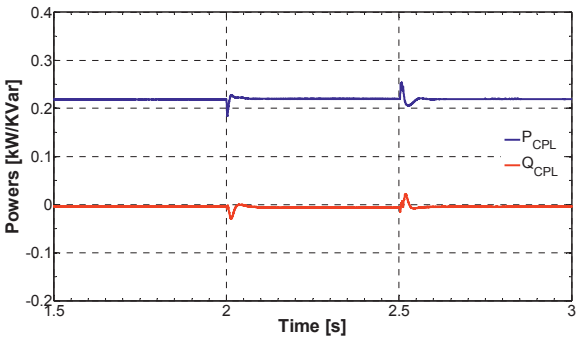


Figure 3.3: CPL powers under voltage dip

Figure 3.4 presents the situation when CPL is allowed to inject the reactive current during the fault to see its impact on voltage. The amount of the injected reactive current is 0.2 pu. An improvement of terminal voltage as a result of the reactive injection can be seen and it is increased by 3%. This improvement in the voltage during the fault results in a small decrease in active component of the current compared to the case of no reactive injection. The active current is decreased by 1.2 %.

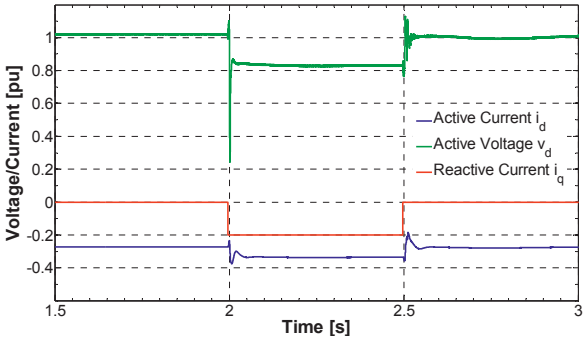


Figure 3.4: Voltage dip under 0.2 pu reactive current injection

Simulations are repeated for the case when CPL injects 0.4 pu reactive current under voltage drop and the results are presented in Figure 3.5. This higher injection of reactive current results in an increase of 6% in the terminal voltage. The decrease in active current component during the fault in this case is 2.2%. The CPL power remains constant under all the voltage conditions.

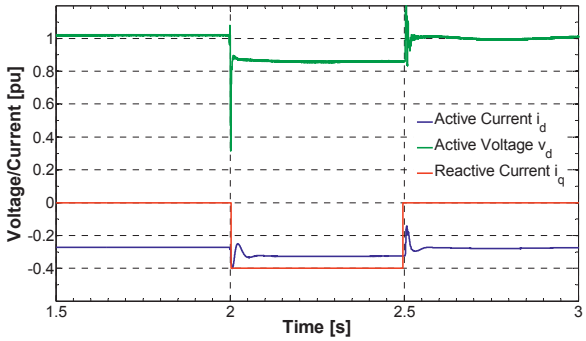


Figure 3.5: Voltage dip under 0.4 pu reactive current injection

## 3.3 Reactive Injection by CPLs and Transient Stability

This section presents a simulation study that is performed to analyse the transient stability in AC distribution system where several CPLs are connected. The impact of reactive injection by the CPLs on the transient stability margins has been investigated. For this analysis, the CPL control injects the reactive components of current during the fault. The reactive injection deactivates automatically when the fault ends. The following three different shares of loads have been considered:

**Case I:** CPLs are consuming 80% of the total generated power by the distributed power source. The stability margins of the system are investigated with and without reactive current injection.

**Case II:** Stability limits of the system are investigated when the amount of load controlled by CPLs and uncontrolled induction motor (IM) load is equal. The investigation is done with and without reactive current injection by the CPLs.

**Case III:** Investigation of stability margins of the distribution system is performed when the amount of load controlled by CPLs is less than that of uncontrolled IM load.

## CASE I

For this analysis, the basic distribution system presented in Figure 3.1 is extended to a system with two CPLs as shown in Figure 3.6. The parameters of the SCIG, medium voltage grid and lines are given in Section 3.1. The length of transmission line between the generator and CPL and between the two CPLs is taken as 6 km and the distance of the grid from $CPL_2$ is taken to be 50 km. The distribution line length is considered to be 100 m. The resistances of the transmission lines are neglected.

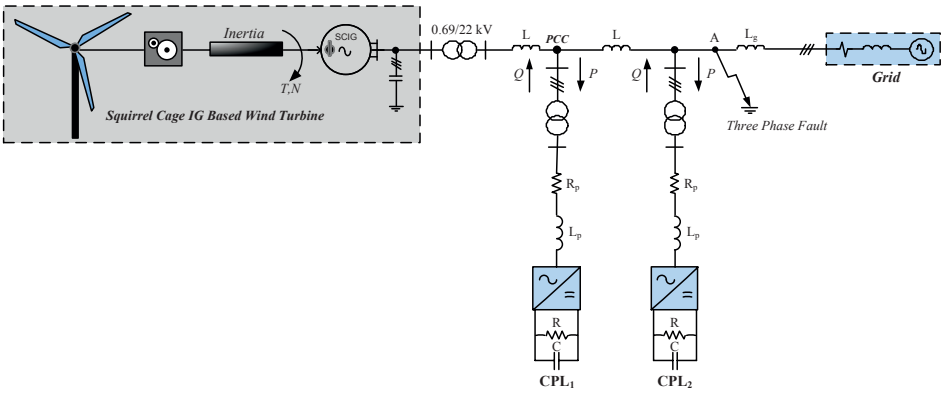


Figure 3.6: AC distribution system with 2CPLs and wind turbine

Each CPL is consuming 300 kW, which corresponds to 40 % of the total power generated by the wind generator. The remaining power produced by the generation system is exported to the grid. A three phase line to ground fault is simulated at point *"A"* between the medium voltage grid and the loads (Figure 3.6). Fault resistance is varied to get a voltage drop equal to 20% of the nominal voltage. The value of the fault resistance found is 110 Ω. Fault occurs at time $t$=2s during the simulation. Several simulations are carried out under this condition to obtain the critical clearing time (CCT) of the system; that is the maximum time during the fault before the system becomes unstable due to voltage collapse.

Voltage at the point of common coupling (PCC) is shown in Figure 3.7 when the system becomes unstable. SCIG becomes unstable under grid voltage sag. A voltage dip increases the rotor slip and SCIG starts consuming more reactive power from the grid (Figure C.1and Figure C.2 in appendix C). It further lowers the voltage and eventually

voltage collapses. When the fault occurs the voltage drop is 0.2 pu. However, it goes on decreasing until it collapses. Figure C.3 in appendix C shows the SCIG losing the torque control during and after the fault. Figure 3.8 shows the voltage just being able to recover the pre-fault value. CCT is found to be 645 *ms*. All the system parameters show oscillations after a step change because of lower value of the generator polar moment of inertia.

Simulations are carried out under the same load conditions, however, this time CPLs are allowed to inject reactive current to support voltage during the fault. The value of fault resistance is kept fixed in this case as well. The obtained voltage drop in this case is 0.17 pu. This 3% improvement in voltage is a result of reactive injection by the CPLs. The amount of injected reactive current is 0.1955 pu for $CPL_1$ and 0.1985 pu for $CPL_2$. This difference of current corresponds to the effects of the severity of fault on each CPL which decrease with the distance from the location of the fault. CPL located nearer to the fault injects slightly more reactive current as the voltage drop across it is slightly higher. This current does not maintain the voltage at its pre-fault value during the fault. Instead, it makes sure that the system recovers from unstable point. Figure 3.9 shows the voltage recovering back the steady state value. The value of CCT is 1.18 s in this case, showing 83% increment corresponding to no reactive injection. The reason for higher value of CCT is the voltage support during the fault due to reactive injection by CPLs. The system is able to tolerate the longer fault. Figure C.4 in appendix C shows that the rotor does not reach the mechanical unstable point and Figure C.5 shows the generator regaining the torque control after the fault.

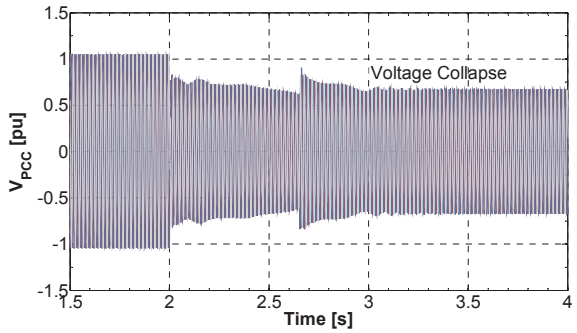


Figure 3.7: Voltage collapse without reactive current control

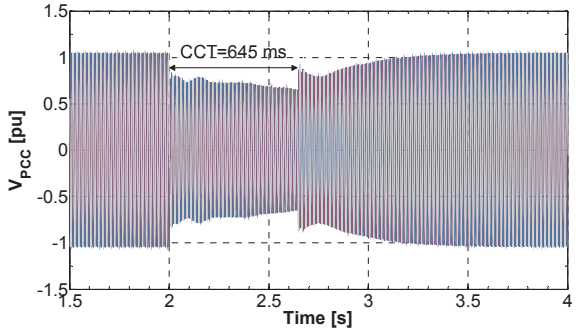


Figure 3.8: CCT without reactive current control

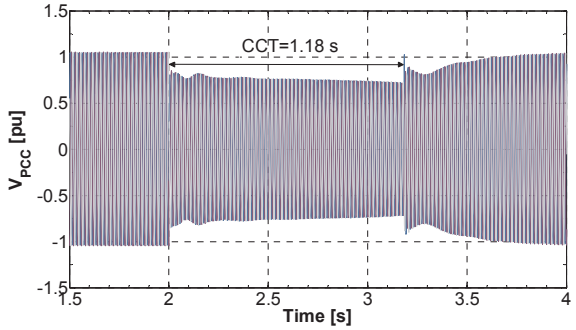


Figure 3.9: CCT with reactive current control

## CASE II

In order to see the impact of uncontrolled load on transient stability margins of the AC distribution system, two CPLs and an additional IM load is considered as presented by Figure 3.10. The amount of load shared by CPLs is equal to that of uncontrolled IM load. Total power consumed by all the loads is 80% of the total produced power with each CPL taking 20% (150 kW) and IM consuming 40%. A three phase line to ground fault is simulated as in the previous case and fault resistance is kept fixed as in the previous case to achieve the same simulation conditions.

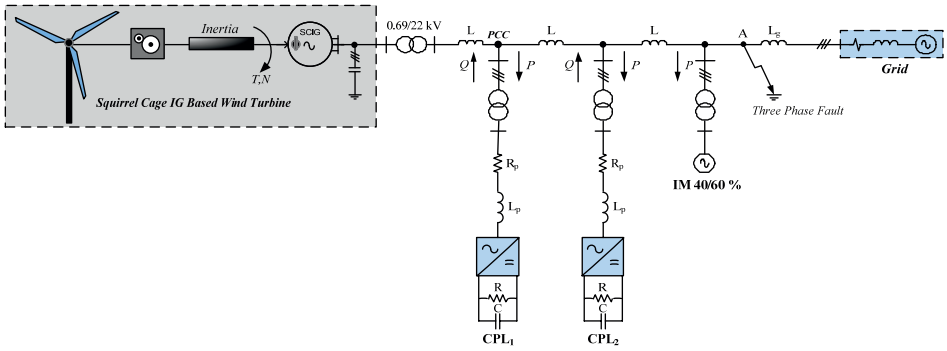


Figure 3.10: Schematic system with two CPLs and an IM load

The simulations are first carried out with no reactive current injection during the fault. The value of CCT is found to be 468 *ms* as presented in Figure 3.11. Low value of CCT is justified by the overall increase in the power system inductance which leads to an earlier voltage collapse. The inclusion of uncontrolled IM load results in a substantial increase in the system inductance. The recovery time after the fault is longer compared to the case of controlled CPLs only.

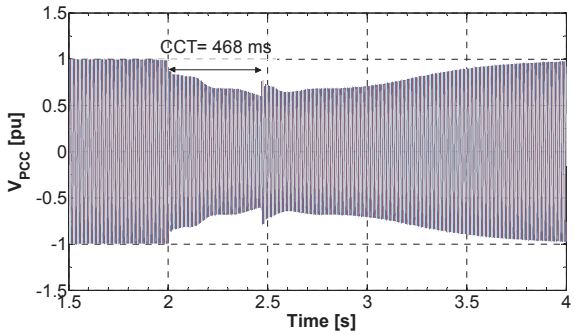


Figure 3.11: Voltage recovery without reactive injection with 40% CPLs and 40% IM

Simulations are repeated under the same fault conditions and CPLs are controlled to inject reactive current during the fault. The Figure 3.12 shows the voltage recovering back to the pre-fault state. CCT is increased in this case and is found to be 660 *ms*. The amount of the injected reactive current is 0.191 pu for $CPL_1$ and 0.193 pu for $CPL_2$. Transient stability margins are highly compromised and it looks that further increase in inductive load will result in further lower value of the CCT.

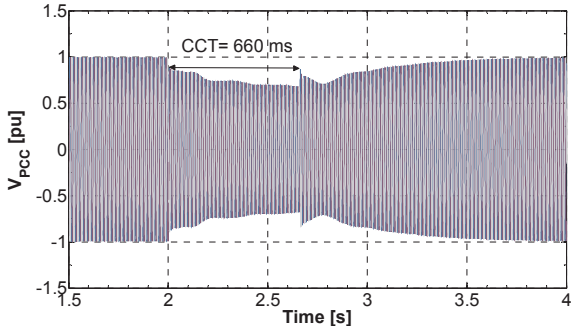


Figure 3.12: Voltage recovery with reactive injection with 40% CPLs and 40% IM

## CASE III

The model of the AC distribution system presented in Figure 3.10 is again considered. However, the amount of load controlled by CPLs is less than that of uncontrolled IM load. Total power consumed by the load is again 80% of the total generated power with each CPL consuming 10% (75 kW) and IM consuming 60% (450 kW). The fault occurs at time $t$=2s and, in the first case, CPLs are not controlled to inject reactive current during the fault.

Figure 3.13 shows the PCC voltage when the system is able to recover back to steady state value. The value of CCT is found to be 340 *ms*. This very low value of CCT justifies highly weak system with a very high value of overall inductance. Simulations are repeated for the same share of load with controlled CPLs being able to provide voltage support during the fault. The voltage recovery to the pre-fault value is shown in Figure 3.14. The CCT is found to be 480 *ms*, which is larger than the case without reactive injection of current. The reactive injection, therefore, helps to increase the transient stability margins of the distributed system.

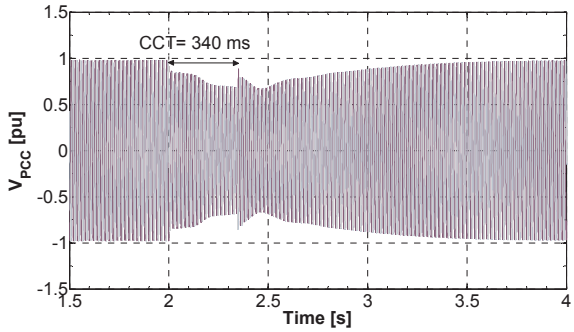


Figure 3.13: CCT without reactive injection by CPLs

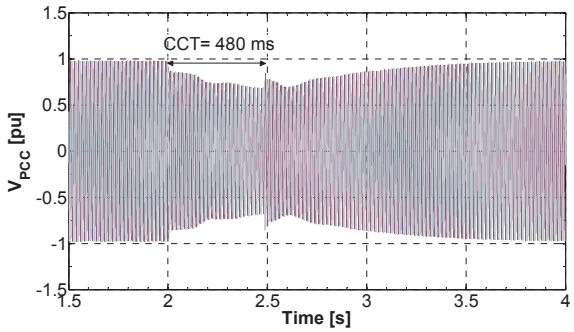


Figure 3.14: CCT with controlled CPLs and uncontrolled IM load

In order to see the stability margins of the system when generator terminal voltage is not symmetrical, the simulations are repeated for all the mentioned cases and 2% phase voltage unbalance rate (PVUR) is simulated at the SCIG terminal. A three phase line to ground fault has been simulated on the medium voltage side as before. The results for the 80% share of CPLs are presented in Figure 3.15 showing the voltage recovery after the fault and the value of CCT is 520 *ms*. This value is lower than the value of CCT obtained for the same share of CPLs under balanced generator terminal voltage.

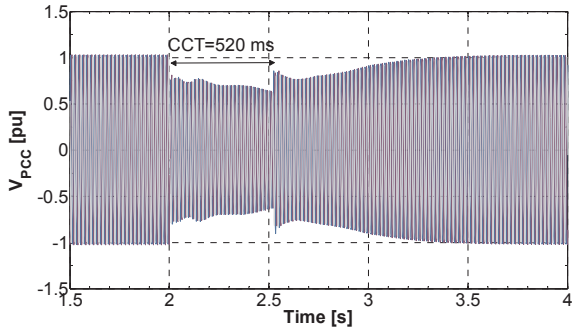


Figure 3.15: Voltage recovery for 80% CPLs for 2% PVUR

Results from all the simulations are summarized in Table 3.1 with and without reactive current injection under balanced and unbalanced SCIG terminal voltage.

Table 3.1: Summary of the simulation results for transient stability

| Type of Loading | Regulation | CCT | |
|---|---|---|---|
| | | Balanced SCIG | 2% PVUR |
| **Case 1:** 80% CPL | *P* constant only | 645 *ms* | 520 *ms* |
| 80% CPL | *P* constant and $i_q$ | 1.18 s | 855 *ms* |
| **Case 2:** 40% CPL, 40% | *P* constant only | 468 *ms* | 360 *ms* |
| 40% CPL, 40% IM | *P* constant and $i_q$ | 660 *ms* | 495 *ms* |
| **Case 3:** 20% CPL, 60% | *P* constant only | 340 *ms* | 275 *ms* |
| 20% CPL, 60% IM | *P* constant and $i_q$ | 480 *ms* | 295 *ms* |

Transient stability limits of the distributed system are different for different load conditions. The best case is found to be the one with all controlled CPLs injecting reactive current during the fault under balanced source voltage, while the worst case is identified with 60% IM load and 20% CPLs without reactive current support under 2% PVUR. When an induction machine has even a very low unbalanced voltage, its stator currents will be highly unbalanced, resulting in unequal heating in the stator winding and torque pulsations in the machine. Therefore, the margins to voltage stability are highly reduced. The system appears to be more stable if a higher amount of load is controlled by the use of CPLs. This is because of the extra functionality of reactive current control to support the system voltage. This extra functionality can, however, be achieved at the expense of an increment in the required current rating of the semiconductor devices in the AC/DC converter.

## 3.4 Incremental Current Rating of the CPL

In this section, a simulation study is performed to investigate the impact of reactive current injection on the total incremental current rating of the converter. To achieve ancillary reactive power for the grid, the CPL current rating has to be increased beyond the total active component of current required to fulfill constant load power. The distribution system model of Figure 3.6 has been considered with each CPL consuming 25% of the total power produced by the distributed resource. The fault resistance is varied to achieve different levels of the grid voltage drops. The higher the fault resistance the lower the voltage dip and vice versa. Several simulations are carried out for different values of voltage sags and CCT is calculated. Simulations are performed with and without the injection of reactive current by the CPLs.

Voltage collapse is illustrated in Figure 3.16 when the fault resistance is reduced to get the 40% voltage drop without injection of reactive current during the fault. It is obvious from the plot that the CCT of the system is very low and it is measured to be 0.12s. The further drop in voltage leads to even lower stability margins of the system and the CCT is further lowered.

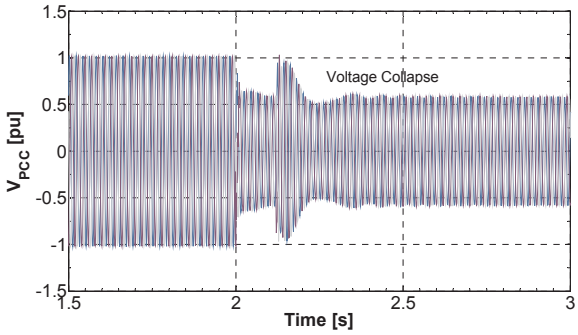


Figure 3.16: Voltage collapse at 40% voltage dip without reactive injection

Figure 3.17 shows simulation results for different converter current components for several levels of voltage dips. In this plot, $i_d$ represent the active current component, $i_q$ the reactive current component and $i_t$ the total current drawn by the CPL. When there is no additional injection of reactive current, the total current rating required by the CPL is represented by only the active component of current, i.e; $i_d^* = i_t^*$. The incremental current magnitude is represented by the difference between the total current with reactive injection $i_t$ and the total current without reactive injection $i_t^*$.

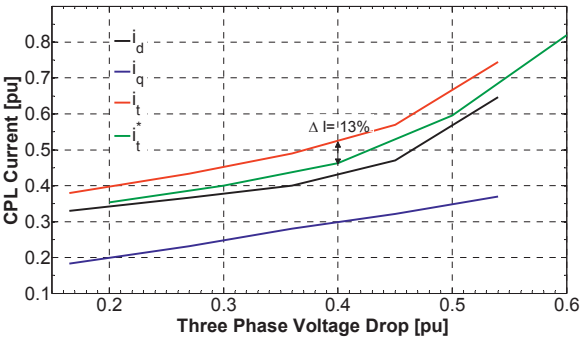


Figure 3.17: Incremental current rating of CPL as a function of voltage drop

The different current components of Figure 3.17 are defined by (3.1) and the relation between them is graphically illustrated in the vector diagram of Figure 3.18.

$$i_t = \sqrt{i_d^2 + i_q^2} \tag{3.1}$$

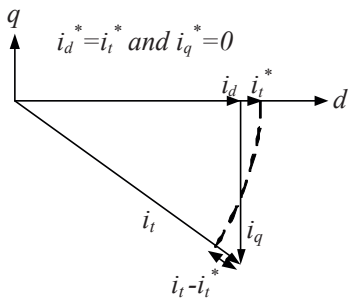


Figure 3.18: Relationship between different current components

It is observed that the CCT of the system is higher for lower values of the voltage drops and lower for the higher values of voltage drop. A different value of incremental current is found for each voltage drop level. During the fault, the voltage cannot be kept at the initial value and the converter injects the sufficient amount of reactive current to avoid the possible voltage collapse. It is obvious from the graph that for all levels of voltage drops the value of active component of current $i_d$ is lower than the value of $i_t^*$. This is because of the small increase in the converter terminal voltage in response to reactive injection. As illustrated in section 3.2 the active current component decreases due to reactive injection to keep the load power constant. From Figure 3.17, it can be observed that when the voltage drop is 40%, the value of $i_d$ is 0.438 pu and the amount of $i_t^*$ is 0.46 pu. Therefore, reactive injection results in 5% reduction in active current component $i_d$ due to voltage increment. However, as the total current $i_t$ represents the quadratic sum of active and reactive components as presented by (3.1). The net increment of 13% is required to avoid the voltage collapse for 40% voltage dip as indicated in Figure 3.17. The improvement in the voltage is prominent as the fault resistance is kept fixed for the cases of with and without reactive injection and the curve for $i_t^*$ in the graph always leads the curve for $i_t$. The results observed in Figure 3.17 indicate that the deeper the fault the higher the required $i_q$ to avoid the voltage collapse. However, this increase in reactive current is not in proportion with the decrease in the active component of the current. Therefore, the required extra current rating of the converter is higher when drop in the voltage is deeper.

## 3.5 Distributed CPLs vs Centralized STATCOM

A simulation investigation is done in order to know whether it is beneficial to implement distributed compensation by CPLs compared to a centralized STATCOM to achieve the same stability margins for the distribution system. The simulation model used for this purpose is shown in Figure 3.19. A comparison between the system with a STATCOM placed at the secondary of the transformer and two non-controlled CPLs is made with the case of two or three CPLs with reactive current control, without a centralized STATCOM. The STATCOM operates according to voltage source principle; however, it differs from the CPL because it does not draw any active power. The total power drawn by the loads in all the studied cases is kept to 50% of the total wind generator power.

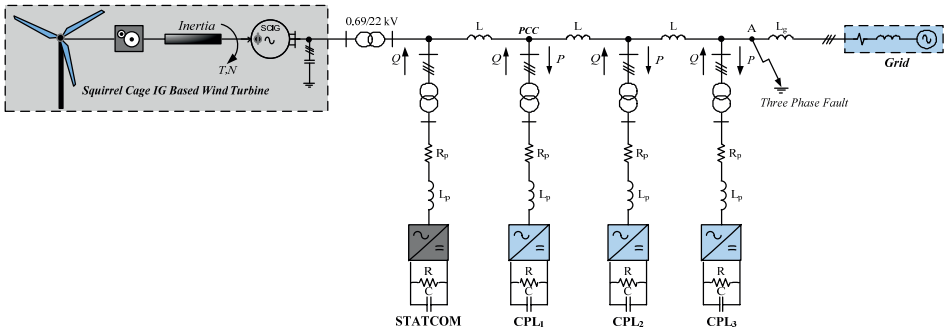


Figure 3.19: Distributed AC system under investigation with 3 CPLs and a STATCOM

Simulations are carried out for different values of fault durations and the fault resistance is varied to get different lengths of the fault before the voltage collapses. In other words, the fault durations represent the CCTs of the system. The higher the fault duration or CCT the higher the fault resistance and lower the fault severity. The amount of reactive current $i_q$ injected by the STATCOM and CPLs ensuring a stable system is measured for a specific fault duration or CCT. It has been observed that the smaller the value of the fault duration the higher the drop in the voltage to provoke an instability in the system and the other way around. The reason for the voltage collapse is the excessive consumption of reactive power by the wind generator from the grid during the fault and the loss of torque control due to rotor over speed.

Figure 3.20 illustrates the situation when only STATCOM is injecting for a fault duration or CCT of 0.4s. If the fault is not cleared beyond this time the voltage collapse will occur. To achieve a better CCT or longer fault duration for the system the fault must be less severe and the fault resistance must be higher. Unlike the previous section, where fault resistance is decreased to get a higher voltage dip, in this case, fault resistance is increased to get a higher CCT of the system.

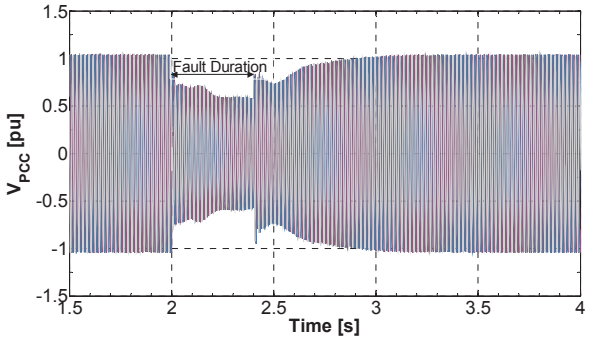


Figure 3.20: Voltage with CCT or fault duration of 0.4s with only STATCOM injecting

The amount of reactive current component $i_q$ that these devices inject for supporting the voltage during the fault is plotted in Figure 3.21. The amount of reactive current

injected by the CPLs is slightly different from each other because of their distances from the fault location. The CPL located closest to the fault experiences slightly higher value of voltage drop at its terminal and, therefore, the injected reactive current is also slightly higher. On the other hand, CPL located far from the fault section is faced with relatively lower value of voltage drop at its terminal and injects slightly less current.

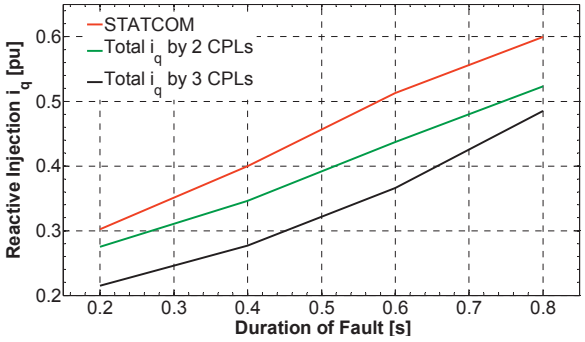


Figure 3.21: Comparison of total reactive current $i_q$ injected by centralized STATCOM and distributed CPLs for different fault durations

The total injected reactive current by the centralized STATCOM is higher for all the fault durations compared to the sum of reactive current injected by the CPLs. Similarly, the sum of reactive current injected by the two CPLs is higher than the sum of reactive current injected by the three CPLs to avoid a voltage collapse for all the considered fault durations. The total amount of reactive current injected by one CPL belonging to a group of three distributed CPLs is roughly four times lower than the total amount of reactive current injected by the centralized STATCOM for all the simulated cases. Similarly, the sum of reactive current injected by one CPL belonging to a group of two CPLs is nearly less than half compared to the total centralized compensation by a STATCOM. If the STATCOM is placed further towards the location of grid fault. It will inject slightly more current to neutralize the fault severity. In general, it can be concluded that the distributed compensation provided by CPLs is always more advantageous than centralized compensation. The lower reactive current requirement, however, comes at the expense of an increased cost of the installed semiconductor switches.

## 3.6 Optimal Current for a CPL

As we have observed in the previous section, for the cases with reactive current support by the CPL, it can be seen from the combination of (2.16) and (3.1) that according to the value of the grid inductance, active current decreases with increased reactive injection because of the voltage improvement. Therefore, an operating point can be achieved where the total converter current will be at its lowest value. A further reactive injection will, however, result in a large increase in total current. This section presents an

analytical investigation to find out the amount of reactive current $i_q$ corresponding to minimum total current $i_t$ for a CPL. The results are then verified by the simulations.

A simplified distribution feeder of Figure 3.22 is considered with one CPL. The total power demand is being supplied by the wind generator and the extra amount of power is delivered to the grid. The length of the distribution branch is considered to be 200 meters. The length of the transmission line is taken to be 50 km.

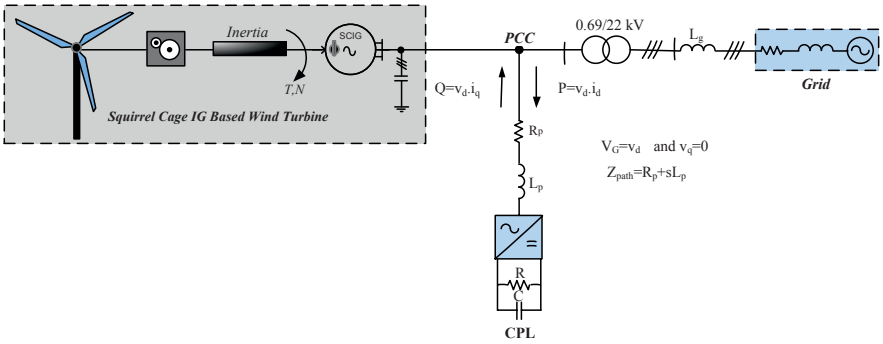


Figure 3.22: Simplified distribution feeder for CPL current optimization

Let $V_G$ be the generation voltage and let's assume that the phase of $V_G$ is 0 (there is no loss of generality since this choice corresponds to arbitrarily choosing a time reference for the analysis). In accordance with the implemented control strategy $V_G = v_d$. Let $P - jQ$ be the active and reactive power supplied to the CPL. We can therefore write:

$$i_t = \frac{P - jQ}{v_d} + o\left(\frac{1}{|v_d|^2}\right) \tag{3.2}$$

where the $o$-notation means that, if f(x) = $o$ (g(x)), then the function $f(x)$ goes to zero faster than $g(x)$, when $x$ goes to 0, i.e;

$$\lim_{x \to 0} \frac{f(x)}{g(x)} = 0 \tag{3.3}$$

This approximation is justified for those networks only where voltage differences across different points are small compared to the nominal voltage $v_d$.

The load voltage $V_{CPL}$ can, therefore, be expressed as:

$$V_{CPL} = v_d - Z_{path} i_t = v_d - Z_{path}\left(\frac{P - jQ}{v_d} + o\left(\frac{1}{|v_d|^2}\right)\right) \tag{3.4}$$

where $Z_{path}$ is the impedance of the path from the source to the load.

Now we write $i_t$ as a function of the reactive power supplied to the load. Therefore, $i_t(0)$ is the supplied current when only active power is demanded and no reactive power is supplied or consumed by the CPL. We have the exact expression:

$$i_t(Q) = \frac{P - jQ}{V_{CPL}^*} \tag{3.5}$$

Using (3.4) in (3.5), we have:

$$\begin{aligned} i_t(Q) &= \frac{P - jQ}{v_d - Z_{path}^* \left( \frac{P + jQ}{v_d} + o\left( \frac{1}{|v_d|^2} \right) \right)} \\ &= \frac{P - jQ}{v_d - Z_{path}^* \left( \frac{P + jQ}{v_d} \right)} \end{aligned} \tag{3.6}$$

Let's express $Z_{path}$ as $ze^{j\theta} = z(\cos\theta + j\sin\theta)$. We can then compute the squared absolute value of $i_t$(Q):

$$\begin{aligned} |i_t(Q)|^2 &= \frac{P^2+Q^2}{\left( v_d - Z_{path}^* \frac{P + jQ}{v_d} \right)\left( v_d - Z_{path} \frac{P - jQ}{v_d} \right)} \\ |i_t(Q)|^2 &= \frac{P^2+Q^2}{v_d^2 - 2z(P\cos\theta + Q\sin\theta) + \frac{z^2}{v_d^2}(P^2+Q^2)} \end{aligned} \tag{3.7}$$

We have a minimum of the absolute value of the current $i_t$(Q) in the zeros of its derivative. However, finding the zeros of (3.7) is not easy. One possible solution could consist in neglecting irrelevant terms of (3.7). The irrelevant terms depend on the values of the parameters $v_d$,$P$,$z$ and $\theta$. However, in most realistic cases, the terms $2zP\cos\theta$ and $z^2/v_d^2 \cdot (P^2+Q^2)$ should be much smaller compared to the others, and we could, therefore, approximate $|i_t(Q)|^2$ with the simpler expression:

$$|i_t(Q)|^2 \approx \frac{P^2+Q^2}{v_d^2 - 2zQ\sin\theta} \tag{3.8}$$

The derivative of (3.8) becomes:

$$\frac{d|i_t(Q)|^2}{dQ} = 2z\sin\theta(P^2 - Q^2) + 2v_d^2 Q \tag{3.9}$$

This is a second order equation that can be easily solved, obtaining the optimal reactive power injected by CPL:

$$Q_{opt} = \frac{v_d^2 - \sqrt{v_d^4 - 4z^2(\sin\theta)^2 P^2}}{2z\sin\theta} \tag{3.10}$$

The reactive component of the converter current $i_q$ is represented by:

$$i_q = \frac{Q}{v_d} \tag{3.11}$$

During a steady state operation we can, therefore, say that $i_q$=$Q_{opt}$. However, a perfect steady state condition is not possible under reactive injection because reactive compensation results in a small increase in the terminal voltage and the value of $v_d$ will be slightly more than 1.0 pu. Equations (3.10) and (3.11) do not take into account this small increase in $v_d$. In a real online system, the control system of the converter will always keep on modifying the value of $v_d$ in response to reactive injection $i_q$. The value of reactive current found through simulations, therefore, will differ by a small amount from the value of $i_q$ that we get using (3.11). This can be observed by conducting a comprehensive simulation study. For a CPL consuming 500kW, using (3.10), the optimal reactive power that is dispatched by the CPL to have minimum total branch current is 0.102 pu or 75 kVar. The amount of optimal reactive injection by CPL for 750 kW consumption is calculated to be 0.21 pu.

The variations of grid parameters also play important role and the optimal operating point for the CPL can vary significantly. If the grid impedance is doubled for load power of 500 kW, then for the steady state case the value of $Q_{\text{opt}}$ obtained from (3.10) is 0.205 pu. However, for 10% drop in grid side voltage the obtained result for $Q_{\text{opt}}$ is 0.278 pu and the value of optimal reactive current using (3.11) is 0.309 pu.

### 3.6.1 Simulation Results

The model of distribution feeder shown in Figure 3.22 is used for the simulation analysis. The CPL is consuming 500 kW from wind generator. The amount of active component of current is related to the power consumed by the load as indicated by (2.16). To find out the amount of reactive current corresponding to minimum attainable total current, different amounts of reactive current are injected into the network and the decreasing values of active currents are measured. The results are summarized in Table 3.2 and plotted in Figure 3.23. The plot confirms that injection of reactive current $i_q$ decreases the amount of total current $i_t$ and when the amount of reactive current is 0.1 pu, the value of total current is minimum. The total current starts increasing from here onwards and reaches to its initial value when the reactive current is nearly 0.18 pu and then it increases rapidly with the further increase in reactive injection.

Table 3.2: Summary of simulation results, $P_{CPL}$= 500 kW

| $i_d$ [pu] | $i_q$ [pu] | $i_t$ [pu] |
|---|---|---|
| 0.667 | 0 | 0.667 |
| 0.66 | 0.05 | 0.661 |
| 0.652 | 0.1 | 0.657 |
| 0.647 | 0.15 | 0.662 |
| 0.642 | 0.2 | 0.672 |
| 0.638 | 0.25 | 0.685 |
| 0,632 | 0.3 | 0.699 |
| 0.627 | 0.35 | 0.718 |
| 0,621 | 0.4 | 0.74 |
| 0.617 | 0.45 | 0.763 |
| 0.613 | 0.5 | 0.791 |

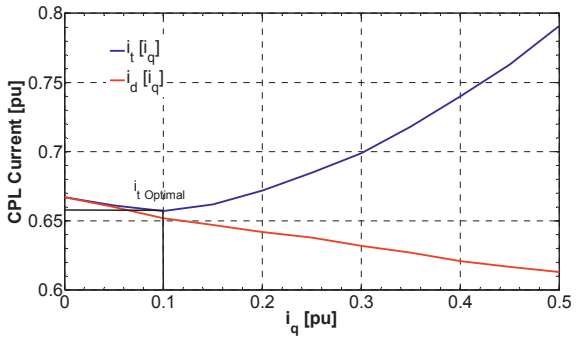


Figure 3.23: Optimal total current for a CPL consuming 500 kW

The active component of current $i_d$ always decreases with the increase in reactive current. As the simulations take into account the changes in system voltage $v_d$, therefore, we get about 2% smaller value of the optimal total CPL current.

Simulations are repeated for the case when CPL is consuming 750 kW and the results are presented in Table 3.3 and plotted in Figure 3.24. In this case, 0.2 pu reactive current is needed to be injected to get the minimum attainable total current in the distribution branch. The error is 5% compared to the result obtained using (3.11) because more reactive compensation resulted in more increase in voltage. It is obvious from the plots that the amount of reactive current that must be injected to get the optimal amount of total current increases with the increase in load active power requirements.

Table 3.3: Summary of simulation results, $P_{CPL}$= 750 kW

| $i_d$ [pu] | $i_q$ [pu] | $i_t$ [pu] |
|---|---|---|
| 1 | 0 | 1 |
| 0.994 | 0.05 | 0.995 |
| 0.986 | 0.1 | 0.991 |
| 0.977 | 0.15 | 0.988 |
| 0.966 | 0.2 | 0.986 |
| 0.957 | 0.25 | 0.989 |
| 0.95 | 0.3 | 0.996 |
| 0.943 | 0.35 | 1.005 |
| 0.935 | 0.4 | 1.017 |
| 0.929 | 0.45 | 1.032 |
| 0.922 | 0.5 | 1.05 |

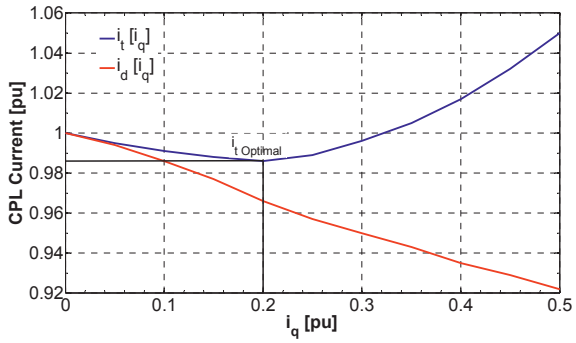


Figure 3.24: Optimal total current for a CPL consuming 750 kW

Figure 3.25 shows the simulation results for the two cases with double grid impedance while CPL is consuming 500 kW. In this case, the operating point has moved further to the right and the injected reactive current is now 0.2 pu for steady state to get the optimal total current. The higher inductance of the system resulted in comparatively larger changes in the system voltage and the error obtained from calculations using (3.11) is more. For the low voltage condition, the value of reactive current found from the simulations is 0.3 pu. For this case, the value of total current in the distribution line at the start is higher compared to the steady state condition. This is because of the increased active component of the current to maintain a constant load power.

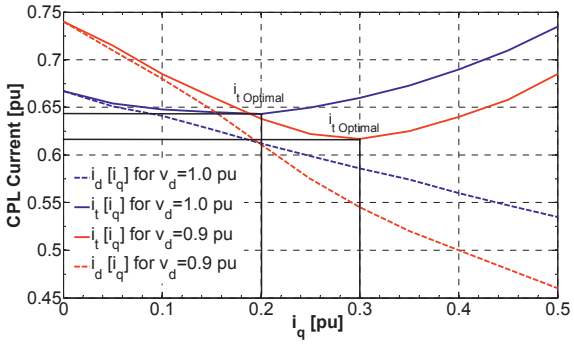


Figure 3.25: Optimal total current for a CPL consuming 500 kW with modified grid parameters

Optimization of total current for a CPL will play an important role with regards to the future development of loss minimization algorithms for residential and industrial microgrids. There has been some studies conducted using grid-connected converters of DERs for loss minimization. However, no such effort has been made using the regulated PE load interfaces. This work will provide a foundation to develop optimization algorithms as ancillary services using controlled loads.

## 3.7 Distribution Loss Minimization

Energy losses in power system take place as power flows through the network to meet the customer load demands. Some of the input energy is dissipated in the conductors and transformers along the delivery route. These losses are inherent in the processing and delivery of power but can be minimized [90, 91]. Losses represent a considerable operating cost, estimated to add 6 to 10 percent to the cost of electricity and some 25 percent to the cost of delivery.

Distribution loss minimization has been an area of extensive research for last few years. Most of the recent literature available on this topic mainly concentrates on the utilization of the PE generation interfaces only. In the following sections, a methodology is introduced to provide lower distribution losses and local voltage support based on the reactive current injection by both the generation and load PE interfaces.

### 3.7.1 Loss Minimization Methodology

The impact of reactive current $i_q$ on the total branch current in a distribution system is investigated analytically and through simulations in the last section. Based on the analysis for the optimal reactive injection under different load powers, a methodology is proposed for loss minimization in AC distribution system. Figure 3.26 shows the distribution system used for this analysis. The distribution system is comprised of two DERs with PE interfaces called controllable power sources (CPS). The transmission and distribution lines, medium voltage grid and CPL parameters are kept the same as

presented in appendix A. The distance between the connection point of the distribution system and $DER_1$ is taken to be 50 meters and the distance between the $DER_1$ and $DER_2$ is also considered as 50 meters. The length of the distribution line between each load is taken as 25 meters. The length of the distribution branches is 200 meters. The length of the high voltage transmission line is considered as 50 km.

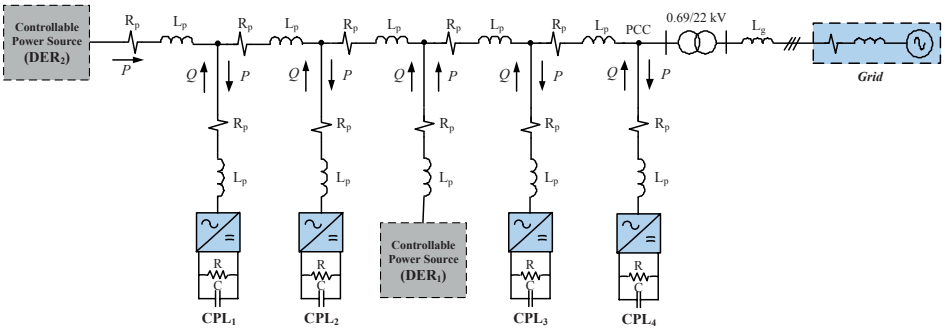


Figure 3.26: Distribution system dominated by power electronic interfaces

It is supposed that the intervention of both the DERs will reduce the overall distribution losses as they are located very close to the point of utilization. A major part of the overall losses is composed of the losses in the long transmission line. The lower the power supplied from the grid to the local loads the lower will be the losses.

In the system under consideration, the loss calculation is performed by measuring the input and output powers for the complete system and for each distribution line. The input power is the sum of the powers generated by the grid and the DERs in response to a particular load demand. The load powers are measured at the point of connection to find out the total distribution losses for a specified load demand. The powers by the DERs are measured to have an idea of how the CPS reacts to a particular load demand.

The methodology involves the following three steps:

- Intervention of DERs or controllable power sources located very close to the load centre for load sharing.
- Cancellation of grid side reactive power by using the controllable power source located closer to the point of connection.
- Injection of reactive current $i_q$ by the loads corresponding to the minimum total current $i_t$ for a CPL.

### 3.7.2 Application of the Methodology

In order to implement the methodology, simulations are carried out for the load condition when each CPL is consuming 750 kW of active power from the power system. The total power demand by the distribution loads is 3000 kW. At the start, simulations are run for one second without connecting the loads because of the

simulation software limitations. The simulation software PSCAD/EMTDC is time sensitive for a step change in load power and it is difficult to get the rated voltage when connecting the loads at the very start of the simulation. The loads are, therefore, connected to the system at time $t$=1s. Initially, only the grid is making sure to fulfill all the load power demand. At time $t$=2s, $DER_1$ is turned on and starts contributing to the local load demand. At time $t$=3s, $DER_2$ is turned on and result is further decrease in the power supplied from the grid. At time $t$=4s, $DER_1$ injects reactive power to cancel out the reactive power supplied by the grid. At time $t$=5s, each CPL injects reactive current corresponding to the total minimum current obtained in the previous section for load power of 750 kW.

When the loads are connected at time $t$=1s, all the power is being supplied by the grid. The amount of active power supplied by the grid is 3360 kW and the total local load demand is 3000 kW. The grid is generating 940 kVar reactive power. At this point the total losses in the system are 360 kW. The power input to each distribution line is 790 kW. The process is illustrated by the following plots.

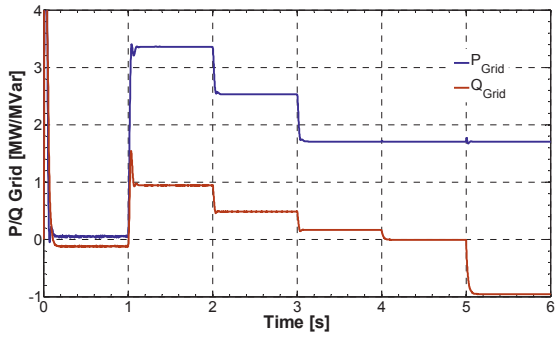


Figure 3.27: Powers supplied from the grid

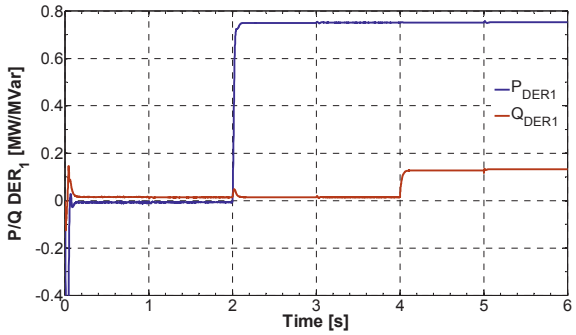


Figure 3.28: : Active and reactive powers supplied from $DER_1$

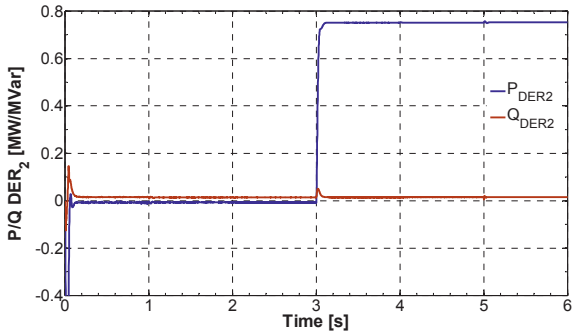


Figure 3.29: Active and reactive powers supplied from $DER_2$

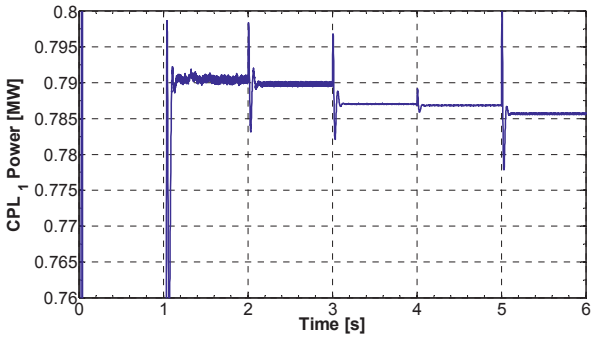


Figure 3.30: Active power input for $CPL_1$

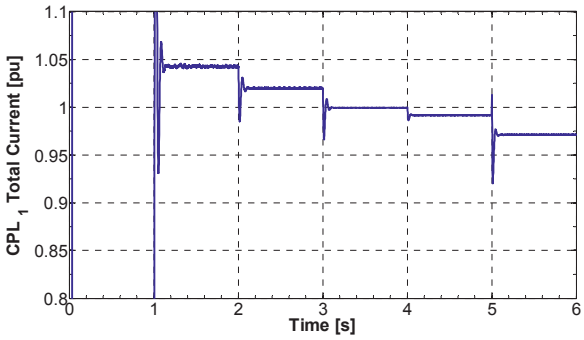


Figure 3.31: Total branch current for $CPL_1$

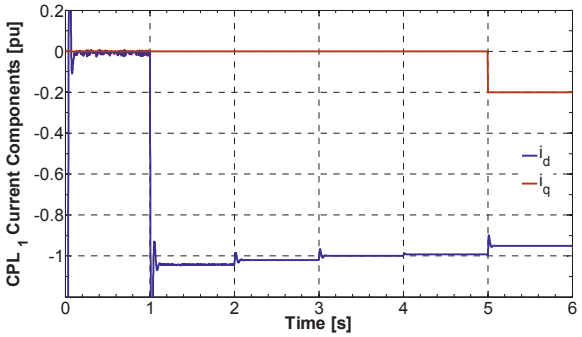


Figure 3.32: Active and reactive current components of $CPL_1$

### 3.7.3 DER Intervention

At time *t*=2s, the $DER_1$ is turned on and it starts supplying 750 kW of power to the loads as shown in Figure 3.28. The power supplied from the grid reduces to 2529 kW. The introduction of $DER_1$ unit also results in the reduction of reactive power from the grid and decreases it to almost half of the initial value. The total supplied power at this point is 3279 kW in demand to 3000 kW. Therefore, introduction of $DER_1$ unit reduces the losses to 279 kW.

At time *t*=3s, the $DER_2$ is turned on to share the load demand (Figure 3.29). The DER units are now supplying 750 kW each. The power supplied from the grid comes down to 1705 kW. The losses are reduced from the initial value of 360 kW to 205 kW. The intervention of $DER_2$ unit also reduces the reactive power supplied from the grid to a value of 163 kVar.

### 3.7.4 Grid Reactive Power Cancellation

At time *t*=4s, $DER_1$ unit is enabled to inject the reactive current to cancel out the remaining reactive power from the grid. The reactive power from the grid comes down to zero value. At this stage the power calculations are as follows:

$P_{total} = P_{DER1} + P_{DER2} + P_{Grid}$ = 1700 +750+750 = 3200 kW

In this step the total losses in the system are reduced to 200 kW.

### 3.7.5 Reactive Injection by CPLs

At time *t*=5s, each CPL injects 0.2 pu reactive current corresponding to total minimum attainable current for a load power of 750 kW. As a result of reactive injection, the line losses in each distribution line are reduced by 2.5 kW in this step as shown in the Figure 3.30. Same results are found for the other three loads. It can also be observed that the power input to the distribution line is decreased from 790 kW to 785 kW after implementation of this three step methodology.

Figure 3.31 shows the total current for $CPL_1$. It is obvious that the total current decreases with the implementation of each step in the methodology. In the last step at time $t$=5s, the decrease in current is nearly 3% in response to reactive current injection. This continuous decrease in current suggests the decrease in the distribution line losses. The losses in the distribution line cannot be further reduced as this is the minimum achievable value of the total current for the distribution line. The reactive injection for minimum current may also improve the terminal voltage that is otherwise unachievable.

At this last stage, the grid is supplying 1680 kW and the power delivered by each DER unit is 750 kW. The total power delivered from the system is 3180 kW .Therefore, the losses are reduced to 180 kW. The total reduction in the losses is 180 kW which is 50% of the initial value. The Figure 3.30 shows that the total losses in the four distribution lines are still 140 kW and the losses in the rest of the system are 40 kW. The total losses in the system are now only 6% of the total power demand.

The time behaviour of the distribution losses is shown in Figure 3.33. The intervention of DER units and reactive injection reduces the losses to 50% of initial value. This methodology incorporates the efficient utilization of the DERs interfaced to the grid through PE interfaces, voltage support at the load terminals, and lower distribution losses as a result of the decrease in total branch current.

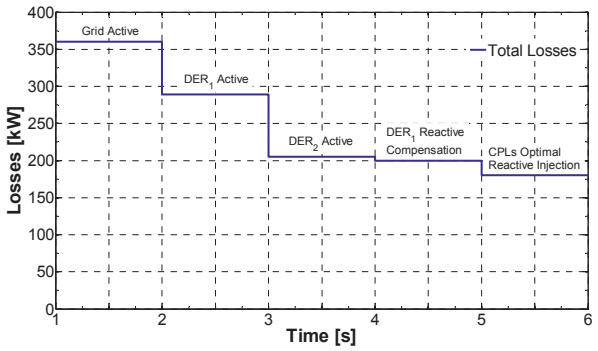


Figure 3.33: Time behaviour of distribution system total losses

## 3.8 Summary

This chapter first discribes the basic AC distribution sytem used for the simulation study. It then presents the effects of injection of reactive current by the CPL on the terminal voltage. It has been observed that the higher the amount of reactive injection the higher the increase in voltage. An investigation has been done to highlight the benefits of introducing the extra functionality of reactive current injection by the CPLs in the events of voltage dips to support voltage stability. The transient stability limit has been investigated for different combinations of CPLs and IM loads. The CCT is chosen as a performance index to compare the investigated cases. The simualtion results indicate that

the larger the number of CPLs that controls the reactive current, the higher the stability margin.

The incremental current rating of the semiconductor switches of the AC/DC converters in the case of reactive current injection is studied and it is noticed that the deeper the voltage drop, the higher the current rating required for the converter to maintain the transient stability. SCIG consumes more reactive power from the utility when the grid fault is severe and therefore more reactive injection is required by the controlled CPLs to avoid a possible disconnection of the system.

The required reactive current rating of converters when all CPLs in the system inject reactive current is compared with the required rating of a centralized STATCOM. The comparison proves advantages to the distributed reactive current compensation by the converter driving each CPL rather than one centralized STATCOM. This has been stated in some prevoius studies where distributed reactive power injection proved beneficial than centralized reactive power compensation by capacitors or SVCs. This work, however, changes the compensation format to reactive current $i_q$ instead of reactive power. This is possible only with controlled PE converters.

An analytical investigation to find the minimum total branch current is also presented for a basic AC distribution feeder with one CPL connected between wind generator and grid. It is observed that the amount of reactive injection increases with the increase in load power, grid impedance and voltage drop to get an optimal CPL current. A simulation analysis is perfomed to see the effects of the simplifications introduced during calculations. The results obtained from the simulations are very close to the results achieved from analytical study.

A methodology is developed for the reduction in losses, based on the use of local DERs and distributed reactive injection by the CPLs. The methodology is based on the three steps. The intervention of the CPS to fulfill the load power demands, the reactive power cancellation on the grid side and the optimal reactive injection by the distributed CPLs. The simulation results for a total load power of 3MW, with each CPL consuming 750 kW, indicate that a reduction of 50% in overall losses in the distribution system is achieved. The methodology, therefore, provides the maximum exploitation of the available PE generation and load interfaces, local voltage support at the load terminals, and lower distribution losses.

# 4 Asymmetrical Grid Fault Mitigation by CPLs

*This chapter introduces the use of CPLs for asymmetrical grid fault ride through enhancement. The CPL control structure is discussed in detail for compensating the positive and negative sequence voltages in a distribution system. A microgrid structure comprising of several CPLs has been considered and CPLs current rating under fault ride through has been evaluated. A comparison is presented between the current ratings of distributed CPLs and a centralized STATCOM to achieve the extra service of asymmetrical grid fault mitigation.*

Although fixed speed SCIG provides a cost effective solution for wind turbines, it also consumes reactive power from the grid. During a grid voltage sag it consumes large amounts of reactive power as its speed deviates from the synchronous speed, resulting in a voltage collapse and further fault propagation within the electrical network. Therefore, enhancement of SCIG fault ride through (FRT) capability is indispensible in order to improve the overall stability and reliability of the power system [92, 93]. Most of the work about FRT enhancement of the fixed speed SCIG based wind turbine is related to balanced grid voltage sags. However, in general more than 90% of the grid faults result in unbalanced voltage sags with both positive and negative sequence components [93]. Unbalanced voltage problems generate heating in the machine windings and toque oscillations, leading to mechanical vibrations and noise.

Grid code requirement demands the FRT enhancement and reactive current injection in wind power systems during a fault. Some grid codes also require real power support during the fault [94-97]. In UK, FRT capability requirements demand that terminal voltage of the wind farm should not be less than 15% of the nominal voltage during the fault and it must be restored to 90% within 0.5s. Grid codes in Denmark set the minimum voltage level during the fault to 25% of the nominal voltage and it should be restored to 75% within 0.75s [98-100]. In the absence of a PE interface between the SCIG and the utility grid, the adjustable reactive power control cannot be performed and a dedicated device is required to fulfill the grid code requirements.

Different methods have been investigated to fulfill the grid code requirements and enhance the FRT capability of a wind farm. These include the use of DFIG wind farm and a centralized STATCOM [101-106].It has been observed that DFIG experiences

inherent difficulties to ride through grid faults due to the high voltage induced in the rotor circuit. Many practical strategies of STATCOM reactive power control under asymmetrical grid faults and load unbalances have been discussed in [93, 103] and proved to be very effective. However, the installation of a dedicated switching compensator or a STATCOM is not very cost effective. The rapidly changing modern power infrastructure can utilize some of its installed resources for the services that were earlier provided by the dedicated devices.

This chapter proposes the application of tightly regulated PE load interfaces or CPLs, connected to SCIG based wind farm, for FRT enhancement under unbalanced grid faults. The main contribution of this work is based on the fact that a dedicated device (STATCOM or DFIG) is not needed for FRT enhancement and industrial motor drives or other CPLs available in the vicinity of the SCIG based wind farm can be utilized to provide this extra service. In addition to the typical positive sequence reactive current injection, the proposed method suggests a negative sequence reactive current compensation during the FRT operation to mitigate the unbalanced grid voltages. By taking into account both the positive and the negative sequence reactive currents, the proposed method can inject the real power and the reactive current demanded by grid codes and alleviate the grid voltage imbalance without exceeding the peak current limit of the PE load interface.

## 4.1 Proposed Control Scheme

The CPL control scheme for asymmetrical fault mitigation slightly differs from the basic control structure presented in chapter 2. An independent control of positive and negative sequence voltages demands the precise sequence extraction to be incorporated into the control structure. To achieve the FRT enhancement, the CPL control algorithm injects the negative sequence active current and both the positive and the negative sequence reactive current. Four PI regulators have been added in the outer voltage control in this case. Positive sequence reactive current $i_q^+$ compensates the positive sequence active voltage drop $v_d^+$ while the negative sequence reactive current $i_q^-$ compensates for the negative sequence active voltage drop $v_d$. Negative sequence active current $i_d^-$ is injected by CPL to compensate the negative sequence reactive voltage drop $v_q^-$. CPL also absorbs the positive sequence active current $i_d^+$ to meet the load power requirements and maintain the DC link voltage. The basic control structure is presented in Figure 4.1.

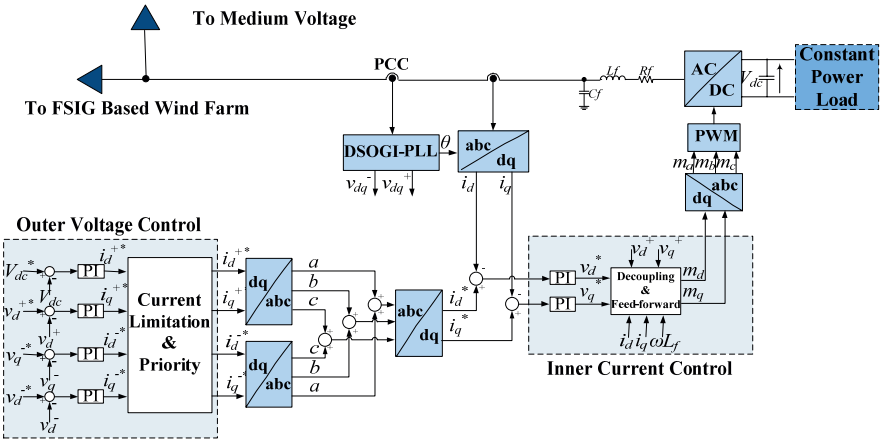


Figure 4.1: CPL control structure with independent control of positive and negative sequence voltages at PCC

A phase lock loop (PLL) based on dual second order generalized integrator (DSOGI) has been employed for this purpose [107-110]. Using the DSOGI-PLL sequence separation scheme, the positive and negative sequence of the voltage appear as DC values in SRF and can be easily controlled by using PI controller. The current limitation and priority block presented in Figure 4.1 adjusts the level of positive and negative sequence active and reactive currents so that a predefined ampere constraint (1.0 pu) of the CPL is not exceeded; thus, the risk of overcurrent tripping of the CPL can be greatly reduced. The priority has been given to the positive sequence reactive current $i_q^+$ to compensate the positive sequence voltage, thereby making sure the maximum FRT and stability enhancement of the SCIG based wind farm. The remaining current capacity of the CPL will be used to compensate the negative sequence voltage in order to reduce the torque pulsations during the unbalanced grid fault. The negative sequence voltage is the quadratic sum of negative sequence active and reactive voltage components. The total negative sequence current injection will therefore be the quadratic sum of negative sequence active and reactive current components.

### 4.1.1 Positive and Negative Sequence Calculation in SRF

DSOGI-PLL sequence separation technique translates the three phase voltage from the *abc* to stationary *αβ* reference frames. A dual SOGI-based quadrature signals generator (QSG) is employed for filtering and obtaining the 90° shifted versions from the *αβ* voltages. The SOGI-QSG scheme is presented by Figure 4.2 and its characteristic transfer functions are given by:

$$D(s) = \frac{v'}{v}(s) = \frac{k\omega' s}{s^2 + k\omega' s + \omega'^2} \tag{4.1}$$

$$D(s) = \frac{qv'}{v}(s) = \frac{k\omega'^2}{s^2 + k\omega' s + \omega'^2} \tag{4.2}$$

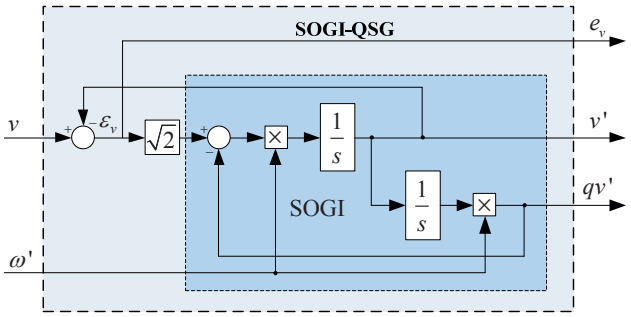


Figure 4.2: SOGI-QSG scheme

These signals act as inputs to the positive and negative sequence calculator (PNSC). The positive and negative sequence $\alpha\beta$ voltages are then translated to the rotating SRF and a PLL (SRF-PLL) is employed to make the system frequency adaptive [108].

The instantaneous positive and negative sequence components, $\mathrm{v}^{+}_{abc}$ and $\mathrm{v}^{-}_{abc}$ of a generic voltage vector $\mathrm{v}_{abc}=[\ v_a \quad v_b \quad v_c\ ]^{\mathrm{T}}$ are written as:

$$\begin{aligned} \mathrm{v}^{+}_{abc} &= \begin{bmatrix} v^{+}_a & v^{+}_b & v^{+}_c \end{bmatrix}^T = \begin{bmatrix} T_+ \end{bmatrix} \mathrm{v}_{abc} \\ \mathrm{v}^{-}_{abc} &= \begin{bmatrix} v^{-}_a & v^{-}_b & v^{-}_c \end{bmatrix}^T = \begin{bmatrix} T_- \end{bmatrix} \mathrm{v}_{abc} \end{aligned} \tag{4.3}$$

where $[T_+]$ and $[T_-]$ are represented as:

$$\begin{bmatrix} T_+ \end{bmatrix} = \frac{1}{3}\begin{bmatrix} 1 & a & a^2 \\ a^2 & 1 & a \\ a & a^2 & 1 \end{bmatrix} and \begin{bmatrix} T_- \end{bmatrix} = \frac{1}{3}\begin{bmatrix} 1 & a^2 & a \\ a & 1 & a^2 \\ a^2 & a & 1 \end{bmatrix} \tag{4.4}$$

where $a=e^{j2\,\pi/3}$. Clarke transformation allows voltage vector translation from the *abc* to the $\alpha\beta$ reference frames such that:

$$\mathrm{v}_{\alpha\beta} = \begin{bmatrix} T_{\alpha\beta} \end{bmatrix} \mathrm{v}_{abc} = \sqrt{\frac{2}{3}} \begin{bmatrix} 1 & -\frac{1}{2} & -\frac{1}{2} \\ 0 & \frac{\sqrt{3}}{2} & -\frac{\sqrt{3}}{2} \end{bmatrix} \mathrm{v}_{abc} \tag{4.5}$$

Therefore, the instantaneous positive and negative sequence voltage components in stationary $\alpha\beta$ reference frame are represented by:

$$\begin{aligned} \mathrm{v}^{+}_{\alpha\beta} &= \begin{bmatrix} T_{\alpha\beta} \end{bmatrix} \mathrm{v}^{+}_{abc} = \begin{bmatrix} T_{\alpha\beta} \end{bmatrix} \begin{bmatrix} T_+ \end{bmatrix} \mathrm{v}_{abc} \\ &= \begin{bmatrix} T_{\alpha\beta} \end{bmatrix} \begin{bmatrix} T_+ \end{bmatrix} \begin{bmatrix} T_{\alpha\beta} \end{bmatrix}^{-1} \mathrm{v}_{\alpha\beta} = \frac{1}{2}\begin{bmatrix} 1 & -q \\ q & 1 \end{bmatrix} \mathrm{v}_{\alpha\beta} \end{aligned} \tag{4.6}$$

$$\begin{aligned} \mathrm{v}^{-}_{\alpha\beta} &= \left[T_{\alpha\beta}\right]\mathrm{v}^{-}_{abc} = \left[T_{\alpha\beta}\right]\left[T_{-}\right]\mathrm{v}_{abc} \\ &= \left[T_{\alpha\beta}\right]\left[T_{-}\right]\left[T_{\alpha\beta}\right]^{-1}\mathrm{v}_{\alpha\beta} = \frac{1}{2}\begin{bmatrix} 1 & q \\ -q & 1 \end{bmatrix}\mathrm{v}_{\alpha\beta} \end{aligned} \tag{4.7}$$

where $q=e^{-j\,\pi/2}$ is a phase shift time domain operator to obtain in-quadrature version of an original waveform. Finally, the stationary positive and negative sequence voltage components are transformed to synchronously rotating voltage components, such that:

$$\begin{aligned} \mathrm{v}^{+}_{dq} &= \left[T_{dq}{}^{+}\right]\mathrm{v}^{+}_{\alpha\beta} = \begin{bmatrix} \cos\theta & \sin\theta \\ -\sin\theta & \cos\theta \end{bmatrix}\mathrm{v}^{+}_{\alpha\beta} \\ \mathrm{v}^{-}_{dq} &= \left[T_{dq}{}^{-}\right]\mathrm{v}^{-}_{\alpha\beta} = \begin{bmatrix} \cos\theta & -\sin\theta \\ \sin\theta & \cos\theta \end{bmatrix}\mathrm{v}^{-}_{\alpha\beta} \end{aligned} \tag{4.8}$$

Figure 4.3 represents the QSG and PNSC used for the extraction of positive and negative sequence voltage in SRF.

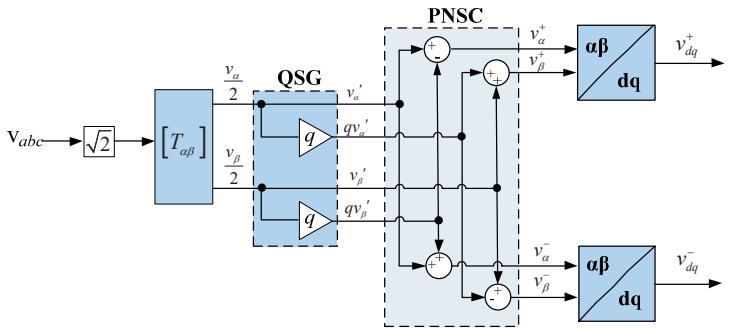


Figure 4.3: Positive and negative sequence calculation in SRF

## 4.2 Operation of SCIG under Asymmetrical Grid Voltage Sag

Apart from many advantages such as low price, robust design, overload handling and little maintenance, the biggest disadvantage of fixed speed SCIG is the uncontrollable reactive power consumption. The compensation for the reactive power consumption needs shunt capacitor banks at no-load [111, 112]. SCIG easily becomes unstable under low voltage conditions as low terminal voltage increases the rotor slip and consumption of reactive power, thereby, further lowering the voltage which leads to disconnection of the turbine.

The torque $T^{+}$ of the induction generator has a quadratic dependence on the positive sequence stator voltage magnitude [112], and can be represented by:

$$T^{+}(s) = 3.\frac{p}{2}.\frac{R_r}{s\omega_s}.\frac{V_s^{+2}}{(R_s + R_r/s)^2 + j(X_s + X_r)^2} \tag{4.9}$$

where $R_s$, $R_r$, $X_s$ and $X_r$ are the stator and rotor resistance and impedance parameters of the SCIG equivalent circuit, $p$ is the number of pole pairs, $s$ is the slip and $\omega_s$ is the grid frequency. For a smaller voltage dip, the SCIG may regain a stable operating point, but for a deep voltage dip the SCIG loses its torque control and may have to be disconnected from the grid due to over speed or a voltage collapse may happen in the network due to high reactive power consumption.

Under the unbalance voltage conditions, the stator currents become unbalanced too and even a small amount of negative sequence voltage $V_s^-$ results in a very high negative sequence current $I_s^-$, such that:

$$I_s^- = \frac{V_s^-}{\omega_s . \sigma . L_S . I_{s,N}} \tag{4.10}$$

where $L_s$ is the stator inductance, $I_{s,N}$ is the rated stator current and $\sigma$ is the leakage factor. Average torque is not much affected by the negative sequence current; however, it causes the torque ripples of double grid frequency. The magnitude of the positive sequence torque and negative sequence torque $T^-$ can be represented by [112]:

$$T^+ \approx 3 . \frac{p}{2\omega_s} . V_s^+ . I_s^+ \tag{4.11}$$

$$T^- \approx 3 . \frac{p}{2\omega_s} . V_s^+ . I_s^- \tag{4.12}$$

Due to the decreased positive sequence voltage magnitude, the average torque is reduced, leading to the acceleration of the generator. The additional torque oscillations of the double grid frequency result in the heating of the stator windings and reduced lifetime of the turbine drive train. The average torque and the torque ripples can only be controlled independently if the CPLs are able to control the positive and negative sequence voltages.

## 4.3 Structure of the Distribution System

The investigated AC distribution system for unbalanced grid fault mitigation is shown in Figure 4.4. It consists of a 750 kW wind turbine with a fixed speed SCIG connected directly to the grid through a transformer and a 750 kVA CPL connected at the terminals. CPL is connected to the low voltage bus. The transformer is rated for wind turbine and CPL power. The main grid is a three phase AC source with internal impedance. The grid fault occurs at the medium voltage bus. The power system parameters in pu are presented in Table 4.1. In the beginning, the FRT enhancement analysis is restricted to single machine generation system and will be further extended to multi-machine generation system.

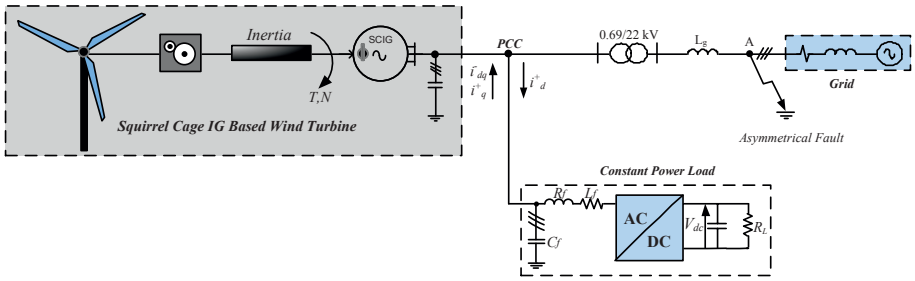


Figure 4.4: System under study with wind turbine connected to the grid and a CPL connected at the terminals

Table 4.1: Power System Parameters

| | |
|---|---|
| **Induction Generator** | |
| Base Apparent Power | 800 kVA |
| Rated Active Power | 750 kW |
| Rated Voltage (line to line) | 690 V |
| Stator resistance | 0.0092 pu |
| Stator leakage inductance | 0.1580 pu |
| Mutual inductance | 3.87 pu |
| Rotor mutual inductance | 0.0651 pu |
| Polar moment of inertia | 5 s |
| Mechanical damping | 0.008 pu |
| **Constant Power Load** | |
| Rated Power | 750 kVA |
| Rated Voltage (line to line) | 690 V |
| Filter Inductance $L_f$ | 0.05 pu |
| Filter Resistance $R_f$ | 0.01 pu |
| DC Link Voltage $V_{dc}$ | 1126 V |
| **Grid and Transmission Line** | |
| Rated Voltage (line to line) | 22 kV |
| Rated Frequency | 50 Hz |
| Resistance | 0.84 pu |
| Inductance | 2.51 pu |
| Transmission Line Inductance $L_g$ | 105.5 pu |

### 4.3.1 Simulations Results for Asymmetrical FRT

In this section, a comprehensive simulation study has been carried out to investigate the FRT capability of an installed CPL at the distribution level supplied by SCIG based wind turbine. CPL starts consuming 30% (225 kW) of the SCIG power at time $t$ = 1s. This has been done to achieve a steady state operating point for the SCIG. An asymmetrical fault (single phase amplitude falls to 78%) is simulated at the medium voltage bus as shown in Figure 4.3 at time $t$ =2s for a duration of 1 second. The

unbalanced grid fault results in highly unbalanced currents in the stator of the SCIG. Figure 4.5 presents the PCC voltage and stator current before and after the unbalanced grid voltage dip.

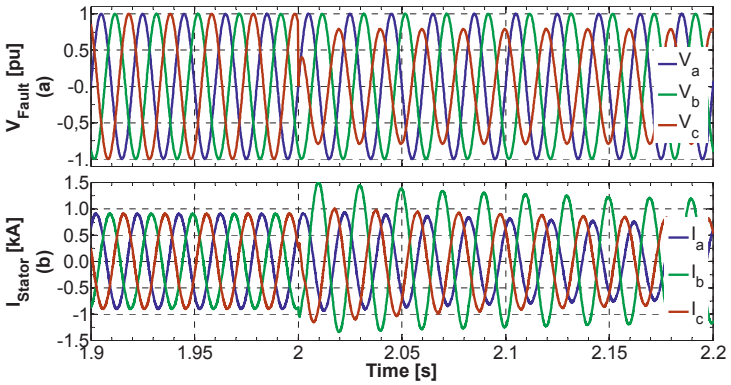


Figure 4.5: System voltages and currents. (a) Voltage at the fault (b) SCIG stator currents

In the presence of positive and negative sequence components in both voltage and current, the total apparent power can be expressed as:

$$\begin{aligned} S = VI^* &= (V^+ + V^-)(I^+ + I^-)^* \\ &= (v_d^+ + jv_q^+ + v_d^- + jv_q^-)(i_d^+ + ji_q^+ + i_d^- + ji_q^-)^* \end{aligned} \tag{4.13}$$

Further expansion of (4.13) results in real and reactive powers, such that:

$$\begin{aligned} P_{CPL} &= v_d^+ i_d^+ + v_d^- i_d^- + v_q^- i_q^- + v_d^+ i_d^- + v_d^- i_d^+ + v_q^- i_q^+ \\ Q_{CPL} &= v_d^+ i_q^+ + v_d^- i_q^- - v_q^- i_d^- + v_d^- i_q^+ - v_q^- i_d^+ - v_d^+ i_q^- \end{aligned} \tag{4.14}$$

where $P_{CPL}$ and $Q_{CPL}$ are the CPL active and reactive powers. In (4.14), the last three terms represent the product of opposite sequences of voltage and current, representing the oscillatory active and reactive powers at double grid frequency.

1. *CPL without voltage support*

At the initial stage of the analysis, CPL's positive and negative sequence voltage control has been kept disabled. The DC link voltage control remains active as it is the basic constituent of the CPL control structure. The simulation results are presented in Figure 4.6 for the complete time duration. SCIG cannot attain the nominal voltage at the very start due to the time constant associated with the stator winding. The asymmetrical fault leads to a negative sequence voltage as depicted in Figure 4.6a. The negative sequence voltage causes negative sequence flux circulation in the air gap and, therefore, results in important torque ripples of the system as presented by Figure 4.6b. The torque oscillations put a huge stress on the mechanical part. The drop in the positive sequence voltage leads to a decrease in the torque and the speed of the rotor keeps on increasing (Figure 4.6c). However, this fault does not drive the system to a mechanical unstable

point and voltage collapse does not occur. Therefore, increase in rotor speed is not very substantial. SCIG returns to the rated operating point after the fault. Figure 4.6d shows the component of positive sequence current $i_d^+$ corresponding to the CPL active power input.

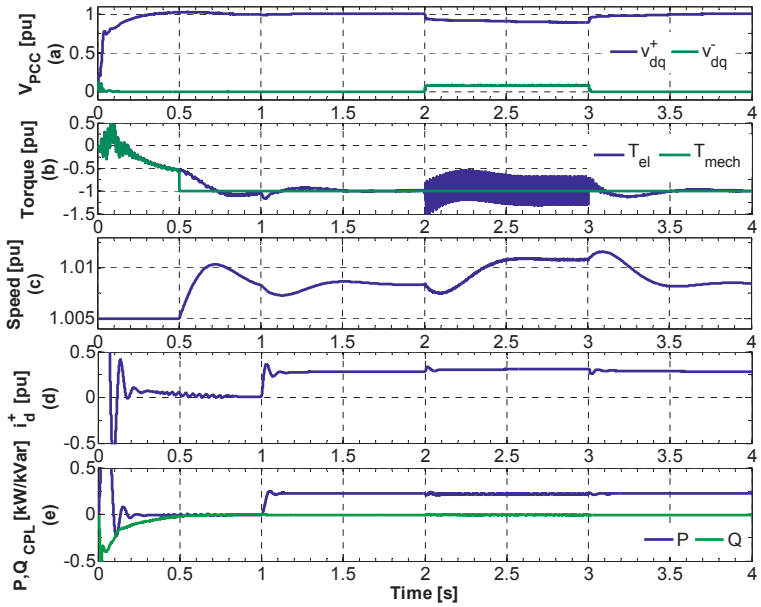


Figure 4.6: Simulation results for asymmetrical grid fault without CPL voltage compensation (a) Positive and negative sequence voltages at PCC (b) SCIG Torque (c) SCIG speed (d) Active component of current representing the load power (e) CPL active and reactive powers

The presence of only current $i_d^+$ reduces the power relationship presented by (4.14), such that:

$$\begin{aligned} P_{CPL} &= v_d^+ i_d^+ + v_d^- i_d^+ \\ Q_{CPL} &= -v_q^- i_d^+ \end{aligned} \tag{4.15}$$

A very small amount of active and reactive power oscillations of double grid frequency are also present during the fault due to the interaction of negative sequence voltages with positive sequence input current as indicated by (4.15). Section C.2.1 in appendix C presents the details of the generation and grid side powers.

2. *CPL with positive sequence voltage support*

In the second phase of simulation study, the CPL is controlled to compensate for positive sequence voltage only, while negative sequence voltage remains in the system. The fault conditions are the same and the simulation results are shown in Figure 4.7. The CPL is able to compensate the positive sequence voltage at PCC by injecting the

component of positive sequence reactive current $i_q^+$ (Figure 4.7d). The positive sequence voltage recovers back to the pre-fault value. CPL also consumes positive sequence active current component representing the load power. The transient in the speed and torque can be observed when the fault occurs and it lasts for some time. Due to the positive sequence voltage compensation, the speed of the rotor does not increase, confirming a stable operating point for the system. The torque ripples in the SCIG still remain due to the presence of negative sequence voltage in the system.

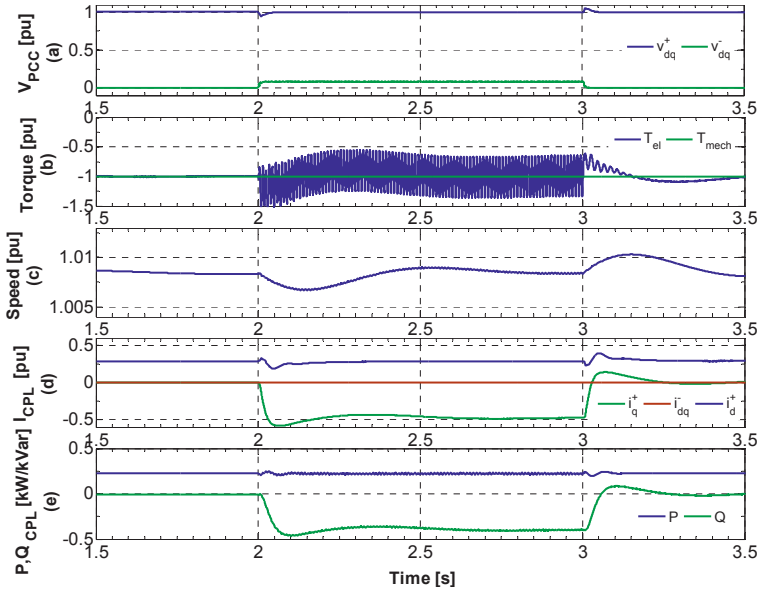


Figure 4.7: Simulation results with CPL positive sequence voltage control (a) Positive and negative sequence voltages at PCC (b) SCIG Torque (c) SCIG speed (d) Positive and negative component of compensating current (e) CPL active and reactive powers

The active and reactive powers associated with CPL are shown in Figure 4.7e and are represented by:

$$\begin{aligned} P_{CPL} &= v_d^+ i_d^+ + v_d^- i_d^+ + v_q^- i_q^+ \\ Q_{CPL} &= v_d^+ i_q^+ + v_d^- i_q^+ - v_q^- i_d^+ \end{aligned} \tag{4.16}$$

3. *CPL with negative sequence voltage support*

Figure 4.8 illustrates the results when CPL is controlled to compensate the negative sequence voltage only. The CPL control strategy completely eliminates the negative sequence component of the PCC voltage as shown in Figure 4.8a. This result in the removal of heavy torque ripples during the fault (Figure 4.8b). CPL injects the negative sequence component of active and reactive current $i_{dq}^-$ for this purpose (Figure 4.8d) and the positive sequence reactive current $i_q^+$ is zero. As the positive sequence component of the voltage is not compensated, therefore, the rotor keeps on accelerating

(Figure 4.8c), and SCIG consumes more reactive power, resulting in a continuous decrease in the positive sequence voltage component. The system, however, does not reach the mechanical unstable point and returns to the rated operating point after the fault. Figure 4.8e shows the oscillating CPL active and reactive powers during the fault.

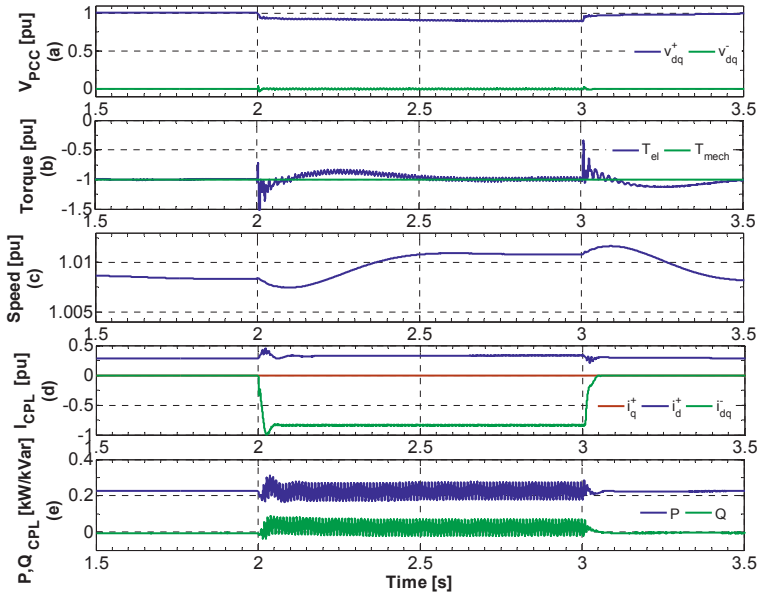


Figure 4.8: Simulation results with CPL negative sequence voltage control (a) Positive and negative sequence voltages at PCC (b) SCIG Torque (c) SCIG speed (d) Positive and negative component of compensating current (e) CPL active and reactive powers

In this case, the active and reactive powers can be represented by:

$$\begin{aligned} P_{CPL} &= v_d^+ i_d^+ + v_d^- i_d^- + v_q^- i_q^- + v_d^- i_d^+ + v_d^+ i_d^- \\ Q_{CPL} &= v_d^- i_q^- - v_q^- i_d^- - v_q^- i_d^+ - v_d^+ i_q^- \end{aligned} \tag{4.17}$$

During the fault, both the active and reactive powers exhibit second order harmonic as a result of interaction between the opposite sequence voltage and current components. The input active power oscillates around a constant load demand. The power oscillations under fault conditions are higher in this case as confirmed by (4.17) compared to the previously discussed two cases. In this case, there is more interaction of opposite sequences of voltage and current. From the load side perspective, these oscillations are undesirable. However, even without the negative sequence voltage compensation through injection of negative sequence current $i_{dq}^-$, the system will be exposed to oscillation due to unbalanced nature of the grid fault as seen in the case without positive or negative sequence voltage control.

4. *CPL with both positive and negative sequence voltage support*

The compensation of positive and negative sequence voltage simultaneously can only be achieved when the CPL has unused current capacity (remaining current after fulfilling the load active power requirements). The coordination between the positive and negative sequence voltage compensation is dependent on the severity of the grid fault. For smaller unbalanced voltage sag, CPL may be able to achieve the independent compensation of both the positive and negative sequence of PCC voltage. The current limiter block shown in Figure 4.1 ensures that the total current capability of the CPL must not be exceeded. The total CPL current rating $I_{CPL,N}$ can be represented by (4.18):

$$\begin{aligned} I_{CPL,N} &= \sqrt{(i_d^+)^2 + (i_q^+)^2 + (i_{dq}^-)^2} \\ &= \sqrt{(i_{dq}^+)^2 + (i_{dq}^-)^2} \;\; \leq \;\; 1 \text{ pu} \end{aligned} \tag{4.18}$$

Figure 4.9 shows the simulation results for the same fault severity when CPL control strategy allows the compensation of both the positive and negative sequence voltage components independently. In this case, CPL injects both the positive and negative sequence of the current for compensation purpose without exceeding its nominal current. It can be observed that coordinated voltage control results in the elimination of torque ripples and the acceleration of the rotor during the fault is also avoided (Figure 4.9b & Figure 4.9c). The power relationship is represented by (4.14) because all the positive and negative sequence voltage and current components are present in this case and double grid frequency oscillation can be observed in both the active and reactive powers. The magnitude of the oscillation is the highest in this case. They may look lower due to the limits of the vertical axis set for this case (Figure 4.9e). The details of generation and grid side powers for the different cases discussed above are presented in section C.2 in appendix C.

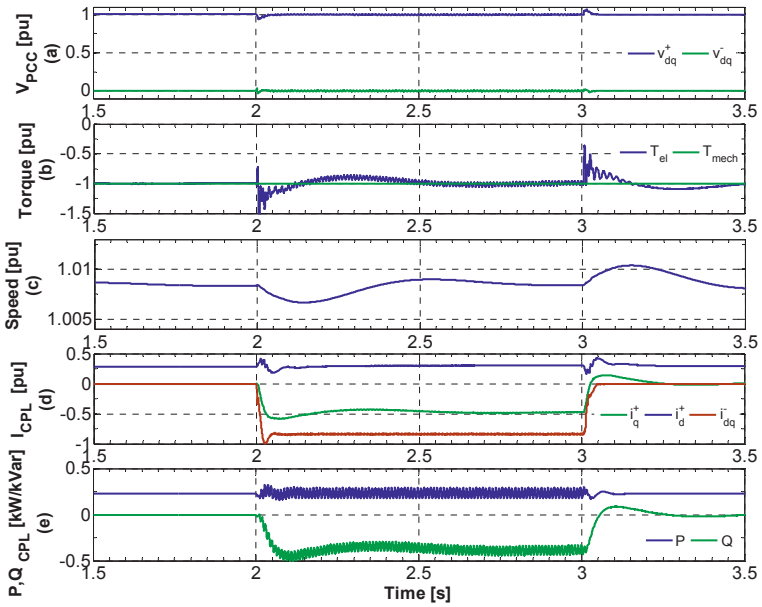


Figure 4.9: Simulation results with CPL coordinated positive and negative sequence voltage control (a) Positive and negative sequence voltages at PCC (b) SCIG Torque (c) SCIG speed (d) Compensating current (e) CPL active and reactive powers

For higher voltage sag, the CPL may not have the sufficient current capacity left to achieve the coordinated voltage control. In this case, the priority is given to positive sequence voltage compensation; because the speed of the rotor keeps on increasing out of control and a voltage collapse becomes unavoidable. Figure 4.10 shows the results for a more severe fault (single phase amplitude drops to 58%). The fault results in comparatively higher negative sequence voltage (Figure 4.10a). The CPL is able to compensate the positive sequence voltage by injecting its full allowed current capacity. If the fault is even more severe, then the CPL will not be able to fully compensate the positive sequence voltage. However, in that case, it can avoid the voltage collapse by supporting the PCC voltage by injecting maximum current without exceeding its current rating. The disadvantage in this case is that there is no extra current to compensate the negative sequence voltage and the torque oscillations will remain during the fault, resulting in unbalanced heating in the stator windings.

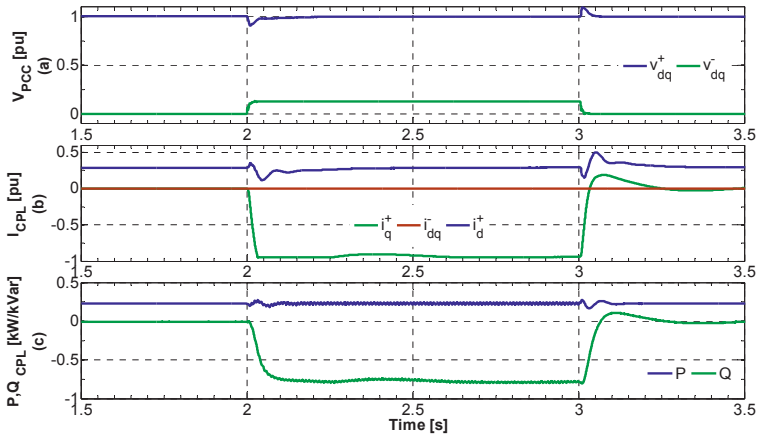


Figure 4.10: Simulation results for higher voltage sag with CPL coordinated positive and negative sequence voltage control (a) Positive and negative sequence voltages at PCC (b) Compensating current (c) CPL active and reactive powers

## 5. *Simulation Results with Multi-Machine Wind Farm*

In this section, a simulation analysis is performed for a medium size wind farm to confirm the validity of the proposed FRT enhancement method discussed in the previous subsections. The single machine system of Figure 4.4 is replaced with multi-machine system and a 2.225 MW fixed speed SCIG-based wind farm connected directly to the medium voltage grid. An aggregate model of the wind farm is used so that the sum of the turbines is modeled as one generator using the standard T-equivalent circuit. The rating of the each SCIG is the same as considered in the previous section and presented in Table 4.1. The fault resistance for the asymmetrical grid fault is kept the same as in the previous sections and the single phase voltage amplitude falls to 78% on the medium voltage side.

Figure 4.12 presents the simulation results for the case when CPL voltage control is disabled. The overall inductance of the system is increased due to the introduction of many SCIGs and it is clear from Figure 4.11a that the magnitude of the positive sequence voltage drops continuously during the fault and finally reaches to a lower value compared to single machine system (Figure 4.6). The component of the negative sequence voltage is not that higher. The smaller negative sequence component results in comparatively lower torque oscillations as presented in Figure 4.11b. The rotor speed increases during the fault (Figure 4.11c). In this case, the system does not reach the mechanically unstable point and the system slowly regains the pre-fault operating conditions after the fault is cleared. CPL consumes 225 kW power at time $t$ = 1 s. An increase in positive sequence active current component can be observed during the fault when the voltage decreases as shown in Figure 4.11d.

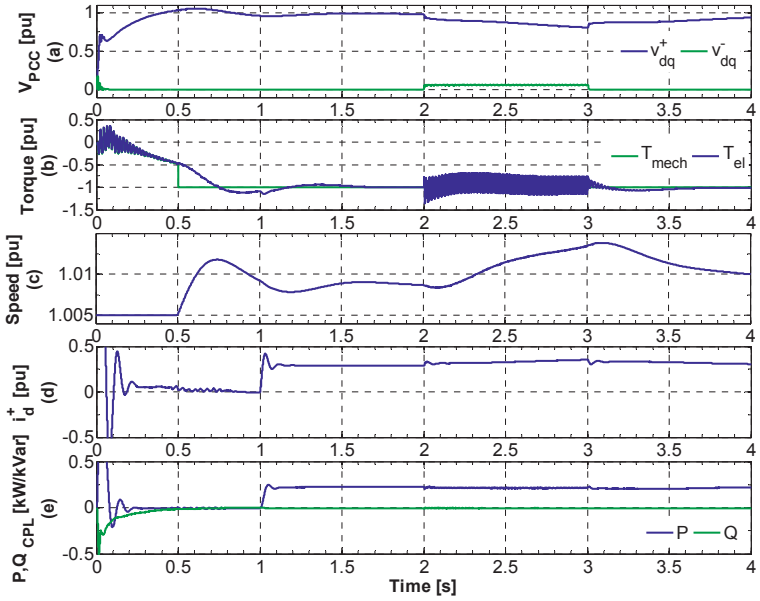


Figure 4.11: Simulation results for multi-machine medium size wind farm without CPL voltage control (a) Positive and negative sequence voltages at PCC (b) SCIG Torque (c) SCIG Speed (d) Active component of current representing the load power (e) CPL active and reactive powers

Simulation results for the case when CPL is controlled to provide both the positive and negative sequence voltage support are presented in Figure 4.12. CPL control affectively maintains the voltage during the fault to the specified values. The torque ripples are largely reduced after the negative sequence voltage compensation. The positive sequence voltage avoids the acceleration of the rotor during the fault and helps to improve the overall system stability and the possible disconnection of the wind farm as shown by Figure 4.12c. CPL injects the positive and negative sequence compensating currents and the current limiter block shown in Figure 4.1 does not impose any restrictions on the amount of injected current. Figure 4.12d illustrates the different CPL current components. The total CPL current in this case is 1.44 pu. This is 44% increase in the total CPL current rating even though the wind farm power rating is increased by three-fold. However, as the overall inductance of the system is very high in this case, the CPL does not need to inject three times more compensating current.

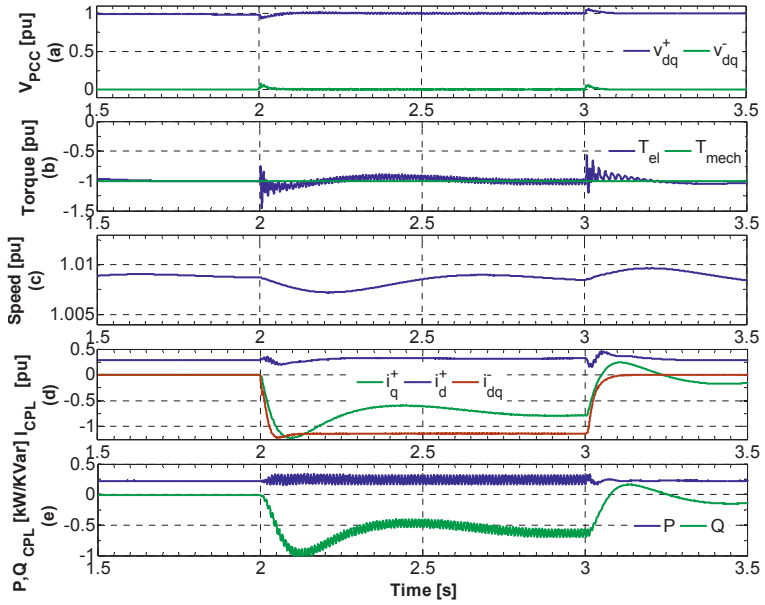


Figure 4.12: Simulation results for multi-machine medium size wind farm with CPL voltage control (a) Positive and negative sequence voltages at PCC (b) IG Torque (c) IG Speed (d) Compensating current (e) CPL active and reactive powers

## 4.4 FRT Enhancements with Distributed CPLs

This section presents a simulation analysis for FRT enhancement in a microgrid consisting mainly of distributed CPLs. A simulation analysis is carried out to find the impact of negative sequence voltage support on the incremental current rating of the CPLs. A comparison between the distributed compensation of positive and negative sequence voltages and the centralized compensation by a STATCOM has also been presented.

### 4.4.1 Microgrid Structure with High Share of CPLs

The investigated microgrid is shown in Figure 4.13. It consists of a 3 MW fixed speed SCIG based wind farm connected directly to the medium voltage grid. Several CPLs are connected to the low voltage distribution bus. It has been assumed that the distribution level is entirely dominated by the consumers with PE interfaces at the front end. An aggregate model of the wind farm is used so that the sum of the turbines is modeled as one generator using the standard T-equivalent circuit. The grid fault occurs at the medium voltage bus. All the power system parameters are presented in Table 4.2.

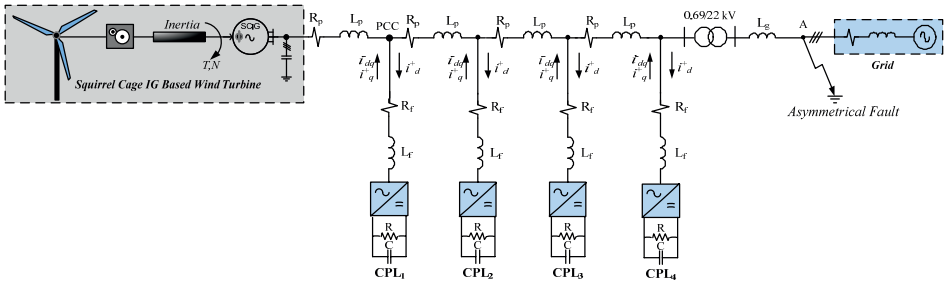


Figure 4.13: Structure of the investigated microgrid with SCIG based wind farm and distributed CPLs

Table 4.2: Wind Farm, CPL, Grid and Lines Parameters

| **Wind Farm** | |
|---|---|
| Base Apparent Power | 3.36 MVA |
| Rated Active Power | 3 MW |
| Rated Voltage (line to line) | 690 V |
| Stator resistance | 0.0092 pu |
| Stator leakage inductance | 0.1580 pu |
| Mutual inductance | 3.87 pu |
| Rotor mutual inductance | 0.0651 pu |
| Polar moment of inertia | 0.5 s |
| Mechanical damping | 0.008 pu |
| **Constant Power Load (Individual Device)** | |
| Rated Power | 3 MVA |
| Rated Voltage (line to line) | 690 V |
| Filter Inductance $L_f$ | 0.21 pu |
| Filter Resistance $R_f$ | 0.042 pu |
| DC Link Voltage $V_{dc}$ | 1126 V |
| **Grid and Lines** | |
| Rated Voltage (line to line) | 22 kV |
| Rated Frequency | 50 Hz |
| Resistance | 3.52 pu |
| Inductance | 11 pu |
| Transmission Line Inductance | 66.5 pu |
| Distribution Line Inductance $L_P$ | 0.11 pu |
| Distribution Line Resistance $R_P$ | 0.0353 pu |

### 4.4.2 Simulation Results for Unbalanced FRT Enhancement with Distributed CPLs

For this simulation analysis, all the four CPLs are controlled to provide the FRT services and are equipped with both the voltage and current controllers. Each CPL starts consuming 450 kW power from the wind farm at time $t$=1s. An asymmetrical fault (single phase amplitude falls to 60% as shown in Figure 4.14a) is simulated at the medium voltage bus as presented in Figure 4.13 at time $t$=2s for a duration of 1 second.

The unbalanced grid fault leads to highly unbalanced currents in the stator of the SCIG as shown in Figure 4.14b.

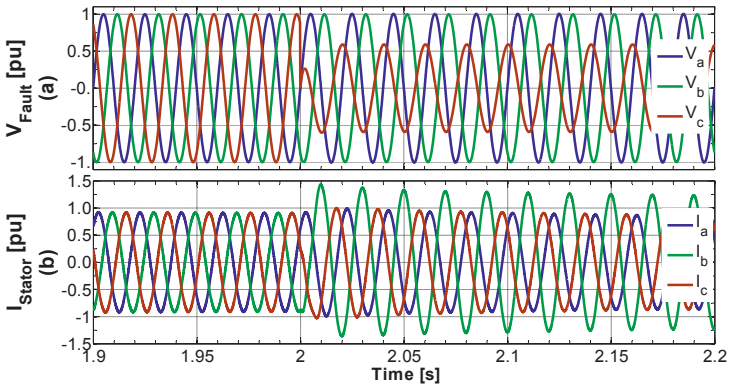


Figure 4.14: (a) Voltage at the fault (b) SCIG stator currents

1. *CPLs without voltage support*

At the very start of the simulation analysis, the AC voltage control has been disabled for all the CPLs and the results are presented in Figure 4.15. DC link voltage control; however, remains active. The system is not able to maintain the nominal voltage level due to the time constant associated with the stator circuit (Figure 4.15a). Similarly, when the CPLs are connected, a transient in voltage can be observed. Torque and speed also exhibit transients at the start and when the fault occurs. The unbalanced fault leads to a negative sequence voltage as depicted in Figure 4.15a. Due to the negative sequence voltage, negative sequence flux circulates in the air gap. This leads to torque ripples of the system during system contingency and the mechanical part suffers huge stress. The drop in the positive sequence voltage leads to a decrease in the torque (Figure 4.15b) and the speed of the rotor keeps on increasing as shown in Figure 4.15c. The severity of the fault drives the system to a mechanical unstable point and a complete voltage collapse occurs due to high reactive power consumption by the SCIG as illustrated in Figure 4.15a unlike the case presented in section 4.3 where the system does not achieve voltage collapse. In this case, SCIG cannot return to the rated operating point after the fault. Figure 4.15d shows the component of positive sequence active current $i_d^+$ corresponding to the $CPL_1$ active power input.

During the fault, CPLs try to keep the active power constant by increasing the positive sequence active current; however, due to the complete voltage collapse the CPL control does not remain very effective and the input power cannot be kept constant as shown in Figure 4.15d. During the fault, the interaction of opposite sequence voltages and currents results in small oscillations in active and reactive power (Figure 4.15e).

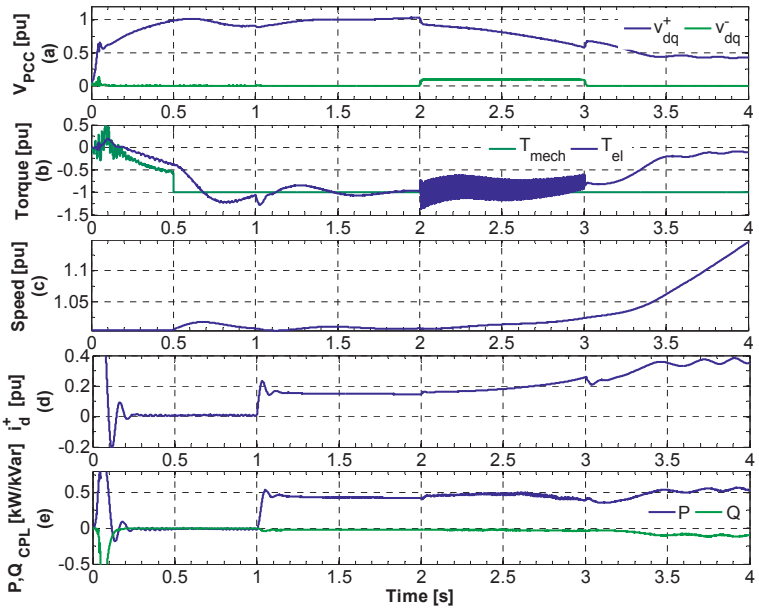


Figure 4.15: Simulation results for CPLs without voltage control (a) Positive and negative sequence voltages at PCC (b) SCIG torque (c) SCIG speed (d) Active component of $CPL_1$ current representing the load power (e) $CPL_1$ powers

2. *CPLs with positive sequence voltage control*

In this case, the simulations are repeated for the same fault condition and CPLs are controlled to compensate for the positive sequence voltage only. The negative sequence voltage control remains inactive. The results have been presented in Figure 4.16. All the CPLs are able to compensate the positive sequence voltage at PCC by injecting the component of positive sequence reactive current $i_q^+$ as shown in Figure 4.16d. Each CPL also consumes positive sequence active current component in accordance with the active power requirement (Figure 4.16e). The positive sequence voltage support avoids an increase in the positive sequence active current component during the fault as is observed in the case without voltage control. Due to the positive sequence voltage compensation, the speed of the rotor does not increase to an unstable point, ensuring a stable operating point for the system unlike the previous case. The torque ripples in the SCIG are still present as illustrated by Figure 4.16b because of the absence of negative sequence voltage compensation.

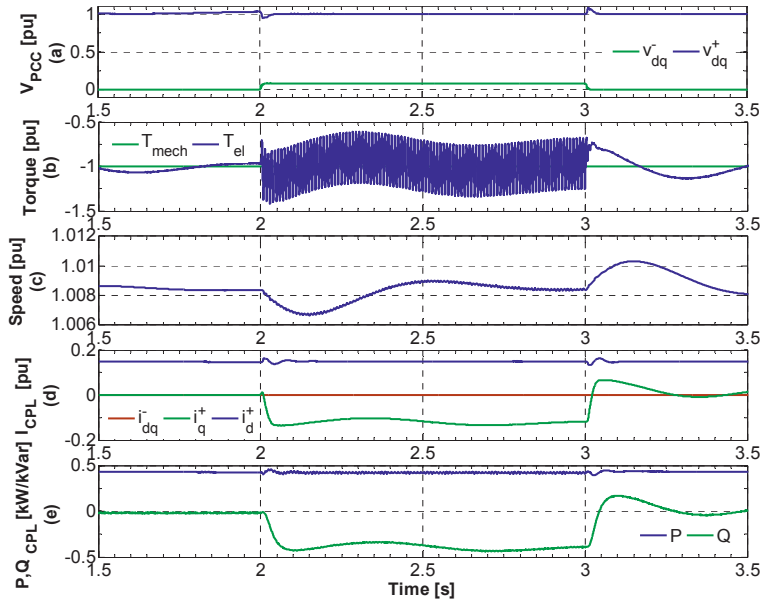


Figure 4.16: Simulation results for positive sequence voltage control (a) PCC voltages (b) SCIG torque (c) SCIG speed (d) $CPL_1$ compensation currents (e) $CPL_1$ powers

3. *CPLs with negative sequence voltage support*

In this case, all the CPLs are controlled to compensate the negative sequence voltage only and the results are presented in Figure 4.17. The CPLs are able to compensate effectively the negative sequence component of the PCC voltage (Figure 4.17a), removing the heavy torque oscillation as shown in Figure 4.17b. All the four CPLs inject the negative sequence component of active and reactive current $i_{dq}^-$ for this purpose as illustrated by Figure 4.17d. As the positive sequence component of the voltage is not compensated, therefore, the rotor keeps on accelerating (Figure 4.17c), and due to the excessive reactive power consumption by SCIG from the grid, a complete voltage collapse occurs (Figure 4.17a). The system reaches the mechanical unstable point and cannot return to the rated operating point after the fault. Figure 4.17e shows the CPL active and reactive powers of double grid frequency during the fault and represented by (4.17). In this case as well, the active power during and after the fault does not remain constant as the CPL control is not activated to avoid the voltage collapse and the positive sequence active current component $i_d^+$ keeps on increasing to maintain a constant load power (Figure 4.17d).

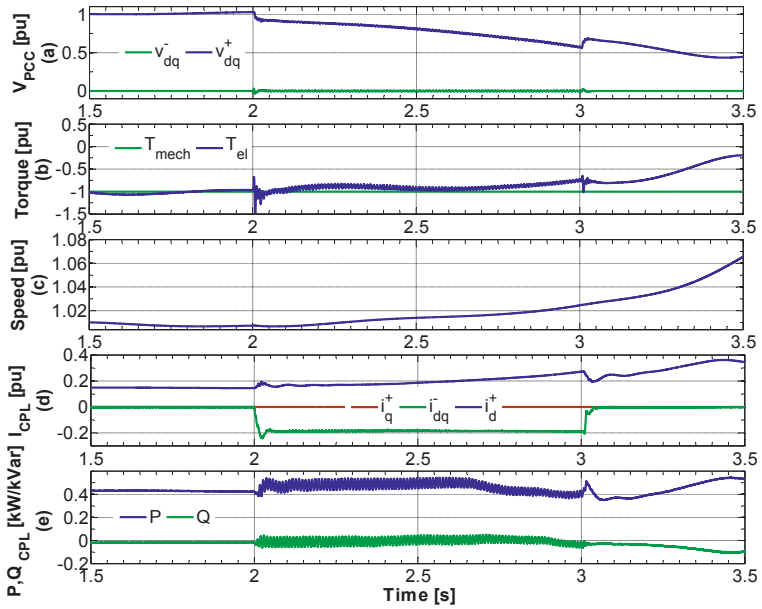


Figure 4.17: Simulation results with negative sequence voltage control (a) PCC voltages (b) SCIG torque (c) SCIG speed (d) $CPL_1$ compensation currents (e) $CPL_1$ powers

4. *CPLs with positive and negative sequence voltage control*

In this case, all the CPLs are allowed to independently compensate both the positive and negative sequence voltage components for the same fault conditions. The results are illustrated in Figure 4.18. Each CPL injects both the positive and negative sequence of the active and reactive current components for compensation purpose as presented by Figure 4.18d. The CPL control efficiently compensates the positive and negative sequence voltages during the fault (Figure 4.18a). The complete voltage compensation effectively eliminates the torque ripples during the fault (Figure 4.18b). The acceleration of the rotor during the fault is avoided and the voltage collapse does not occur (Figure 4.18c). SCIG regains the rated operating point during and after the fault as shown by Figure 4.18a.

Simulation results enhance the understanding of the operation of fixed speed SCIG-based wind turbine when CPL is controlled to provide the positive and negative sequence voltage compensation independently. The positive sequence voltage compensation enhance the torque capability of the SCIG and avoids the acceleration of the rotor, while the negative sequence voltage compensation helps increasing the lifetime of the generator drive train by removing the torque ripples. However, voltage compensation capability is totally dependent on the chosen current rating of the CPL. It can only provide the compensating current if there is some current left after fully providing the load power needs. The overall impedance of the power system also plays an important role. The voltage compensation capability of the CPL is high for a weak power grid.

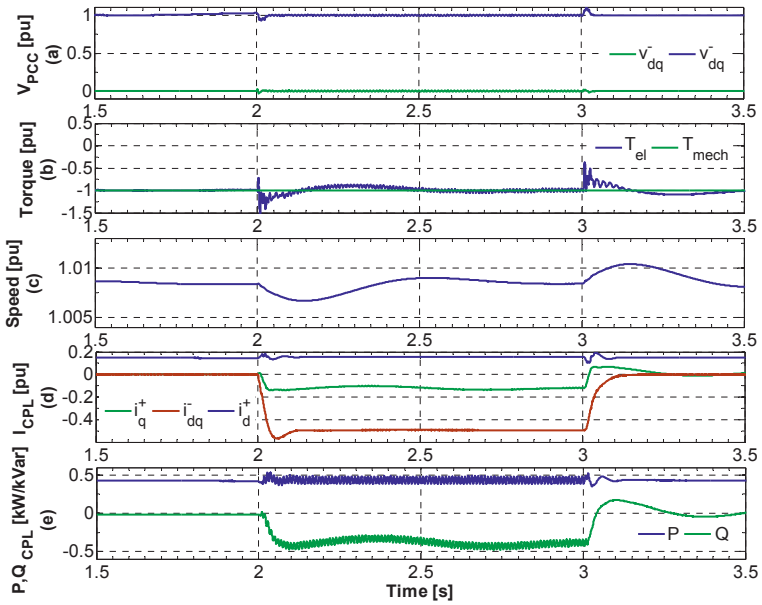


Figure 4.18: Simulation results with coordinated positive and negative sequence voltage control (a) PCC voltages (b) SCIG torque (c) SCIG speed (d) $CPL_1$ compensation currents (e) $CPL_1$ powers

The obvious advantage of the proposed scheme is that the installed resources at the distribution level can be used to achieve the performance of a STATCOM that has been specifically used for compensation purpose. However, in order to achieve this, the CPL current rating must either be enhanced or it must be operated below its rated active power to allow the injection of extra current for voltage compensation.

## 4.5 Impact of Unbalanced FRT Enhancement on Current Rating of a CPL

This section presents the impact of negative sequence voltage compensation on the total current rating of the CPL. As indicated by (2.16), the voltage support comes at the cost of reactive current injection under balanced grid faults. The improvement in the voltage profile leads to the reduction of active component of current to keep the input power constant. This is analogous to the previously discussed case of positive sequence voltage compensation under unbalanced grid faults, while the negative sequence voltage still remains in the system. Under this condition, total CPL current $I^{+}_{t}$ can be expressed by (3.1) which can be rewritten to distinguish the currents components such that:

$$I_t^+ = \sqrt{(i_d^+)^2 + (i_q^+)^2} \tag{4.19}$$

It is supposed in this investigation that CPL is designed to provide the positive sequence voltage compensation through reactive power ancillary service. In order to mitigate the

negative sequence effects in the system, the CPLs have to inject the negative sequence active and reactive current components during the fault. This demands an increment in the total current rating of the each CPL comprising a microgrid. In this case, the total CPL current $I_{CPL,N}$ can be represented by:

$$\begin{aligned} I_{CPL,N} &= \sqrt{(i_d^+)^2 + (i_q^+)^2 + (i_d^-)^2 + (i_q^-)^2} \\ &= \sqrt{(I_t^+)^2 + (I_t^-)^2} \end{aligned} \tag{4.20}$$

where $I_t^-$ is the total negative sequence current in SRF.

The microgrid model of Figure 4.13 is considered with each CPL consuming 450 kW. Single phase to ground fault at the medium voltage bus is simulated to get the different values of voltage sags. Simulations are performed with and without the compensation of negative sequence voltage and the results are presented in Figure 4.19. It can be observed that the total CPL current is higher for unbalanced FRT enhancement of deeper voltage dip. This is due to the increment in the positive and negative sequence compensation currents for FRT enhancement. Before the fault occurs, each CPL is consuming only the active component of positive sequence current corresponding to the load requirements. The value of this current is 0.15 pu. For a single phase voltage dip of 70%, the total CPL current increase to 0.37 pu. This is 150% increment in the total CPL current compared to the pre-fault value. However, for a higher single phase voltage dip, the positive sequence voltage drops rapidly at the low voltage bus and CPL has to draw more positive sequence active current in accordance with (2.16) if there is no FRT enhancement provided by CPLs. This also requires an increment in the total CPL current and the system is highly vulnerable to a voltage collapse. Therefore, a demand for an increase in the current rating of the CPL is essential to avoid a complete voltage collapse.

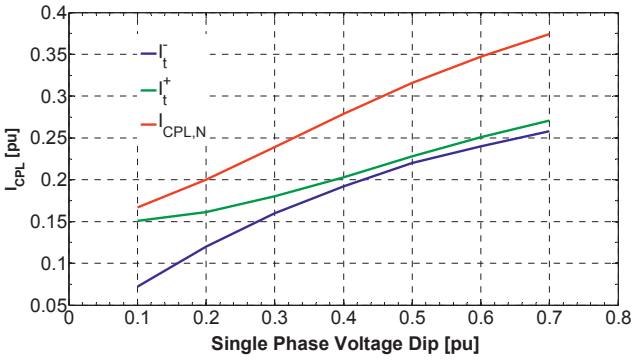


Figure 4.19: Incremental current rating of the CPL as a function of single phase to ground fault

## 4.6 Centralized STATCOM vs Distributed CPLs

In order to evaluate the extra functionality of each CPL belonging to a group of distributed CPLs for FRT enhancement, a comparison is made with the operation of a centralized STATCOM. A simulation study is performed in order to know the impact of distributed compensation on the total current of each device compared to a STATCOM. The microgrid model used for this purpose is shown in Figure 4.20. $CPL_1$ will be occasionally replaced with the centralized STATCOM.

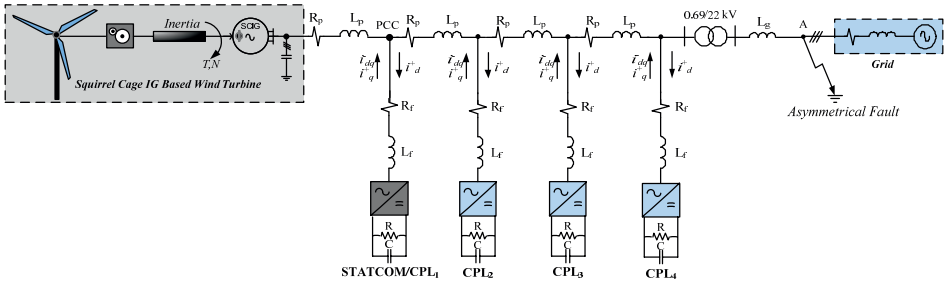


Figure 4.20: Investigated microgrid with SCIG based wind farm, STATCOM and distributed CPLs

A comparison between the system with a STATCOM and three non-controlled CPLs is made with the case of two, three and four CPLs with FRT capability. Like the previous cases, the total power drawn by the each CPL is 450 kW. Simulations are carried out for different levels of single phase to ground voltage dips at medium voltage bus. The total compensating current $I_{COMP}$ in this case is represented by:

$$I_{COMP} = \sqrt{(i_q^+)^2 + (i_d^-)^2 + (i_q^-)^2} \tag{4.21}$$

The amount of total compensating current for FRT enhancement is plotted in Figure 4.21 for different single phase fault levels. Each individual CPL injects an amount of current according to the voltage drop at PCC. The voltage drop across each CPL is almost the same, therefore, all the CPLs inject almost equal amount of current for FRT enhancement. It can be observed that the total compensating current by the STATCOM for all the fault levels is higher compared to the total compensating current by a single CPL belonging to a group of two, three and four distributed CPLs. The higher the number of distributed CPLs in the microgrid, the lower the compensating current injected by individual device. However, the sum of total distributed compensating current for all the studied cases is higher compared to the centralized STATCOM. This is because of the varying distances of the CPLs from PCC. The total compensating current has to be higher to overcome the increasing impedance of the system due to addition of each CPL device. In general, it can be concluded that the distributed compensation as an ancillary service provided by CPLs is beneficial than centralized compensation and it demands the lower current rating for the individual devices.

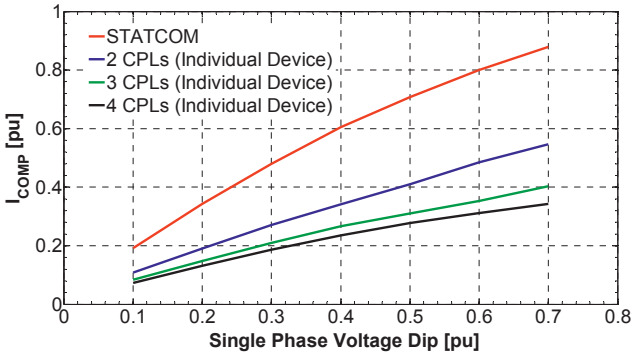


Figure 4.21: Total compensating current comparison between STATCOM and distributed CPLs for FRT enhancement

## 4.7 Summary

This chapter introduces the idea of using a CPL to mitigate the asymmetrical grid faults in a fixed speed SCIG-based wind farm instead of using dedicated devices such as a STATCOM or DFIG wind turbine. A detailed simulation analysis is carried out to understand the voltage control performed by CPL and the resulting operation of the SCIG under unbalanced fault. A tightly regulated VSC utilizing vector control method is used as a CPL. DSOGI-PLL is employed in the control strategy for the precise extraction of positive and negative sequence components of the PCC voltage. A CPL control structure is proposed to achieve the independent compensation of positive and negative sequence of the voltage. The priority has been assigned to the positive sequence voltage control for the maximum FRT enhancement of the wind turbine.

The positive sequence voltage compensation avoids the acceleration of the rotor and improves the voltage stability. The negative sequence voltage control is activated when there is remaining current capacity to remove the torque oscillation in the machine during the unbalanced fault. The simulation results for multi-machine wind farm confirm that the CPL effectively provides the positive and negative sequence voltage compensation and the increase in CPL compensation currents is not in proportion with the increase in system power rating.

A detailed model of microgrid comprising of several distributed CPLs has been considered. A more severe grid fault leading to a complete voltage collapse has been simulated. All the CPLs are taking part in unbalanced FRT enhancement and they effectively provide the positive and negative sequence voltage compensation thereby avoiding the mechanical instability of the wind farm.

The incremental current rating of the semiconductor switches of the CPLs for unbalanced FRT enhancement is studied and it is observed that the deeper the voltage drop, the higher the CPL current rating required for FRT enhancement.

The total compensating current injected by the individual CPL belonging to a group of distributed CPLs is compared with the total compensating current by a centralized STATCOM. It is found that the each distributed CPL injects less current for FRT enhancement compared to one centralized STATCOM.

# 5 Power Quality Enhancement by CPL

*This chapter addresses the power quality issues in AC distribution system with CPL acting as active power filter in addition to serve the load. The analysis has been performed under both ideal and non-ideal source voltage conditions. A slightly different control strategy for the CPL based on time and frequency domain reference signal generation has been presented in detail.*

As has been investigated in previous chapters, CPLs can be used for improving the transient stability and FRT enhancements in a distribution system through provision of active and reactive powers under grid voltage dips. This chapter explores the possibility of using them for active power filtering in the presence of harmonic generating non-linear loads under both ideal and non-ideal voltage conditions.

The inclusion of power electronics based devices at the transmission as well as at the distribution level in large numbers has badly deteriorated the power quality in the recent times. These devices and PE load interfaces, if not tightly regulated, draw non-sinusoidal current from the utility. Elimination of harmonic pollution in power grid and improving quality of electrical power supply to consumers has become one of the important research subjects in modern electrical power system. In a microgrid, employing local DG units, harmonics and voltage sags have been identified to be the most serious problems for the industrial consumers. Shunt active power filters (APF) can be used to alleviate some of the major power quality issues. They generally provide reactive power compensation, harmonic compensation and flicker/unbalance compensation [113-118].

In this chapter, it is proposed that the CPL installed in an AC distribution system can be used to provide active power filtering as an ancillary service in the presence of non-linear harmonic producing loads. The reference generation of compensating currents has been done using both the time domain and frequency domain approaches. Time domain approach is based on the instantaneous reactive power (IRP) *p-q* theory and frequency-domain approach is based on current's physical components (CPC) theory, utilizing Fourier analysis of the distorted current to extract the compensating current. Simulation results indicate that the controlled load can be applied to achieve active power filtering in addition to providing constant power to consumers under both ideal and non-ideal source voltage conditions.

## 5.1 Reference Signal Generation Schemes

In the presence of non-linear loads, the source current will have very high harmonic content. It is essential to remove the lower order harmonics from the utility to avoid the harmonic voltage drops across the electrical network. Therefore, harmonic requirement of the non-linear loads has to be fulfilled by a source located close to them as presented in Figure 5.1. Reference signal generation schemes calculate the harmonic components of the load current to be further used as set points in the control system of the APF. In this section, two reference signal generation schemes based on two most common power theories will be discussed. The compensation purpose for both the reference signal techniques is to make the source current sinusoidal with the source supplying only the constant active power to the load.

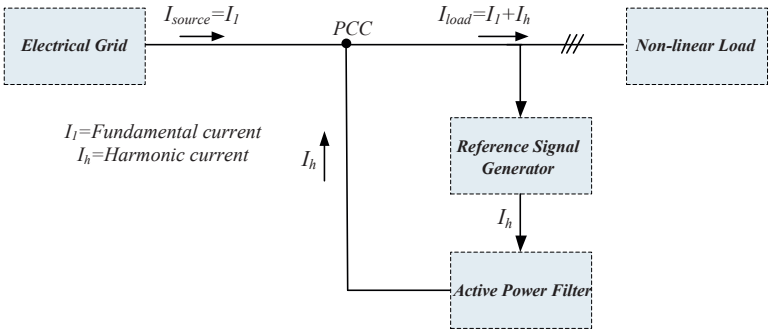


Figure 5.1: Functional diagram of an active compensator with reference signal generator

### 5.1.1 IRP p-q Based Time Domain Approach

*IRP p-q* theory [119, 120] is the most widely used to generate reference signals for the control system of switching compensators. The theory is based on the assumption that the instantaneous active power of an ideally compensated load must always be constant and the oscillating components of the instantaneous power should be compensated [121]. It utilizes Clark transform of the line current and phase voltages. For a balanced three phase three wire system, we can write:

$$\begin{bmatrix} x_\alpha \\ x_\beta \end{bmatrix} = C \begin{bmatrix} x_a \\ x_b \end{bmatrix} \tag{5.1}$$

where $x$ represents either the phase voltage or line current and $C$ is a constant, such that:

$$C = \begin{bmatrix} \sqrt{3/2} & 0 \\ \sqrt{1/2} & \sqrt{2} \end{bmatrix} \tag{5.2}$$

The instantaneous active and reactive power as defined in [119-121] is:

$$\begin{aligned} p &= v_\alpha i_\alpha + v_\beta i_\beta \\ q &= v_\alpha i_\beta - v_\beta i_\alpha \end{aligned} \tag{5.3}$$

Using the instantaneous powers, instantaneous active and reactive currents in stationary reference frame can be defined as:

$$\begin{aligned} i_\alpha &= i_{\alpha p} + i_{\alpha q} = \frac{v_\alpha}{v_\alpha^2 + v_\beta^2} p^{\sim} - \frac{v_\beta}{v_\alpha^2 + v_\beta^2} q \\ i_\beta &= i_{\beta p} + i_{\beta q} = \frac{v_\beta}{v_\alpha^2 + v_\beta^2} p^{\sim} + \frac{v_\alpha}{v_\alpha^2 + v_\beta^2} q \end{aligned} \tag{5.4}$$

where $p^{\sim}$ is the oscillating active power that needs to be compensated. A generic reference signal generation scheme based on the *IRP p-q* theory is shown in Figure 5.2.

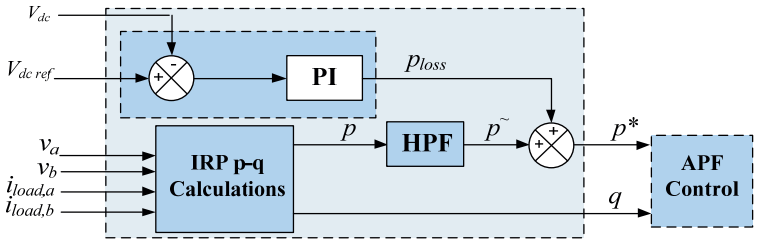


Figure 5.2: *IRP p-q* based reference signal generation scheme

Control methods based on SRF are very similar to the control methods based on *IRP p-q*. In this case, the currents are transformed into SRF that is synchronized with the AC supply voltage such that:

$$\begin{bmatrix} i_d \\ i_q \end{bmatrix} = \begin{bmatrix} \cos\theta & \sin\theta \\ -\sin\theta & \cos\theta \end{bmatrix} \begin{bmatrix} i_\alpha \\ i_\beta \end{bmatrix} \tag{5.5}$$

The *d* and *q* components of currents represent the active and reactive components of the load current. Figure 5.3 shows the reference current extraction scheme in SRF for the system under investigation. Both the methods employ filters to extract the load current components to be compensated. The filters are not needed for the *q* component if total reactive power is to be compensated.

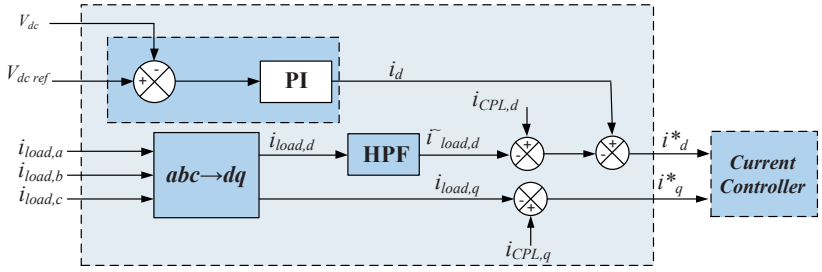


Figure 5.3: Reference signal generation scheme in SRF

### 5.1.2 CPC Based Frequency Domain Approach

The *CPC* theory [122] is a frequency based approach to describe the power properties of an electrical circuit. *CPC* provides orthogonal decomposition of currents into physical components [123-130]. Phase voltages and line currents are expressed in terms of Fourier series and presented in the form of vector **u** and **i** such that:

$$\mathrm{u} = \begin{bmatrix} u_a \\ u_b \\ u_c \end{bmatrix} = \sum_{n\in N} \mathrm{u}_{(n)} = \sum_{n\in N} \begin{bmatrix} u_{(n)a} \\ u_{(n)b} \\ u_{(n)c} \end{bmatrix} = \sqrt{2}\,\mathrm{Re} \sum_{n\in N} \mathrm{U}_{(n)} e^{jn\omega(1)t} \tag{5.6}$$

$$\mathrm{i} = \begin{bmatrix} u_a \\ u_b \\ u_c \end{bmatrix} = \sum_{n\in N} \mathrm{i}_{(n)} = \sum_{n\in N} \begin{bmatrix} i_{(n)a} \\ i_{(n)b} \\ i_{(n)c} \end{bmatrix} = \sqrt{2}\,\mathrm{Re} \sum_{n\in N} \mathrm{I}_{(n)} e^{jn\omega(1)t} \tag{5.7}$$

where $\mathrm{u}_{(n)}=[U_{(n)a}\ U_{(n)b}\ U_{(n)c}]^{\mathrm{T}}$ and $\mathrm{i}_{(n)}=[I_{(n)a}\ I_{(n)b}\ I_{(n)c}]^{\mathrm{T}}$ are the vectors of voltage and current complex rms values [122, 123]. $N$ is the set of current and voltage harmonics. The complex power for the $n$th order harmonics is represented by:

$$S_{(n)} = \mathrm{U}^T_{(n)} \mathrm{I}^*_{(n)} = P_{(n)} + jQ_{(n)} \tag{5.8}$$

where $P_{(n)}$ and $Q_{(n)}$ are the $n$th order active and reactive load powers. In the presence of harmonic generating loads (HGLs), harmonic frequencies generate active power that is transmitted from the load to the source. The set of these harmonics can be represented by $N_C$. According to *CPC*, the current of HGL can be decomposed into five components:

$$\mathrm{i} = \mathrm{i}_a + \mathrm{i}_s + \mathrm{i}_r + \mathrm{i}_u + \mathrm{i}_c \tag{5.9}$$

All these current components can be defined as:

$$
\begin{aligned}
\mathrm{i}_a &= \sqrt{2}\,\mathrm{Re}\sum_{n\in N} G_e \mathrm{U}_{(n)} e^{jn\omega(1)t} \\
\mathrm{i}_r &= \sqrt{2}\,\mathrm{Re}\sum_{n\in N} jB_e \mathrm{U}_{(n)} e^{jn\omega(1)t} \\
\mathrm{i}_u &= \sqrt{2}\,\mathrm{Re}\sum_{n\in N} A_{(n)} \mathrm{U}^{\#}_{(n)} e^{jn\omega(1)t} \\
\mathrm{i}_s &= \sqrt{2}\,\mathrm{Re}\sum_{n\in N} \left(G_{e(n)} - G_e\right) G_e \mathrm{U}_{(n)} e^{jn\omega(1)t} \\
\mathrm{i}_c &= \sum_{n\in N_C} \mathrm{i}_{(n)}
\end{aligned}
\tag{5.10}
$$

where $\mathrm{i_a}$ is the active current representing the active power transfer to the load, $\mathrm{i_r}$ is reactive current representing the phase shift between voltage and current harmonics, $\mathrm{i_u}$ is the load current unbalance, $\mathrm{i_s}$ is the scattered current representing change of load conductance $G_{e(n)}$ with harmonic order, $\mathrm{i_C}$ represents the flow of active power from load towards source due to harmonic current, $\mathrm{U}^{\#}_{(n)}=[U_{(n)a}\ U_{(n)c}\ U_{(n)b}]^{\mathrm{T}}$ and $\mathrm{A_{(n)}}$ is the unbalanced admittance as reported in [122, 123, 125, 126].

Each of these current components contributes to the power losses independently. The compensation goal is such that the load appears ideal for the source. In this case, it will draw only useful active power. However, only the active power of positive sequence current and fundamental voltage is the useful power for most of the machine loads. Active power resulting from the negative sequence current and voltage and higher order harmonics contribute to the power and torque oscillations.

The asymmetrical source voltage can be decomposed into the positive and negative sequence components of fundamental harmonic $u^p{}_1$, $u^n{}_1$, and higher order harmonic components $u_h$ such that:

$$
\mathrm{u} = u_1 + \sum_{n\in N'} u_n = u_1^p + u_1^n + u_h \tag{5.11}
$$

where $N'$ represents the set without n=1. The active power can be decomposed into the same harmonic components so that:

$$
\mathrm{P} = P_1 + \sum_{n\in N'} P_n = P_1^p + P_1^n + P_h \tag{5.12}
$$

The active power of the positive sequence of the fundamental harmonic $P^p{}_1$ is named as working power in [122, 123] and is represented by $P_w$ such that:

$$
P_w = P_1^p = \left|u_1^p\right|\left|i_1^p\right| \tag{5.13}
$$

where $i^p{}_1$ is the current of minimum value called as working current $i_{\mathrm{w}}$. It provides the power $P^p{}_1$ at the source voltage $u^p{}_1$, and is represented by:

$$
i_w = \frac{P_1^p}{\left|u_1^p\right|^2} u_1^p = \frac{3U_1^p I_1^p \cos\varphi_1^p}{\left(\sqrt{3}U_1^p\right)^2} u_1^p = I_1^p \cos\varphi_1^p \frac{1}{U_1^p} u_1^p \tag{5.14}
$$

where $\varphi^p{}_1$ is the phase difference between the fundamental harmonics of the positive sequence of the voltage and current.

The rms value of the working current is therefore:

$$i_w = I_1^p \cos\varphi_1^p \tag{5.15}$$

When the working current is subtracted from the total load current, the remaining current is the non-useful current reported as detrimental current $i_{det}$ in [122], such that:

$$i_{det} = i - i_w \tag{5.16}$$

The CPL must inject the detrimental current into the power network so that the source only delivers the working current and will see the load as ideal. The *CPC* based reference signal generation scheme is shown in Figure 5.4. DFT is used to extract the magnitude and phase angles of the fundamental harmonics of the voltage at point of common coupling (PCC) and load current. The frequency domain algorithm makes it easy to calculate any harmonic component of the current or voltage. Working current is found using (5.15) and is subtracted from the active component of the load current. All the other components given in (5.10) are the part of detrimental current. *CPC* based reference signal generation scheme is not purely frequency domain approach. The detrimental current is specified in time domain and working current is calculated using frequency domain approach. Therefore, it is a hybrid reference signal generation technique.

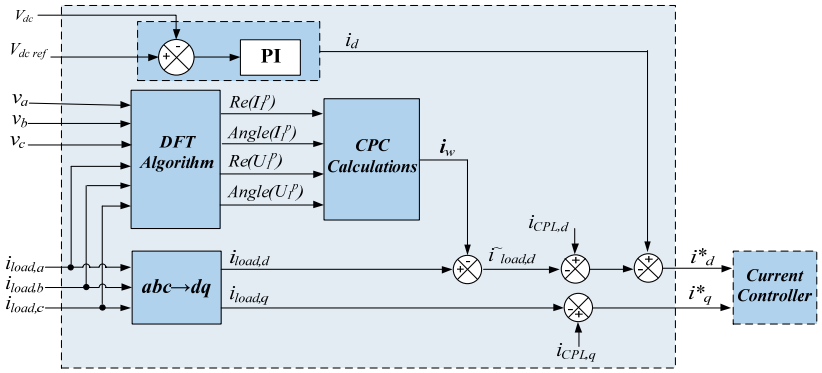


Figure 5.4: CPC based hybrid reference signal generation method

## 5.2 Active Power Filtering under Ideal Source Voltage

A simplified model of microgrid as depicted in Figure 5.5 is considered for simulation analysis under balanced source voltage. The model consists of an ideal voltage source, a CPL and a non-linear load. The non-linear load is an uncontrolled diode bridge supplying a resistive load. The system parameters are presented in Table 5.1. To investigate the effectiveness of CPL control for an unbalance and distorted PCC voltage, the source inductance $L_s$ of the phase-b is kept lower. CPL is used as APF using

the reference signals generated from both the time and frequency domain approaches presented in the previous section. Simulation parameters are kept identical for both methods.

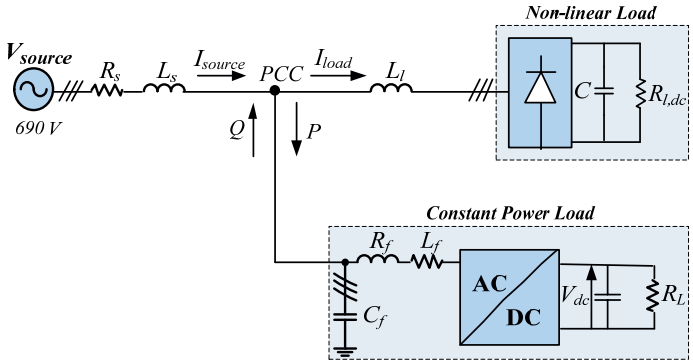


Figure 5.5: Model of the microgrid under investigation with CPL and non-linear load

Table 5.1: Simulation Model Parameters

| Parameter | Value |
|---|---|
| Rated frequency $f$ | 50 Hz |
| Rated Voltage $V_{s(L\text{-}L\ rms)}$ | 690 V |
| DC link Voltage $V_{dc}$ | 1126 V |
| DC link Capacitor $C$ | 4000 μF |
| Filter Inductance $L_f$ | 0.1 mH |
| Filter Resistance $R_f$ | 6 mΩ |
| Line Inductance $L_l$ | 0.8 mH |
| Load Resistance $R_{l,dc}$ | 4.15 Ω |
| $L_s$ (Phase a &c) | 0.75 mH |
| $L_s$ (Phase b) | 0.075 mH |
| Source Resistance $R_s$ | 0.2 Ω |
| P non-linear load | 161 kW (0.215 pu) |
| Q non-linear load | 53 kVar (0.07 pu) |
| $P_{CPL}$ | 150 kW (0.2 pu) |

### 5.2.1 Simulation Results for Time Domain Approach

In this section, the simulation results obtained from *IRP p-q* approach are discussed. Simulations are run for a total time of 0.6 second. At the very start, CPL is disconnected from the system and only the non-linear load is connected. At time $t$=0.2s, CPL is connected, however, it is acting only as APF and does not draw any power from the source. CPL injects the reference compensating current obtained from *IRP p-q* approach using (5.4). The main compensation objective is to eliminate the harmonics in the source current.

Figure 5.6 shows the source and non-linear load currents and PCC voltage before and after the compensation. The load and source currents before compensation are identical. However, after compensation the source current effectively becomes sinusoidal. Some harmonics in the PCC voltage can also be observed due to voltage drop across source impedance when harmonic current flows through it. After compensation, as source current harmonics are mitigated, the PCC voltage becomes perfectly sinusoidal as well, because now the voltage drop across the source impedance is also sinusoidal.

Figure 5.7a presents the non-linear load active and reactive components of currents that oscillate around a fixed value. The higher frequencies are filtered out and the filter output is shown by Figure 5.7b. These oscillating currents must be compensated to make the supply current sinusoidal along with the fixed reactive current component. CPL closely follows the reference signal (Figure 5.7c). The source current has reduced to a lower value because the CPL is now supplying the reactive power and harmonics demanded by the non-linear load.

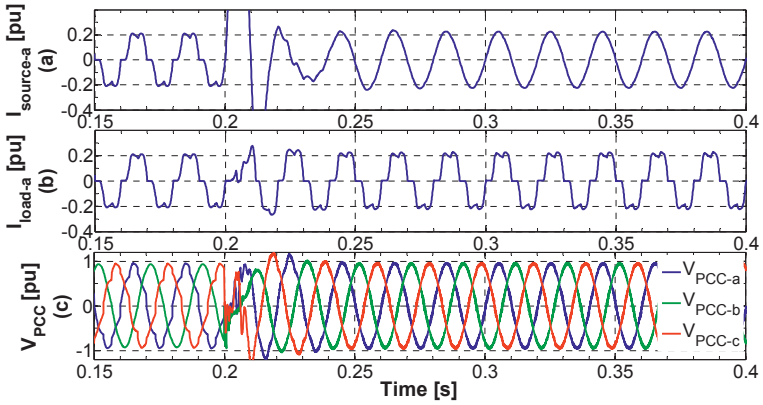


Figure 5.6: (a) Source current (b) Non-linear load current (c) Voltage at PCC

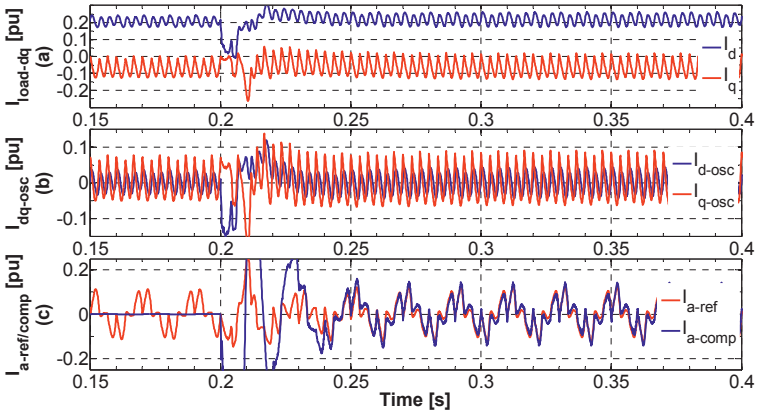


Figure 5.7: (a) Active and reactive components of non-linear load current (b) Oscillating active and reactive components after filtering (c) Phase-a of *IRP p-q* based reference current and compensating current by CPL

Figure 5.8 illustrates the simulation results when the CPL starts acting as an interface ensuring a constant power demanded by the load. The source is providing the active power demanded by the non-linear load only till time $t$=0.4s. The active power supplied by the source is almost doubled at time $t$=0.4s because of the CPL power requirement (Figure 5.8a) and the increase in source current is observed (Figure 5.8b). The amplitude of the PCC voltage is dropped as shown in Figure 5.8c because the increase in source current leads to a slightly more voltage drop across the source impedance.

THD of the source current is reduced from 23.5% to 2.05% as shown in time domain plot of Figure 5.9a when CPL is operating as APF only. This confirms that the lower frequency current harmonics having higher amplitudes are effectively compensated using *IRP p-q*. The distortion produced by the non-linear current across source impedance is effectively improved due to the improvement in source current waveform. The voltage THD is reduced from 10.5% to 1.3% as illustrated in Figure 5.9b.

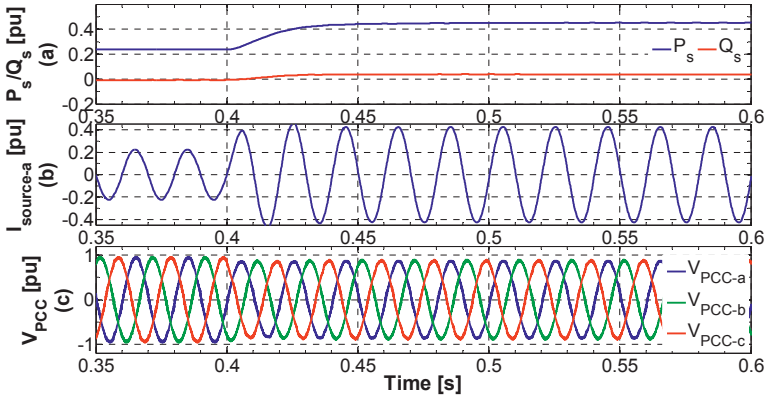


Figure 5.8: (a) Phase-a source current and PCC voltage for total simulation time (b) Source current (c) PCC voltage THD

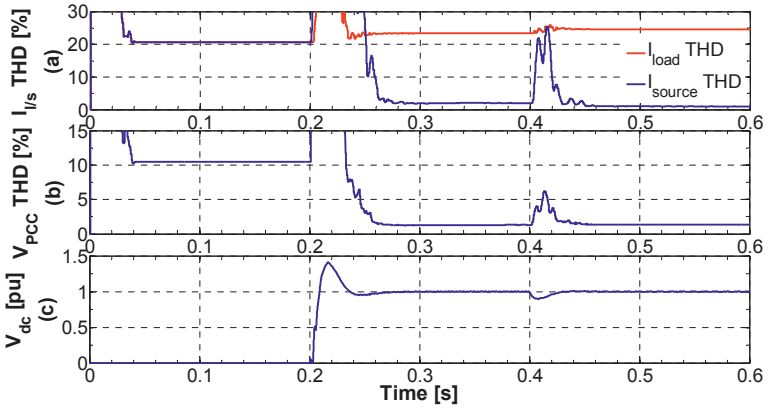


Figure 5.9: (a) Source and load current THD (b) PCC voltage THD (c) DC link voltage

At time *t*=0.4s, when CPL starts consuming active power from the source the THD of the source current is further reduced to 1.1%. The reason for this is the addition of perfect sinusoidal current drawn by the CPL to the total source current that has very small distortion due to CPL switching operation. Figure 5.9c shows that the DC-link voltage controller provides a very stiff control during the whole simulation period irrespective of CPL mode of operation. The voltage remains fixed to the specified value. Shunt active filtering as an ancillary service is an added feature of the CPL if its control is modified in accordance with the application requirements.

### 5.2.2 Simulation Results for Frequency Domain Approach

*CPC* based hybrid signal generation scheme has a major advantage over *IRP p-q* that it can separate the current into its components such as positive sequence, negative sequence and higher order harmonic current. In this way, it can compensate for the negative sequence fundamental and higher current harmonics when the loads are mainly induction or synchronous machines to avoid overheating in the machine windings.

Simulations are carried out for *CPC* based method for the same duration as in the case of *IRP p-q* approach. CPL does not consume power till time $t$=0.4s, like the previous case. Figure 5.10a shows the source current. After the compensation the source current reduces to the value of working current as specified by (5.15). CPL injects the amount of detrimental current represented by (5.16) to compensate for the reactive, scattered, unbalance and harmonic components of the non-linear load current as depicted in Figure 5.10b. The source current is exactly in phase with the voltage at PCC as shown in Figure 5.10c. The PCC voltage harmonics caused by the voltage drop across the source impedance are largely eliminated after the compensation by CPL.

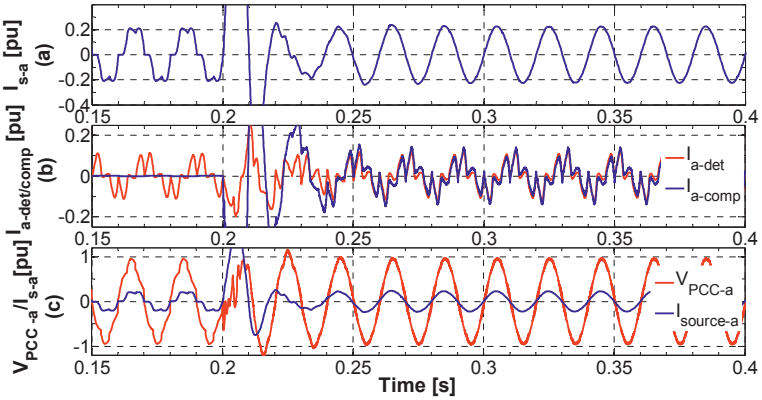


Figure 5.10: (a) Source current (b) Phase-a of CPC based detrimental current and compensating current (c) Phase-a source current and PCC voltage

THD in the source current is reduced from 23.5% to 1.46% as presented by time domain plot of Figure 5.11b when the CPL does not consume active power from the source. The PCC voltage THD is reduced from 10.5% to 1.15 % (Figure 5.11c). At time $t$=0.4s, CPL starts drawing constant active power. The sudden effect of it is the reduction in THD of the source current which reduces to 1.05% (Figure 5.11b). In fact, if CPL draws more active power, the source current THD will further reduce because the more fundamental current component will be added in the total source current. This means that tightly controlled loads in a microgrid not only provide shunt active filtering but they can additionally improve the source current shape by drawing a pure sinusoidal current as switching effects can be neglected. This higher source current results in more voltage drop across the source impedance and the voltage at PCC further reduces. This has been

indicated in Figure 5.11a. Therefore, CPL control needs to be very robust to withstand the drop in AC side voltage.

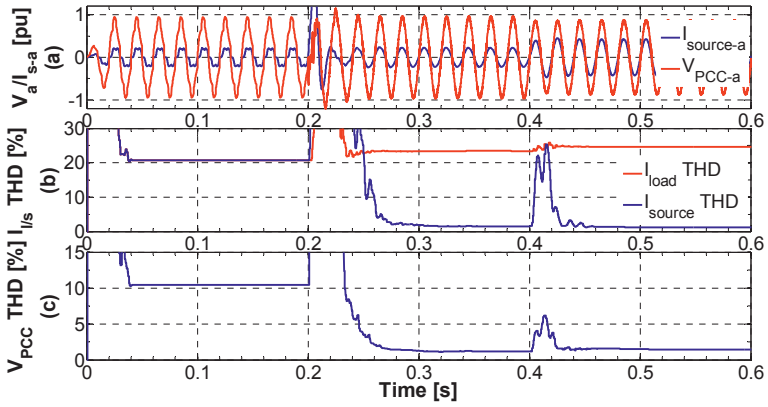


Figure 5.11: (a) Phase-a source current and PCC voltage for total simulation time (b) Source and load current THD (c) PCC voltage THD

## 5.3 Active Power Filtering under Non-Ideal Source Voltage Conditions

The simulation analysis presented in the previous section confirms that under ideal source voltage conditions, both the time and frequency domain reference signal generation techniques perform well. However, *IRP p-q* approach generates erroneous reference signals when the source voltage is unbalanced and distorted with harmonics. Equation (5.3) will yield incorrect values of the active and reactive powers because source voltage is polluted. The reference signal is corrected by using the fundamental positive sequence of the voltage in the CPL control that needs to be modified accordingly. CPC approach, however, is based on the extraction of fundamental components of currents called working current using FFT algorithm and is not affected by the source voltage unbalance.

### 5.3.1 CPL Control Modifications

The control structure of the CPL is modified to incorporate the positive sequence voltage detector. The fundamental positive and negative sequence voltage detection technique based on DSOGI-PLL has been discussed in detail in chapter 4. For the analysis under investigation we will adapt only the positive sequence extraction. The control structure is presented in Figure 5.12.

A dual SOGI-based QSG is employed for filtering and obtaining the 90° shifted versions from the $\alpha\beta$ voltages and (4.8) is used for the extraction of positive sequence voltage extraction. Positive sequence voltage calculator is shown in Figure 5.13.

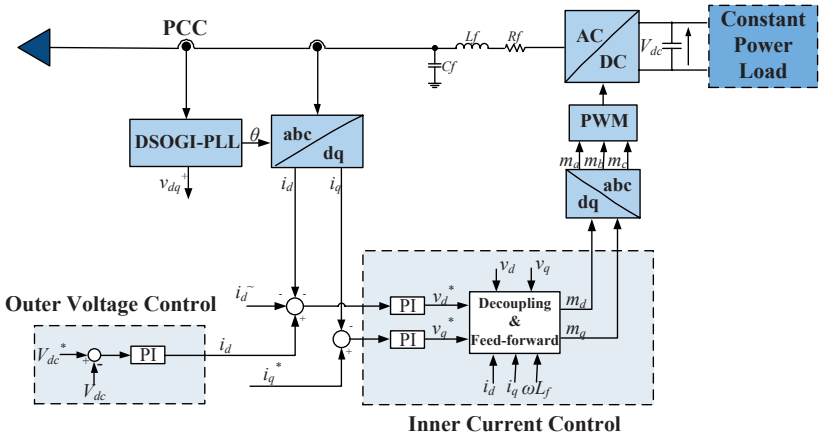


Figure 5.12: CPL control structure for non-ideal source voltage

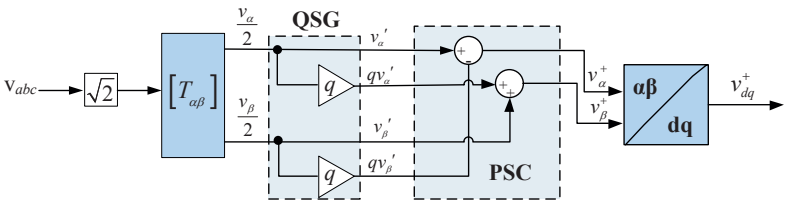


Figure 5.13: Positive sequence calculation in SRF

### 5.3.2 Simulation Model for Non-Ideal Voltage Conditions

The simulation model of the microgrid under non-ideal voltage conditions is shown in Figure 5.14. The source impedance is not considered in this case compared to the case with ideal source voltage discussed in previous section. The objective of this analysis is to make the CPL operate as APF under non-ideal conditions and the harmonics are directly added in the supply voltage using simulation software features. The addition of source impedance would further distort the voltage shape by adding a voltage drop in it. The distribution system parameters are presented in Table 5.2 and are kept identical for all the studied cases. The source voltage is unbalanced and polluted with harmonics and is represented by the following expression:

$$\mathbf{u} = \sum_{n=1}^{7} \begin{bmatrix} u_{(n)a} \\ u_{(n)b} \\ u_{(n)c} \end{bmatrix} = v_s \begin{bmatrix} \sin \omega t \\ 0.917 \sin(\omega t - 120^\circ) \\ \sin(\omega t + 120^\circ) \end{bmatrix} + 0.15 v_s \begin{bmatrix} \sin 3\omega t \\ \sin 3(\omega t - 120^\circ) \\ \sin 3(\omega t + 120^\circ) \end{bmatrix} + 0.1 v_s \begin{bmatrix} \sin 5\omega t \\ \sin 5(\omega t - 120^\circ) \\ \sin 5(\omega t + 120^\circ) \end{bmatrix} + 0.05 v_s \begin{bmatrix} \sin 7\omega t \\ \sin 7(\omega t - 120^\circ) \\ \sin 7(\omega t + 120^\circ) \end{bmatrix} \quad (5.17)$$

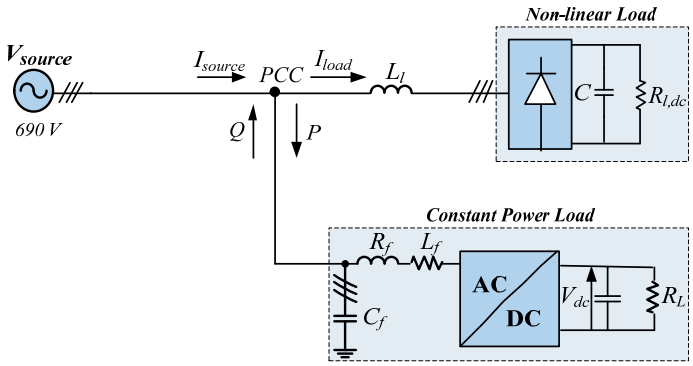


Figure 5.14: Model of the microgrid under investigation with a CPL and non-linear load under non-ideal source voltage

Table 5.2: Microgrid Parameters under Non-Ideal Voltage Conditions

| Parameter | Value |
|---|---|
| Rated frequency $f$ | 50 Hz |
| Rated Voltage $V_{s(L\text{-}L\ rms)}$ | 690 V |
| DC link Voltage $V_{dc}$ | 1126 V |
| DC link Capacitor $C$ | 4000 µF |
| Filter Inductance $L_f$ | 0.1 mH |
| Filter Resistance $R_f$ | 6 mΩ |
| Line Inductance $L_l$ | 0.8 mH |
| Load Resistance $R_{l,dc}$ | 4.15 Ω |
| $P_{\text{non-linear load}}$ | 167 kW (0.222 pu) |
| $Q_{\text{non-linear load}}$ | 78 kVar (0.104 pu) |
| $P_{CPL}$ | 150 kW (0.2 pu) |

### 5.3.3 Simulation Results for IRP p-q Approach

First the simulation results obtained from *IRP p-q* approach are discussed. The total simulation run time is 0.6 sec. Initially the CPL is not the part of system and only the non-linear load is connected, similar to the simulation analysis done in the previous section. At time $t$=0.2s, CPL is connected so that it acts only as APF and does not draw any power from the source. CPL injects the reference compensating current without incorporating the fundamental positive sequence voltage. However, as the input voltage is unbalanced and highly distorted (Figure 5.15a), the reference currents calculated by control algorithm are erroneous and it does not completely filter the current harmonics demanded by non-linear load as shown in Figure 5.15b. The source current is not sinusoidal. CPL closely follows the reference signal (Figure 5.16a). The source voltage THD level is 18.7%. THD of the source current is reduced from 21.8% to 12.92% as shown in Figure 5.16c. The lower frequency harmonics are still present.

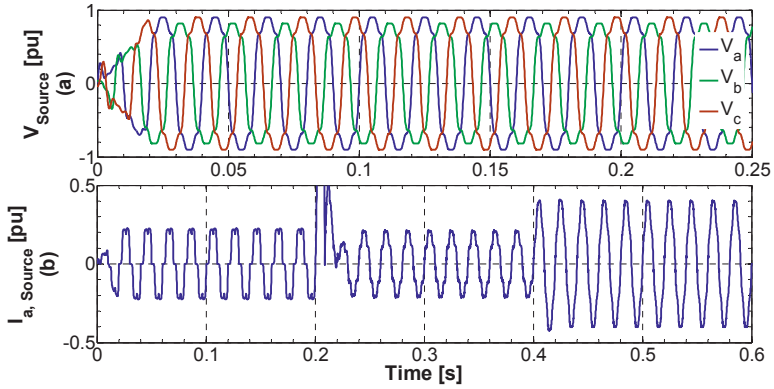


Figure 5.15: System voltages and currents (a) Distorted source voltage (b) Source current without positive sequence voltage inclusion in CPL control

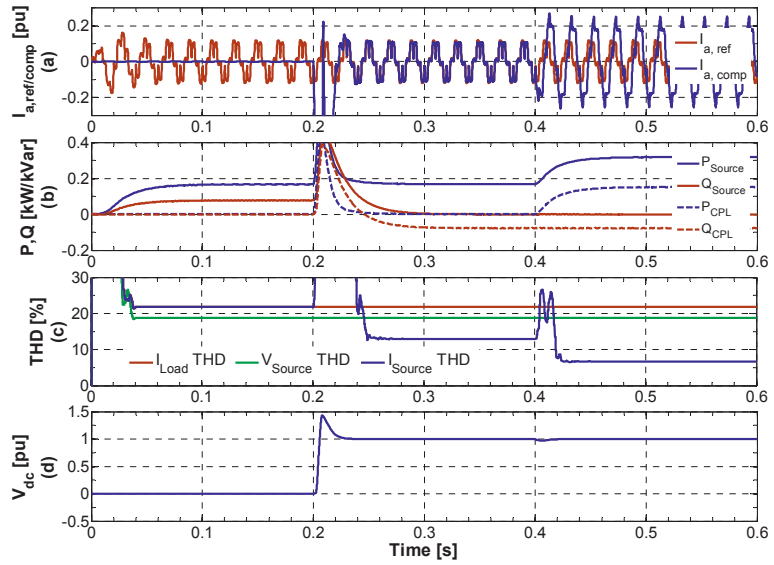


Figure 5.16: Simulation results for *IRP p-q* method without fundamental positive sequence voltage (a) Phase-a reference and compensating current (b) Source and CPL powers (c) THD for the source voltage, source current and load current (d) DC link voltage

At time $t$=0.4s, CPL starts consuming active power from the source. The total source current is increased as shown in Figure 5.15b. THD of the source current is further reduced to 6.72% due to the addition of perfect sinusoidal current drawn by the CPL to the source current. Figure 5.16c provides information about system powers. The source provides reactive power only when there is no active filtering provided by the CPL (Figure 5.16c). At time $t$=0.2s onwards, the source no longer supplies reactive power to the non-linear load and the CPL takes on this responsibility. It can be observed that the

input CPL active power remains constant under all the conditions. Figure 5.16d shows that the DC-link voltage controller provides a very stiff control. The voltage remains fixed to the specified value during the simulation.

Figure 5.17 presents the results for the *IRP p-q* approach when the fundamental positive sequence voltage is incorporated in the control algorithm presented by (5.3). In this case, the harmonics are affectively filtered and the source current THD reduces from 21.8% to 3.0% as shown in Figure 5.17c. When the CPL starts consuming the active power the source current THD is further improved and reduces to 1.48%.

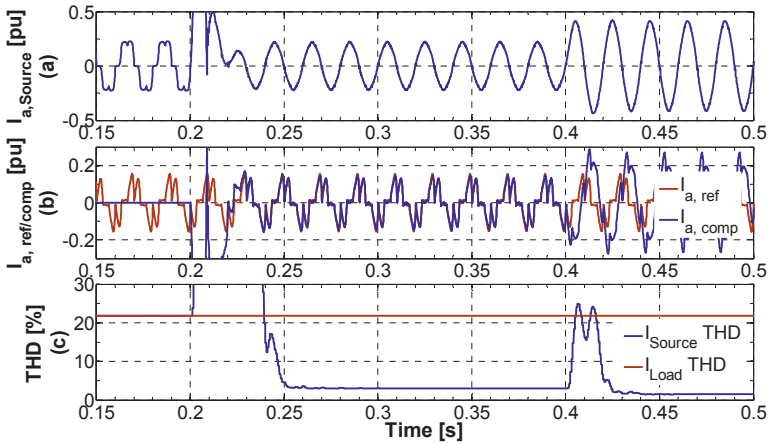


Figure 5.17: Simulation results for *IRP p-q* method with fundamental positive sequence voltage (a) Source current (b) Phase-a reference and compensating current (c) Source and load current THD

### 5.3.4 Simulation Results for d-q Approach

Instead of calculating the oscillating powers for the reference signal generation using (5.3), the time domain *d-q* approach extracts the reference currents for the converter control directly from the measured load currents using filters in SRF. The control of the converter becomes very simple as it avoids many power and current calculations. The CPL control however, needs the precise extraction of the positive sequence voltage to be used in PLL for phase angle calculation.

Figure 5.18 presents the simulation results obtained using time domain *d-q* technique. The CPL is connected to the distribution system at time $t$=0.2s and acts as APF only. It not only effectively compensates the harmonics in the source current, it also supplies the total reactive power required by the non-linear load. The source is only supplying the constant active power to the non-linear load. Figure 5.18a illustrates the different shapes of the source current during the simulation and the impact of harmonic and reactive power compensation on it. The source current THD is reduced from 21.8% to 2.54%, showing the effectiveness of the *d-q* reference signal generation scheme (Figure 5.18c). Figure 5.18b confirms how closely the CPL is following the reference signal, though the

source voltage is highly distorted. At time *t*=0.4s, the CPL acts as a regulated load and consumes the same amount of power as in the previous case. This leads to a further reduction in source current THD, which further comes down to 1.4% and is confirmed by Figure 5.18c.

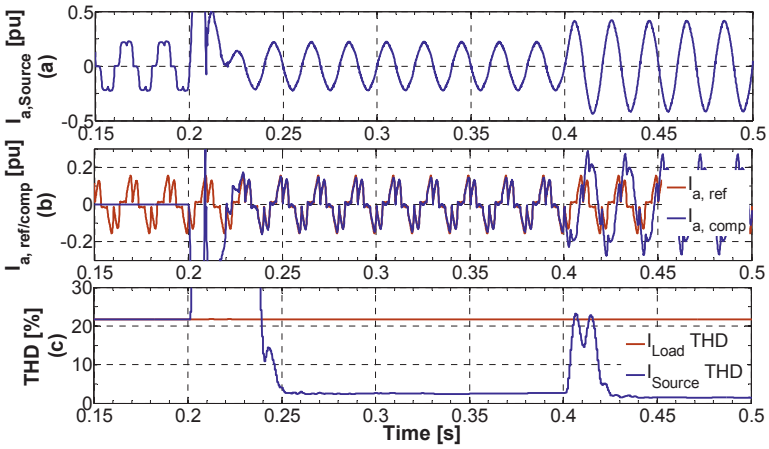


Figure 5.18: Simulation results for *d-q* method (a) Source current (b) Phase-a reference and compensating current (c) Source and load current THD

### 5.3.5 Simulation Results for CPC Approach

Simulations are carried out for *CPC* based method for the same duration as in the case of time domain approaches and the results are presented in Figure 5.19. CPL does not consume power till time *t*=0.4s. Figure 5.19a shows the source current after the reactive power and harmonic compensation using (5.16). The source current is affectively reduced to the value of working current as specified by (5.15). It is also exactly in-phase with the voltage at PCC. CPL control follows the value of detrimental current to compensate for the reactive, scattered, unbalance and harmonic components of the non-linear load current (Figure 5.19b). THD in the source current is reduced from 21.8% to 2.3% as presented by Figure 5.19c.

At time *t*=0.4s, CPL starts drawing constant active power. The sudden effect of it is the reduction in THD of the source current which reduces to 1.3%. The voltage harmonics are not compensated and the distortion in the source voltage is not due to the voltage drop across source impedance. Instead the source voltage is assumed to have fixed harmonics. The harmonics in the source voltage can only be mitigated using series voltage compensation. Shunt compensation, as in our case cannot achieve all the power quality targets.

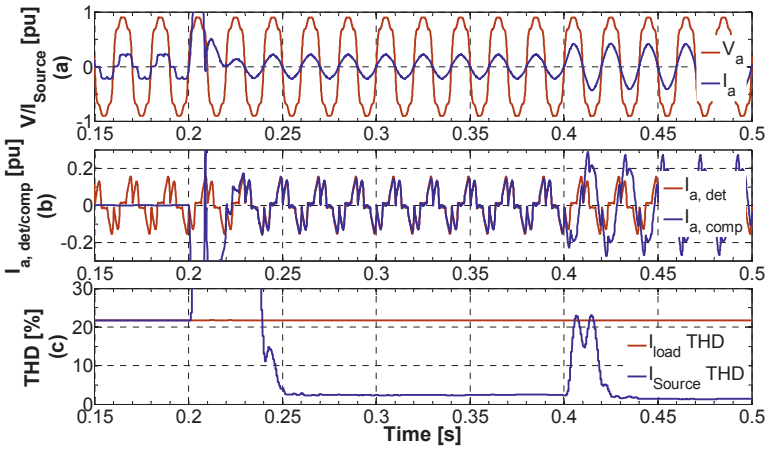


Figure 5.19: Simulation results for *CPC* method (a) Source current (b) Phase-a reference and compensating current (c) Source and load current THD

Appendix D presents the use of generation side PE interface for power quality enhancement. The study highlights the difference between the role of CPL and generation PE interface when employed as APFs in distributed energy systems.

## 5.4 Summary

This chapter explored the possibility of using CPL in an AC distribution system as shunt active filter. A tightly regulated VSC utilizing vector control method is used as a CPL. Generation of reference signal is achieved using both the time and frequency domain approaches. Hybrid reference signal generation approach based on CPC theory uses the time domain approach to measure the detrimental current while the working current is measured with frequency domain approach using DFT. CPL present in proximity of the non-linear load supplies the reactive and harmonic currents demanded by the non-linear load.

For ideal source voltage conditions, the simulation results obtained from the time domain *IRP p-q* approach using high pass filters show that the THD of the source current is reduced from 23.5% to 2.05%. CPL natural action further lowers the THD in the source current to 1.1% by adding a perfect sinusoidal term in the total source current. For *CPC* based frequency domain approach, THD of the source current reduces to a value of 1.05%. The harmonics in the PCC voltage due to the voltage drop in the source impedance are largely eliminated after the compensation performed with both the time and frequency domain approaches.

For non-ideal source voltage conditions, *IRP p-q* method generates erroneous reference signals for compensation and demands a positive sequence voltage detector. Therefore, a SOGI-QSG based PLL is employed in the control structure for the extraction of fundamental positive sequence voltage. The simulation results obtained from the time

domain *IRP p-q* and *d-q* methods using high pass filters show that the THD of the source current is reduced from 21.8% to 2.54%. Compensation of detrimental current by CPL using *CPC* approach reduces the source current to a minimum value called working current. Source current THD reduces to 2.3%. It further reduces to 1.3% when CPL starts consuming active power.

# 6 Conclusions and Future Work

*Some concluding remarks and few recommendations for future work are briefly discussed in this chapter.*

## 6.1 Conclusions

The main conclusions from the work presented above are grouped as follows:

### 6.1.1 CPL Control

Due to the inherent negative resistance instability issue associated with CPLs; the control structure needs to be robust. In this thesis, CPL is an active three phase full bridge rectifier utilizing IGBTs switches. Inner and outer controllers of the CPL are tuned using modulus optimum and symmetrical optimum methods respectively. Frequency and time domain study of the CPL controllers suggests that the proposed control and modelling approach for the CPL is effective. It has been shown through simulations that the negative resistance instability effects of the CPL can be minimized by the injection of reactive component of the current which supports the CPL terminal voltage.

### 6.1.2 Reactive Power Ancillary Service

CPLs have been considered as AC distribution system resources providing ancillary grid services in addition to acting as regulated load interfaces. The role of the distributed CPLs has been discussed for the transient stabilty enhancement of the distribution system. Transient stabilty margins have been investigated through simulations in the events of symmetrical grid voltage sags for different combinations of CPLs and IM loads. It has been observed that the the larger the number of CPLs that controls the reactive current, the higher the stability margin. The injection of reactive power during the grid voltage sag helps to keep the rotor speed well within the mechanical stabilty limits which otherwise could run out of stabilty due to excesive consumption of reactive power by the wind generator.

The provision of reactive power for the stability margins enhancement during grid contingencies demands an increase in the current rating of the PE converters. The incremental current rating of the PE converters in the case of ancillary reactive current

injection is studied and it is observed that the deeper the grid voltage sag, the higher the current rating required for the converter to maintain the generation system stability and avoid the possible disconnection.

A comparison between the current ratings of the distributed CPLs and conventional centralized STATCOM has been made to avoid the generation system disconnonection under voltage collapse. The comparison proves advantages to the distributed reactive current injection by the CPLs rather than using dedicated centralized STATCOM for this purpose.

The injection of reactive current results in a small decrease in the active current component by improving the voltage. At a certain operating point the total current for a CPL reaches to its minimum value before increasing again with further reactive injection. A theoretical study is carried out to find the minimum total branch current in a basic AC distribution feeder. It has been noticed that the amount of reactive injection increases with the increase in load power, grid impedance and voltage drop to achieve an optimal CPL current.

### 6.1.3 FRT Enhancement

Unbalanced FRT enhancement using CPLs has been introduced as an alternative to the existing compensation solutions. For a fixed speed SCIG-based wind farm, a dedicated STATCOM has been generally employed to mitigate the unbalanced grid faults and DFIG is the existing solution for variable speed wind farms. This service has been achieved using the installed CPLs in distribution system. A modification in the CPL control is proposed to extract and incorporate the positive and negative sequence of the voltage. DSOGI-PLL is employed in the control strategy for this purpose and the outer voltage control is modified with the incorporation of positive and negative sequence voltage controllers.

The positive sequence voltage compensation avoids the acceleration of the rotor beyond the mechanical stability limits and avoids possible voltage collapse. The negative sequence voltage control removes the torque and power oscillations in the generation system during the asymmetrical grid fault. This avoids the overheating in the stator windings and improves the life time of the generation system.

FRT enhancement by the CPLs comes at the cost of an increase in the current rating of the PE converters. The more severe the grid voltage sag and the unbalance in the system voltage, the higher the CPL current rating required for FRT enhancement. A comparison between the current rating of the distributed CPLs and a dedicated STATCOM for FRT enhancement indicates that each distributed CPL requires lower currant rating compared to one centralized STATCOM.

### 6.1.4 Power Quality Issues

CPL is used as APF to address the power quality issues in a distribution system polluted with the voltage and current harmonics. Time domain *IRP p-q* and frequency domain

*CPC* approaches are used to extract the compensating current in order to eliminate the harmonics in the source current under ideal and non-ideal voltage conditions. *IRP p-q* based control algorithm generates the erroneous reference signals under non-ideal voltage condition. A positive sequence voltage detector is employed in the CPL control structure.

For both ideal and non-ideal source voltage conditions, it has been observed that the harmonics in the source currents are removed using both the time and frequency domain approaches. *CPC* based control algorithm, however, provides slightly better results. When the CPL starts consuming active power from the source in addition to acting as APF the THD in source current is further decreased due to the addition of a fundamental current component in the total source current.

## 6.2 Recommendations for Future Work

An extensive research is still needed to take the presented work forward. In the following lines few recommendations are proposed.

### 6.2.1 Variable Speed DFIG-Based Wind Farm

The presented work in this thesis mainly focuses on the compensation methods for fixed speed SCIG-based wind farm. Variable speed DFIG-based wind farms are widely used as generation sources employing both the rotor and grid side converters for compensation objectives. CPLs can be used as additional standby compensators thereby sharing the compensation objectives alongside DFIG PE converters. This will reduce the current rating for both the generation and load PE interfaces.

### 6.2.2 Hosting Capacity

Due to the voltage control provided by CPLs, more such loads can be hosted by the network although they have negative resistance instability associated with them. A theoretical investigation is required to find out the critical share of CPLs in a microgrid for balanced/unbalanced grid fault mitigation and other additional grid services. A comprehensive stability study of such a network is also worth doing.

### 6.2.3 Power Quality Issues with High Share of CPLs

This work addressed the power quality issues in a basic distribution system comprising of a CPL which acts as APF. It can provide a foundation to address the power quality issues in a more complex distribution system comprising of many CPLs acting as APFs. A mechanism for sharing the reference current or power between the CPLs can be established resulting in a reduced current rating for each device.

### 6.2.4 Loss Minimization Algorithm for a Microgrid

Loss minimization method presented in this work can be extended to a microgrid comprising of many active and passive loads and generation PE interfaces. The theoretical study presented in this work can be extended to a specific case with reduction of total current and minimum losses as objective function. The control system of each device must be adaptive to the changes in the voltage in response to reactive injection for optimal current.

# Appendices

# A System Parameters and Per Unit Value

*The details of the basic AC distribution system have been discussed in the appendix A. Per unit system used for the simulations has been described and the parameters for the different components comprising the distributed system have been presented.*

AC distribution system discussed in this thesis is composed of a wind turbine utilizing a SCIG for power generation, PE load interfaces, a medium voltage grid, transmission and distribution lines and transformers. Parameters of the all the components of the system have been discussed in details in per unit quantities to make the simulation analysis appear simple.

## A.1 Per Unit System

The implementation and design of the control system of the VSC based CPLs becomes simple by using the per unit (pu) system. In this way, it is easy to determine the real value of a generic quantity by multiplying it with a reference value. First of all, it is essential to choose a reference power and reference voltages. Then the reference currents and impedances can be calculated. This is very common method to select the base values in the electric drives research area [88]. The following reference values have been selected for the system under investigation:

$$S_b = 800\ [kVA]$$

$$V_{b1} = \sqrt{\frac{2}{3}}.690 = 563.38\ [V]$$

$$V_{b2} = \sqrt{\frac{2}{3}}.22000 = 17962.92\ [V]$$

$$\omega_b = 314.159\ [\text{rad/s}]$$

where $S_b$ is the nominal power, $V_{b1}$ and $V_{b2}$ are the primary and secondary side voltages of the main transformer, and $\omega_b$ is the base frequency. The base impedance and current referred to the primary side are given as:

$$Z_{b1} = \frac{V_{b1}^2}{S_b} = 0.595\ [\Omega]$$

$$I_{b1} = \frac{V_{b1}}{\sqrt{3} \cdot Z_{b1}} = 669.5\ [A]$$

The values referred to the secondary side are the following:

$$Z_{b2} = \frac{V_{b2}^2}{S_b} = 605\ [\Omega]$$

$$I_{b2} = \frac{V_{b2}}{\sqrt{3} \cdot Z_{b2}} = 21\ [A]$$

In order to prevent the over-modulation, the DC-link voltage must always be greater than 1.35 times the value of base voltage [88], such that:

$$V_{dc} = 2 \cdot V_{b1} = 1126.77\ [V]$$

The lower value of the DC link voltage will result in serious instabilities in the VSC operation. DC side base current is given by:

$$I_{dc.base} = \frac{3}{4} \cdot I_{b1} = 710\ [A]$$

DC base impedance is calculated as:

$$Z_{dc.base} = \frac{V_{dc}}{V_{dc.base}} = 1.587\ [\Omega]$$

## A.2 Squirrel Cage Induction Generator

An induction machine can operate in either generation or motoring mode. The mode of operation is determined by the sign of the mechanical torque. Positive mechanical torque indicates motoring operation while negative value of the torque represents generation mode. A fixed speed SCIG and a capacitor bank for magnetization, form the DG in the system of Figure 3.1. Need for a separate source of magnetizing reactive power is a main disadvantage of induction generators and, therefore, they are not a preferred choice to be used as sources of electrical power. Synchronous generators are the widespread means of electric power generation. However, small generators used to supply a farm or residence or an industry from wind energy can be SCIGs. Induction generators draw their magnetizing reactive power from the utility system in the absence of capacitor bank at their terminal and generate electrical power for the local load and/or supply power to the utility system. In Europe, SCIG based wind farms represent a

considerable 30% of the installed wind power and they need a compensating device in order to increase the power system stability and reliability [131].

The capacitor bank provides the magnetization to SCIG for the smooth operation. Its value is adjusted in such a way that nominal voltage at the generator terminal can be fixed to1.0 pu for the operation in steady state. The value found is 260 kVar. This value along with the generator power gives the apparent value of 794 kVA, which is very close to the chosen reference value. The value of power factor is, therefore, 0.944.The parameters of induction generator are presented in Table A.1.

Table A.1: Induction Machine Parameters

| Parameter | Value |
|---|---|
| Nominal power | 750000 [W] |
| Nominal voltage | 690 [$V_{rms}$] line to line |
| Nominal current | 628 [$A_{rms}$] |
| Nominal frequency | 50 [Hz] |
| Pole pairs | 2 |
| Stator resistance $R_s$ | 0.0092 pu |
| First cage resistance $R_r$ | 0.0076 pu |
| Second cage resistance | 10 pu |
| Second cage reactance | 10 pu |
| Mutual inductance | 3.8693 pu |
| Stator leakage inductance | 0.1580 pu |
| Rotor mutual inductance | 0.0651 pu |
| Polar moment of inertia H | 0.5 s |
| Mechanical damping F | 0.008 |

## A.3 Three Phase Transformer

Two transformers in Y-Δ configuration are shown in Figure 3.1. This configuration produces a phase shift. Y-winding is a primary winding with a voltage level of 690 V while Δ-winding is secondary winding and operates at 22 kV. Star point of the Y-winding is grounded. Magnetization and saturation currents are neglected. Table A.2 presents the transformer parameters.

Table A.2: Parameters of the Three Phase Transformer

| Parameter | Value |
|---|---|
| Nominal power | 800000 [$VA$] |
| Nominal frequency | 50 [Hz] |
| Winding 1 type | Y |
| Winding 1 nominal voltage | 690 [$V_{3ph\ rms}$] |
| Winding 2 type | Δ |
| Winding 2 nominal voltage | 22000 [$V_{3ph\ rms}$] |
| Δ lags or leads Y | Lags |
| Positive leakage reactance | 0.06 [pu] |
| Ideal transformer model | Yes |
| No load losses | 0.001 [pu] |
| Copper losses | 0.01 [pu] |
| Saturation enabled | No |

## A.4 Medium Voltage Grid and Lines

The induction generator is connected to a medium voltage grid through a three phase transmission line. The inductance of the transmission line is chosen to be 1mH/km. The lines length for this type of system can extend to tens of kilometres depending upon the maximum acceptable losses.The main grid is a three phase AC source with impedance. Resistances of the transmission lines are small compared to reactance so they are neglected. The inductance $L_p$ and resistance $R_p$ of the distribution line is assumed to be 1 mH and 0.1 Ω per kilometre respectively [132]. Capacitances between lines and the ground are neglected. Parameters of main grid and lines are given in Table A.3.

Table A.3: Parameters of the Power Grid and Lines

| Parameter | Value |
|---|---|
| Nominal voltage | 22 [k$V_{rms}$] line to line |
| Nominal frequency | 50 [Hz] |
| Resistance | 2 [Ω] |
| Inductance | 0.2 [H] |

## A.5 Summary

The different components of the AC distribution system under consideration have been discussed. The design and implementation of the control system of the CPLs is easier using the pu system. Reference power and reference voltages have been selected. Then the reference currents and impedances are calculated. Different modes of operation of the fixed speed SCIG have been briefly discussed. Some advantages and disadvantages of using the SCIG have been presented. However, SCIG-based wind turbines represent a significant percentage of the total installed wind power in Europe. Magnetization

requirements of the SCIG have been calculated. Parameters of the three phase transformers, medium voltage grid and transmission and distribution lines have also been discussed.

# B Stability of DC Link Voltage Controller

*The details of the CPL control structure under reduced AC side voltage have been discussed in the appendix. A frequency domain analysis is performed for different values of the AC side voltage and the response of the DC link voltage control is observed. Simulations are carried out on a basic system to investigate the impact of AC voltage sags on the CPL control.*

CPL control structure and modelling has been discussed in detail in chapter 2. The transfer functions for the CPL controllers have been derived and the tuning rules for the identification of controller parameters have been suggested. The transient stability of the power system has been addressed in chapter 3 for different cases. However, the stability of the CPL controllers has not been discussed in detail when there is a reduction in AC side voltage. The following sections present the frequency and time domain investigation to identify the robustness of the DC link voltage control.

## B.1 Frequency Domain Analysis under Reduced AC side Voltage

The open loop transfer function of the DC link voltage controller presented in (2.50) is independent of the value of the grid voltage. However, for the real online systems there are always delays in the control system and the changes in the converter control parameters are not modified instantaneously. The controller parameters are kept the same as calculated for steady state operating conditions. Only the values of $K$ will be modified. For a 20% drop in AC side voltage we have:

$$K = \frac{v_d}{V_{dc}} = 0.8$$

The transfer function for this condition therefore becomes:

$$H_{V,OL}(s) = \frac{0.0018s + 1}{0.27 \times 10^{-9} s^3 + 1.35 \times 10^{-6} s^2}$$

Bode plot for this case is shown in Figure B.1. There is a small reduction in the phase margin compared to the steady state operating conditions (Figure 2.17). The value of phase margin is 52˚ and it occurs at a frequency of 1.38e+3 rad/s. The cross over frequency has also decreased compared to the steady state case. The DC link voltage control is still stable under reduced voltage conditions. The high value of the phase margin suggests that the system is robust as well.

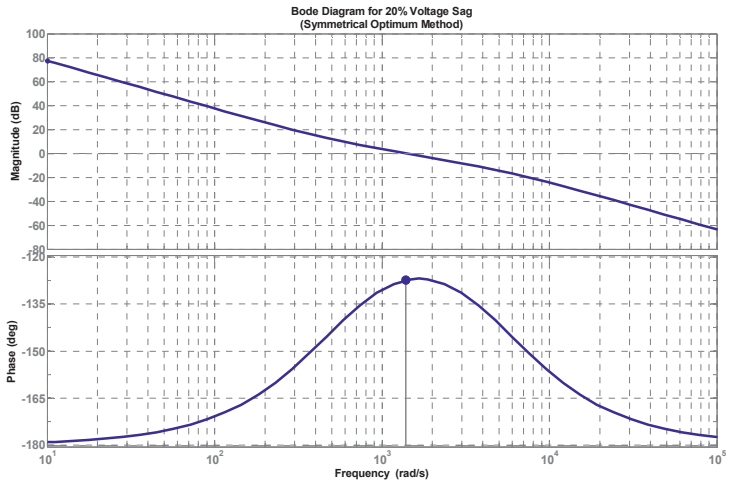


Figure B.1: Bode plot for DC link voltage controller for $v_d$=0.8 pu

Bode plot for 60% drop in AC side voltage is shown in Figure B.2. The phase margin is further reduced to 46˚ and is just greater than the acceptable limit of 45˚. The margins show that system is still within the stable operating conditions [89]. However, any further drop in voltage will result the system to be unstable and a voltage collapse is obvious.

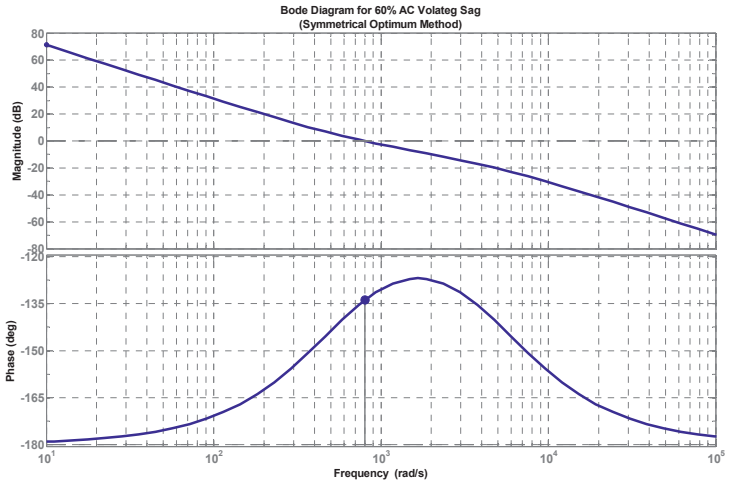


Figure B.2: Bode plot for DC link voltage controller for $v_d$=0.4 pu

Bode plot for 70% drop in voltage as presented in Figure B.3 confirms that the phase margin is 42˚ and the gain margin is infinite. The value of the phase margin is lower than the acceptable value for the stable operation of a system. It is obvious that the stability of the system is compromised with the reduction in grid voltage to this level.

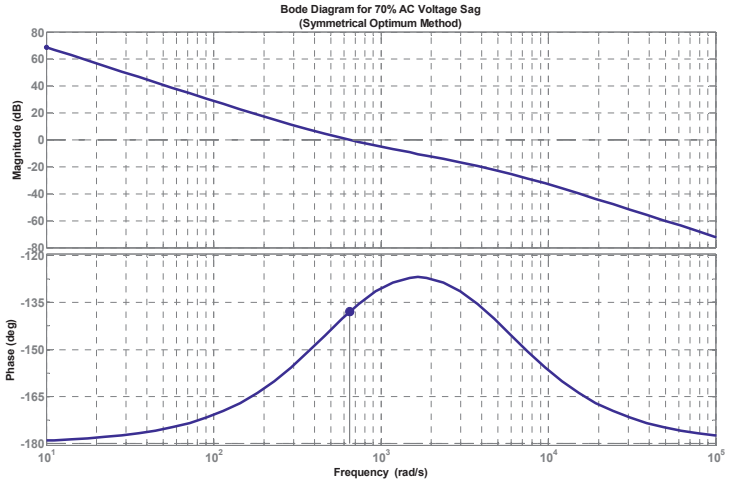


Figure B.3: Bode plot for DC link voltage controller for $v_d$=0.3 pu

## B.2 Simulation Results

The controller parameters found from the tuning methods are incorporated in the control system of the CPL. A simulation study is done to verify the results from the analytical

study. The system used for the simulation analysis is shown in Figure B.4. It consists of a CPL and an ideal grid. The induction generator shown in the system of Figure 3.1is removed for this analysis. The presence of induction generator makes it impossible to distinguish between the instability caused by the converter control and the transient instability following a major grid side disturbance. Transient stability analysis of the power system is performed in chapter 3 where a weak grid with a very high overall inductance results in a less stable system under grid voltage sags. Therefore, in the case presented here, an ideal grid is used to investigate the CPL's control stability. The effectiveness of the converter control strategy and its impact on the system stability can only be judged through simulations when all the other destabilizing factors are removed from the system. For these simulations, the CPL draws 300 kW of active power from the ideal grid.

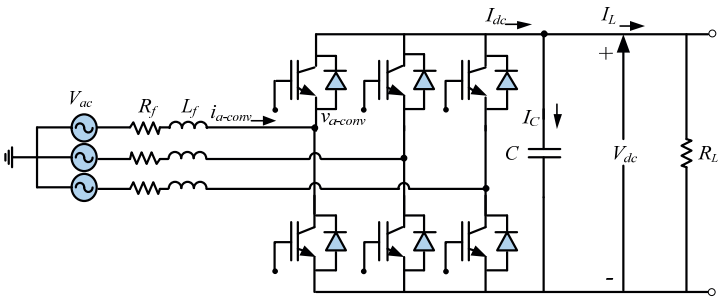


Figure B.4: CPL with an Ideal Grid

Simulations are performed for the steady state conditions. The total duration of the simulation is 4 seconds. The results are shown in Figure B.5. The grid voltage is 1.0 pu and the corresponding value of the DC link voltage is also maintained to 1.0 pu. There is a small overshoot and initial transients in the DC link voltage before settling down to the given reference value. The performance of the system is very stable and the outer voltage controller is following the reference value.

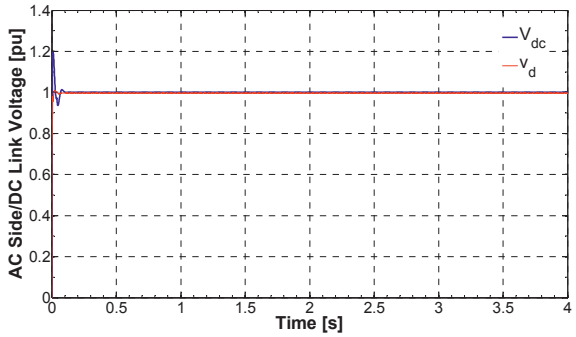


Figure B.5: AC/DC side voltages for steady state operation

The grid voltage is reduced by 20% and 60% respectively and the simulations are repeated to see its impact on the control system. Figure B.6 and Figure B.7 show the simulation results. As can be observed that the control system is still able to maintain the DC link voltage to the specified value of 1.0 pu. The simulation results are very much in accordance with the frequency response of the open loop transfer function of the DC link voltage controller performed under the same AC side voltage dips and presented in the previous section. However, for the 60% drop in voltage the initial transient in the DC link voltage lasts for a relatively longer time before settling to the specified value.

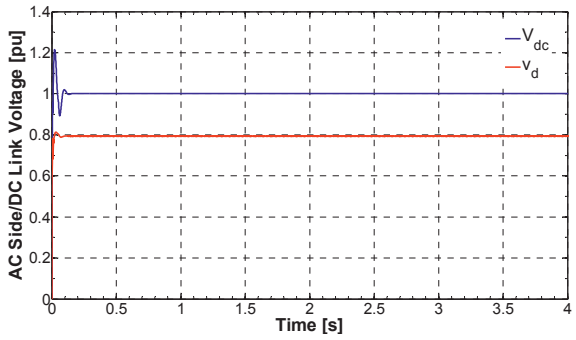


Figure B.6: AC/DC side voltages for 20% grid voltage sag

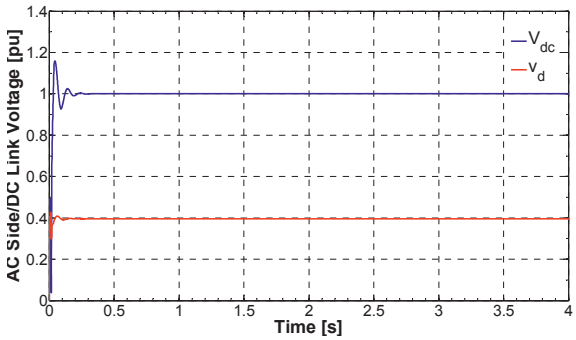


Figure B.7: AC/DC side voltages for 60% grid voltage sag

When the AC side voltage is reduced to 0.3 pu the DC link voltage collapses (Figure B.8). It has been earlier confirmed by the bode plot under the same condition showing the lower value of the phase margin than acceptable limit. At the start of the simulation converter control system tries to maintain the DC link voltage to the specified reference value of 1.0 pu. However, it fails to hold the voltage and a DC link voltage collapse occurs. The DC link capacitor then charges to a value of 0.18 pu for the rest of the simulation. This result also confirms that the input AC voltage must always be kept higher than 0.3 pu for the stable operation of the converter control system. This condition however applies only for the system under consideration to see the stability

and robustness of the CPL control structure. The distribution systems presented in chapter 3 incorporate an induction generator along with a medium voltage grid with a reasonable value of inductance. In such system, the transient stability becomes much important than the stability of the PE interface.

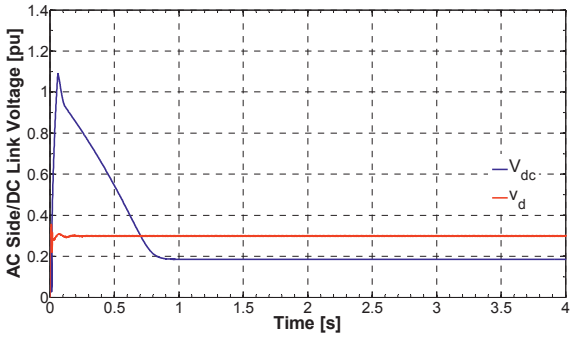


Figure B.8: AC/DC voltages for 70% grid voltage sag

## B.3 Summary

A frequency domain analysis is carried out under different AC side voltage sags and the open loop transfer functions of the DC link voltage controller are plotted. It has been observed that the phase margin reduces with the reduction in AC side voltage. For a 60% drop in AC side voltage, the phase and gain margins are within the acceptable limits. However, when the grid voltage is reduced further, the frequency domain analysis shows a low phase margin and a collapse in DC link voltage is observed through simulations.

# C Generation System Dynamics

*The details of generation system parameters under balanced and unbalanced grid faults are discussed in this appendix. Generation dynamics and grid side powers are first discussed for transient stability analysis. Then the results for asymmetrical grid faults are discussed for different cases of voltage support by the CPL.*

The generation system dynamics play an important role when CPLs are providing the reactive current for transient stability improvement and FRT enhancement under different grid contingencies. In order to enhance the understanding of the analysis presented in chapters 3 and 4, some of the simulation results are presented in following sections.

## C.1 Transient Stability Analysis

Some parameters of the AC distribution system for transient stability analysis are presented in this section. These include the reactive power, speed and the torque for different simulation conditions.

### C.1.1 CPLs without Reactive Injection

Figure C.1 illustrates the reactive power absorbed by the generation system when the CPLs are not injecting reactive current during the fault. It can be observed that before the fault occurs the reactive power consumption is negligible. When the fault occurs the generation system consumes reactive power from the utility and it keeps on increasing leading to a complete voltage collapse at the distribution level. When the fault is cleared the pre-fault value of the reactive power is not restored.

The rotor speed is represented in the plot of Figure C.2. The steady state value is equal to 1.005 pu which means that the machine is working as a generator. Therefore, a negative slip is obtained. As shown in the plot, the rotor accelerates during the fault and a mechanical unstable point is obtained. The distribution system stability is lost. The rotor speed keeps on increasing after the fault is cleared.

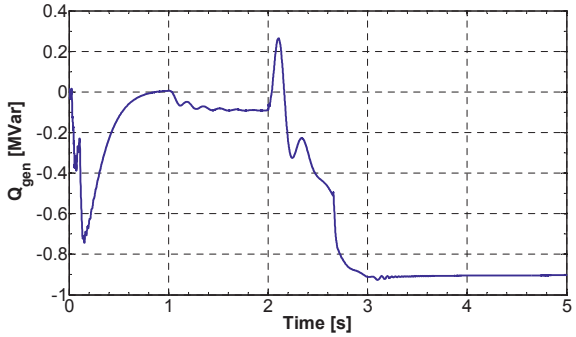


Figure C.1: SCIG reactive power

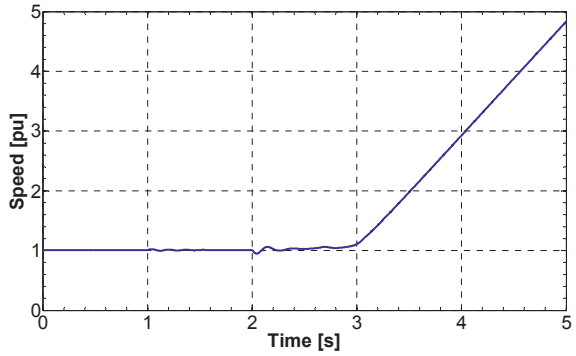


Figure C.2: Rotor accelerating during and after the fault

Figure C.3 shows the electromagnetic and mechanical torque of the SCIG. The electromagnetic torque achieves the steady state value equal to -1.0 pu after a transient lasting for 2 seconds. For the first second during the simulation, the machine control is adjusted to speed control and at time $t$= 1s the torque control is implemented. This initial trend depends on how the simulation software initializes the operation of the machine. The electromagnetic torque has to balance the mechanical torque in order to keep the rotor speed constant. The relationship between the electromagnetic torque and the rotor speed is presented as:

$$T_{mech} - T_{el} = J.\frac{d\omega}{dt} \tag{C.1}$$

where $T_{mech}$ is the mechanical torque, $T_{el}$ is the electromagnetic torque, $J$ represents the moment of inertia and the $\omega$ is the rotor speed. At steady state, the electromagnetic torque and the mechanical torque are almost identical, thus the speed derivative is equal to zero this means that the speed is a constant. However, when the fault occurs the rotor accelerates and the machine loses the control of electromagnetic torque as shown in (C.1). When the fault is cleared the machine is not able to recover the pre-fault value of the electromagnetic torque.

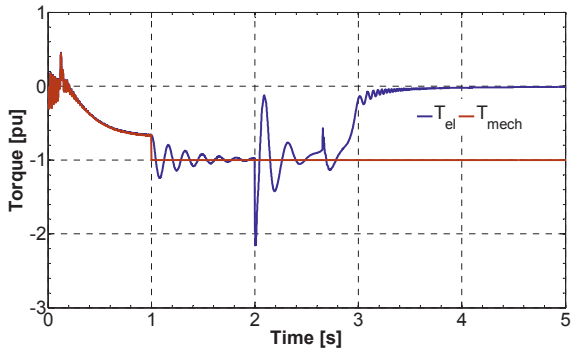


Figure C.3: SCIG losing torque control during and after the fault

### C.1.2 CPLs with Reactive Injection

Figure C.4 shows the rotor speed before and after the fault. During the fault the speed increases as the machine is consuming reactive power form the utility. However, the reactive injection during the fault keeps the rotor acceleration within the tolerable limits so that the machine does not run out of mechanical stability. The rotor speed recovers back to its pre-fault value when the fault is cleared after a transient which lasts for 1 second.

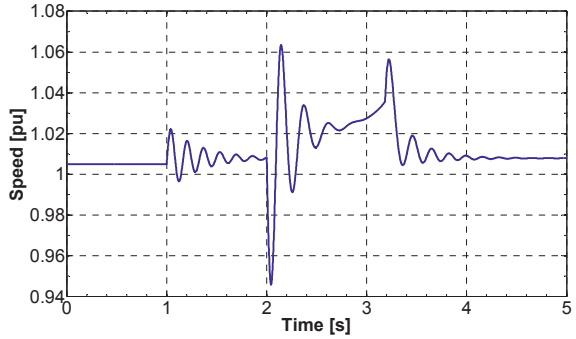


Figure C.4: Rotor speed recovery

Machine torque under reactive injection is presented by Figure C.5. The torque settles to a value of 1.0 pu after an initial transient. During the fault, the generator does not lose control of electromagnetic torque and it follows the mechanical torque. After the fault is cleared the machine regains the specified value of the torque for its normal operation. The oscillation in the speed and torque of the machine can be further reduced by increasing the value of the moment of inertia.

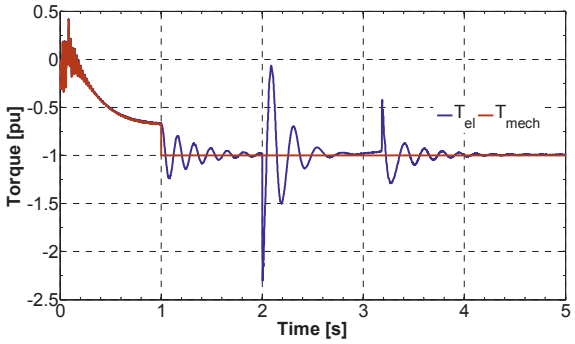


Figure C.5: Torque recovery during and after the fault

## C.2 Asymmetrical Grid Faults

Some of the system parameters for the FRT analysis performed in chapter 4 are presented in the following sections for different cases of voltage support by the CPLs. PCC voltage and generation/grid side powers are the system parameters that must be explained to understand the system behaviour for different voltage support methods.

### C.2.1 No Voltage Support

For the asymmetrical grid faults, the active and reactive powers on the generation side are presented by Figure C.6. CPL is not providing voltage support at this point. The SCIG is producing the rated active power after the initial transient dies out. During the fault at time $t$=2s, the oscillations of double grid frequency are present due to the interaction of opposite current and voltage sequences. SCIG consumes reactive power during the fault and terminal voltage decreases. After the fault is cleared, the powers retain their pre-fault values after a transient.

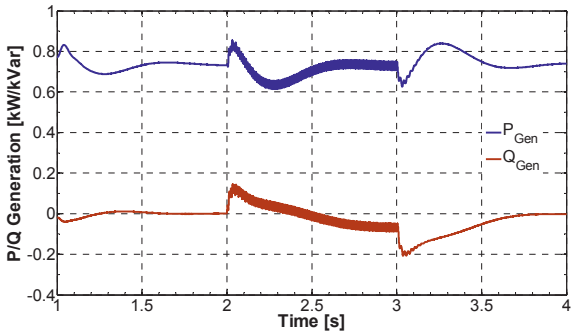


Figure C.6: SCIG powers without voltage support during the fault

Figure C.7 shows the grid side powers without any voltage support. The CPL is consuming 225 kW from the generation system and the rest of the power is being exported to the grid. The oscillations are visible during the fault. The powers regain the pre-fault value after the fault is cleared at time $t$=3s.

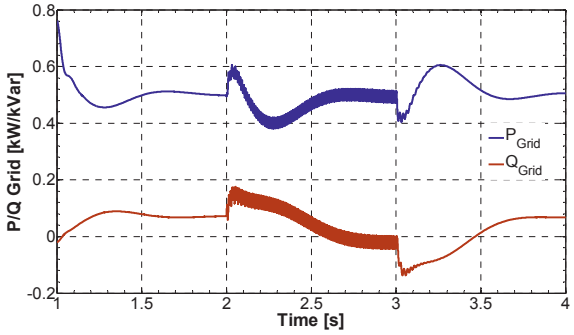


Figure C.7: Grid side powers without voltage support during the fault

## C.2.2 Positive Sequence Voltage Support

The phase voltages at PCC are shown in Figure C.8 when positive sequence voltage support is being provided. The voltage unbalance is clearly visible as the negative sequence of the voltage stays in the system. The generator and grid side powers are shown in Figure C.9 and Figure C.10 respectively. It can be seen that the positive sequence voltage control compensates for the reactive power during the fault and the value stays around pre-fault value (Figure C.9). The negative sequence present in the system, however, results in the power oscillations during the fault.

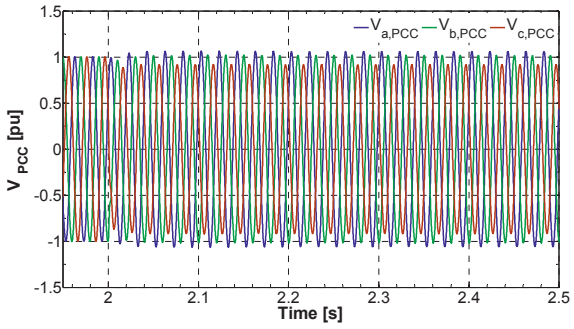


Figure C.8: PCC voltages with positive sequence voltage support

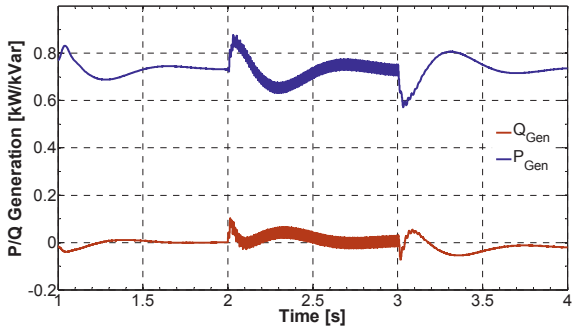


Figure C.9: SCIG powers with positive sequence voltage support

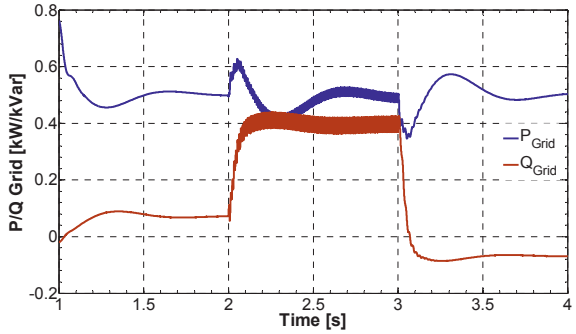


Figure C.10: Grid side powers with positive sequence voltage support

### C.2.3 Negative Sequence Voltage Support

The phase voltages at PCC are shown in Figure C.11 with negative sequence voltage compensation only. The unbalance in the voltage is largely eliminated. Figure C.12 shows the generator powers for the negative sequence voltage support. The oscillations in the active and reactive powers are clearly removed due to the compensation of unbalance present in the system. The SCIG still consumes reactive power during the fault as the positive sequence voltage drop increases during the fault. It recovers the pre-fault values after a transient when the fault ends. The grid side powers are shown in Figure C.13. On the medium voltage side, the effects of the fault are present and the oscillation in the powers can be observed. The magnitude of the oscillations is high because of the addition of the injected powers by the CPL during the fault to compensate for the negative sequence.

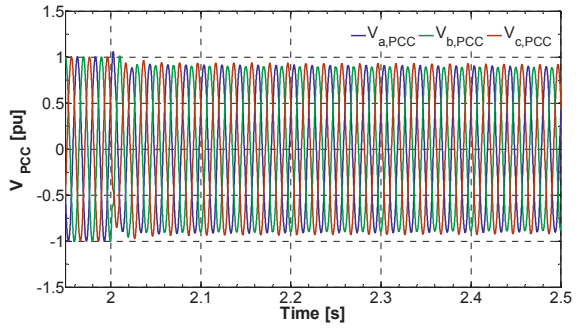


Figure C.11: PCC voltages with negative sequence voltage support

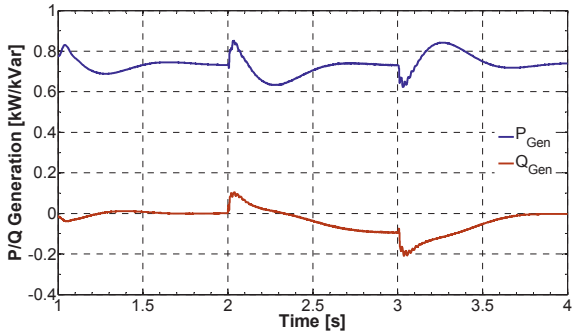


Figure C.12: SCIG powers with negative sequence voltage support

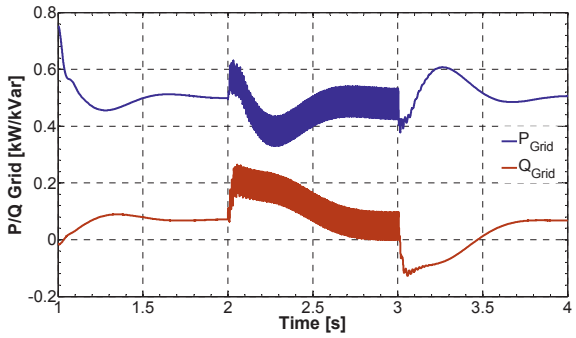


Figure C.13: Grid side powers with negative sequence voltage support

## C.2.4 Positive and Negative Sequence Voltage Support

For the case of coordinated positive and negative sequence voltage support, the phase voltages at the PCC are presented in Figure C.14. The magnitude of the voltage is restored to the pre-fault value as a result of the voltage support for both the sequences. The unbalance present in the system is effectively removed. The oscillations in the generation side powers are no more present (Figure C.15) and the reactive power

consumption by the induction machine during the fault is largely controlled. The result is the reproduction of the pre-fault voltage value. The oscillations in the grid side powers are increased due to the injected oscillating powers by the CPL during the fault as presented by Figure C.16. The removal of oscillations avoids heating in the machine winding and ensures better operational life for the equipment.

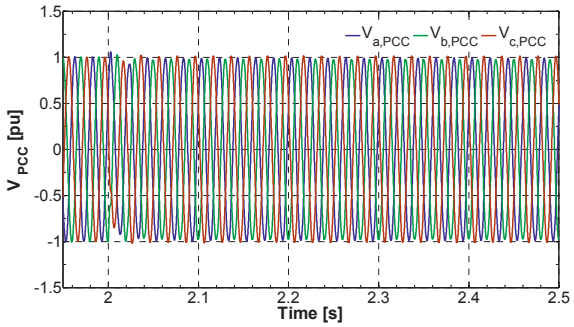


Figure C.14: PCC voltages with both positive and negative sequence voltage support

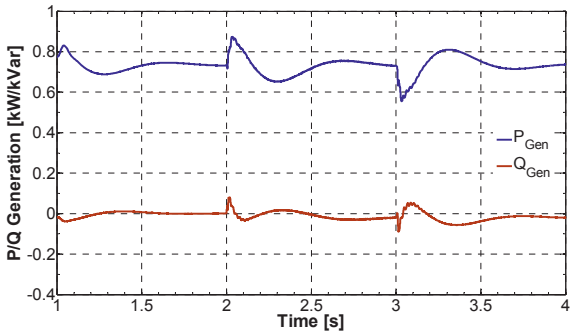


Figure C.15: SCIG powers with both positive and negative sequence voltage support

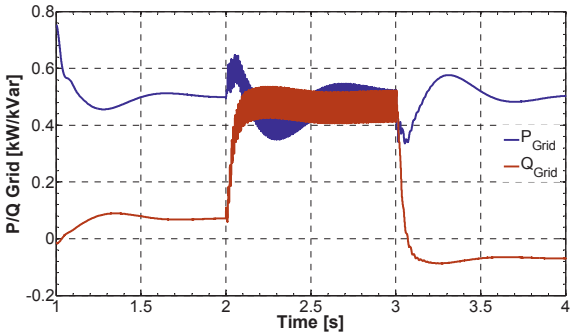


Figure C.16: Grid side powers with both positive and negative sequence voltage support

## C.3 Summary

The generation system parameters presented for the transient stability analysis indicate that the reactive injection by the CPLs during the fault keeps the rotor speed and torque within the mechanical stability limits and the voltage collapse is avoided.

When the distribution system experiences the asymmetrical grid fault the CPL injects the reactive power into the network to compensate for the reactive power consumed by the SCIG. This maintains the positive sequence voltage to the pre-fault value. To compensate for the unbalance in the system the CPL injects the active and reactive powers of double grid frequency. The injected unbalanced powers are translated on the grid side.

# D Active Power Filtering with PE Generation Interface

*This appendix presents a simulation analysis performed to investigate the role of generation PE interface as shunt active filter in a distribution network. Unlike the CPL, a generation PE interface supplies the active power to the non-linear load and hence reduces the fundamental component of the source current. It has been discussed how a CPL acting as APF serves better than a generation PE interface acting as APF.*

In chapter 5, it has been shown by a detailed simulation analysis that a CPL can be affectively used as shunt active filter in a distribution network. However, most of the modern distribution networks have the renewable generation sources interfaced to the network through PE converters. These generation PE interfaces can be used to alleviate the harmonics and address the power quality issues in the network. In the following sections, a simulation analysis has been presented to discuss the role of PE generation interfaces for power quality enhancements. Both the time and frequency domain approaches have been considered for extraction of compensating current for converter control. A brief discussion has been made on the effectiveness of the CPL and PE generation interface both acting as APFs in a distribution network.

## D.1 Simulation Model

This section presents the simulation model for active power filtering when a generation interface is utilized as a APF instead of using a CPL. The distribution system of Figure D.1 has been considered for this purpose. The PE generation interface called here as controllable power source (CPS) is a VSC similar to a CPL. The control structure is also the same as utilized for the CPL. CPS acts as an interface for a distributed energy source and is able to supply active and reactive power to the distribution system. The parameters of the system are same as considered in section 5.3 except that CPS supplies 75 kW of active power at time $t$= 0.4s. The source voltage is distorted with the same harmonic content as presented by (5.17).

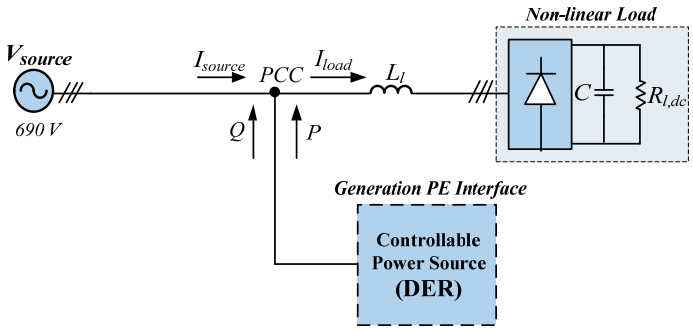


Figure D.1: Distribution system with CPS as active power filter

### D.1.1 Simulation Results for d-q Approach

Simulation results for the *d-q* approach have been presented first. CPS acts as a filter only when it is connected at time *t*=0.2s. Like the cases with CPL acting as active filter presented in the previous section, here also, the distortion in the source current is dropped from a value of 21.8% to 2.5% as shown in Figure D.2c. The CPS control is following the reference value generated by *d-q* approach very accurately (Figure D.2b). CPS is supplying the reactive power and the harmonic contents required by the non-linear load as presented in Figure D.3a. No active power is being supplied by the CPS and all the active power requirements of the load are being provided by the grid.

At time *t*=0.4s, the CPS starts supplying a portion of active power required by the non-linear load and the amount of power supplied is 75 kW (Figure D.3b). The reduction in the source current at this instant can be seen in the plot of Figure D.2a. The distortion in the source current is increased compared to the cases with CPL. This is opposite to the situation when CPL acts as APF presented in section 5.3.4. The source current THD is increased to 5.1% in this case as shown in Figure D.2c. As we know that THD can be presented by the following expression:

$$\text{THD}\,\% = \sqrt{\sum_{n=2}^{\infty} \frac{I_n^2}{I_1^2}} \times 100 \tag{D.1}$$

where $I_1$ is the fundamental component of current and $I_n$ is the component of current with $n$th order harmonics. The APF is providing the harmonic compensation very effectively; however, some harmonic content remains in the system due to switching of the PWM converter. It can be noticed that the fundamental component of the source current is decreased because some portion of it is being provided by the CPS. When a reduced value of the fundamental component is present in the denominator of (D.1) and the same value of the switching harmonics remain in the numerator, we will get a higher value of the THD in the source current. In the CPL case, the fundamental component of the current required by the load is added in the fundamental component of the source current resulting in an overall improvement in the distortion.

Figure D.3a illustrates that the reactive power provided by the source remains zero and the CPS is providing the reactive power to the non-linear load. The DC link voltage stays at the defined value during each stage of the simulation (Figure D.3b).

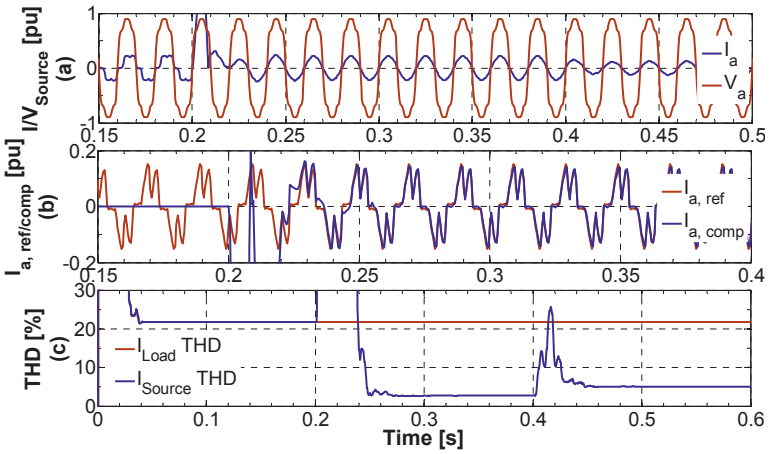


Figure D.2: Simulation results for *d-q* method with CPS as active power filter (a) Source current (b) Phase-a reference and compensating current (c) Source and load current THD

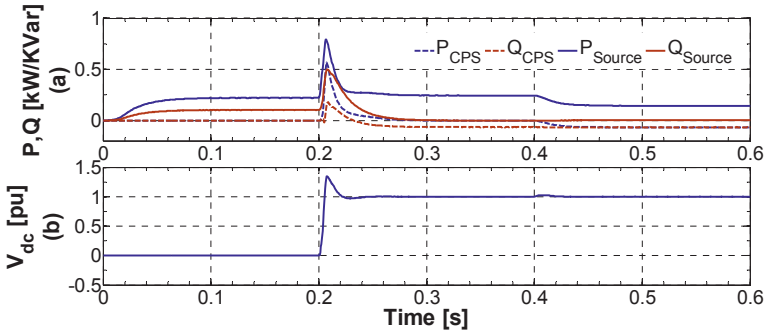


Figure D.3: Simulation results for *d-q* method with CPS as active power filter System (a) Source and CPS powers (b) DC link voltage

## D.1.2 Simulation Results for CPC Approach

Simulation results for *CPC* based reference signal generation scheme are shown in Figure D.4. The results are very much similar to the *d-q* approach. At time *t*=0.2s, when CPS only provides active power filtering the THD in the source current is reduced from 21.8% to 2.3%. CPS control closely follows the reference current signal generated by the *CPC* based method as presented in Figure D.4b.

When CPS starts providing the active power at time $t$=0.4s, the value of the source current is decreased (Figure D.4a) and the THD in the source current is raised to a value of 4.8% as shown in Figure D.4c. However, as in the cases of CPL as APF, in this case also CPC approach provides slightly better and accurate reference signal compared to the time domain method.

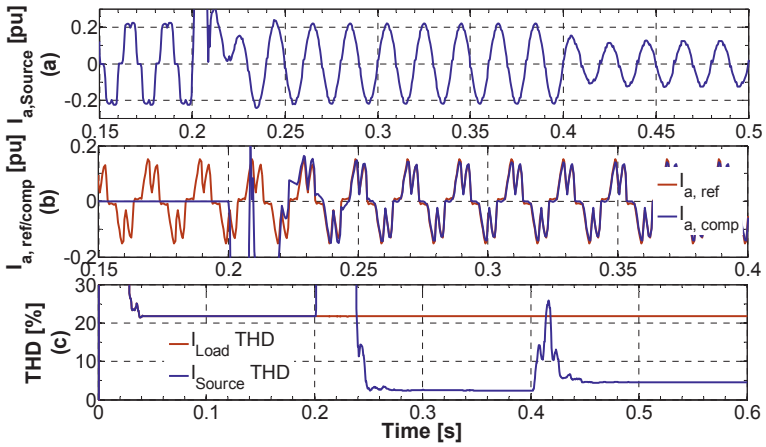


Figure D.4: Simulation results for *CPC* method with CPS as active power filter (a) Source current (b) Phase-a reference and compensating current (c) Source and load current THD

## D.2 Summary

Generation PE interface called CPS used as APF under non ideal voltage conditions has been considered. It has been observed that THD in the source current is increased when CPS starts supplying a part of active power to the non-linear load. This is in opposite to the operation of a CPL acing as shunt active filter. In this case, a sinusoidal term is subtracted from the total source current.

# References


[1] H. Farhangi, "The path of the smart grid," *Power and Energy Magazine, IEEE,* vol. 8, pp. 18-28, 2010.

[2] A. Ipakchi and F. Albuyeh, "Grid of the future," *Power and Energy Magazine, IEEE,* vol. 7, pp. 52-62, 2009.

[3] P. Tenti, H. K. M. Paredes, and P. Mattavelli, "Conservative Power Theory, a Framework to Approach Control and Accountability Issues in Smart Microgrids," *Power Electronics, IEEE Transactions on,* vol. 26, pp. 664-673, 2011.

[4] C. Yuen, A. Oudalov, and A. Timbus, "The Provision of Frequency Control Reserves From Multiple Microgrids," *Industrial Electronics, IEEE Transactions on,* vol. 58, pp. 173-183, 2011.

[5] A. Arestova and Y. Sidorkin, "The use of wind farms and virtual power plants for emergency control in the future smart super grids," in *Strategic Technology (IFOST), 2011 6th International Forum on*, 2011, pp. 437-442.

[6] J. Jin-Hong, K. Jong-Yul, K. Seul-Ki, and K. Jang-Mok, "Unified compensation control of a hybrid energy storage system for enhancing power quality and operation efficiency in a diesel and wind-turbine based stand-alone microgrid," in *Power Electronics for Distributed Generation Systems (PEDG), 2012 3rd IEEE International Symposium on*, 2012, pp. 264-270.

[7] L. Xinbo, Z. Yuanjun, and M. Shuohan, "EMI filter design for constant power loads in more electric aircraft power systems," in *Power Electronics and Motion Control Conference, 2009. IPEMC '09. IEEE 6th International*, 2009, pp. 2664-2668.

[8] J. Brombach, M. Jordan, F. Grumm, and D. Schulz, "Influence of small Constant-Power-Loads on the power supply system of an aircraft," in *Compatibility and Power Electronics (CPE), 2013 8th International Conference on*, 2013, pp. 97-102.

[9] S. C. Smithson and S. S. Williamson, "Constant power loads in More Electric Vehicles - an overview," in *IECON 2012 - 38th Annual Conference on IEEE Industrial Electronics Society*, 2012, pp. 2914-2922.

[10] M. S. Carmeli, D. Forlani, S. Grillo, R. Pinetti, E. Ragaini, and E. Tironi, "A stabilization method for DC networks with constant-power loads," in *Energy Conference and Exhibition (ENERGYCON), 2012 IEEE International*, 2012, pp. 617-622.

[11] G. Sulligoi, D. Bosich, Z. Lin, M. Cupelli, and A. Monti, "Linearizing control of shipboard multi-machine MVDC power systems feeding Constant Power Loads," in *Energy Conversion Congress and Exposition (ECCE), 2012 IEEE*, 2012, pp. 691-697.

[12] X. N. Zhang, D. M. Vilathgamuwa, K. J. Tseng, B. S. Bhangu, and G. Chandana, "A loop cancellation based active damping solution for constant power instability in vehicular power systems," in *Energy Conversion Congress and Exposition (ECCE), 2012 IEEE*, 2012, pp. 1182-1187.

[13] Z. Yue and Q. Wei, "A third-order sliding-mode controller for DC/DC converters with constant power loads," in *Industry Applications Society Annual Meeting (IAS), 2011 IEEE*, 2011, pp. 1-8.

## References


[14] C. H. Rivetta, A. Emadi, G. A. Williamson, R. Jayabalan, and B. Fahimi, "Analysis and control of a buck DC-DC converter operating with constant power load in sea and undersea vehicles," *Industry Applications, IEEE Transactions on,* vol. 42, pp. 559-572, 2006.

[15] C. Rivetta and G. A. Williamson, "Large-signal analysis of a DC-DC buck power converter operating with constant power load," in *Industrial Electronics Society, 2003. IECON '03. The 29th Annual Conference of the IEEE*, 2003, pp. 732-737 vol.1.

[16] C. Rivetta and G. A. Williamson, "Global behaviour analysis of a DC-DC boost power converter operating with constant power load," in *Circuits and Systems, 2004. ISCAS '04. Proceedings of the 2004 International Symposium on*, 2004, pp. V-956-V-959 Vol.5.

[17] A. Khaligh, A. M. Rahimi, and A. Emadi, "Modified Pulse-Adjustment Technique to Control DC/DC Converters Driving Variable Constant-Power Loads," *Industrial Electronics, IEEE Transactions on,* vol. 55, pp. 1133-1146, 2008.

[18] A. Khaligh and A. Emadi, "Mixed DCM/CCM pulse adjustment with constant power loads," *Aerospace and Electronic Systems, IEEE Transactions on,* vol. 44, pp. 766-782, 2008.

[19] A. Khaligh and A. Emadi, "Power Alignment, New Digital Control Approach for a DC-DC Flyback Converter with Constant Power Loads," in *Industrial Electronics and Applications, 2006 1ST IEEE Conference on*, 2006, pp. 1-6.

[20] A. Khaligh, A. M. Rahimi, A. Chakraborty, and A. Emadi, "Analysis and Stabilization of a Buck-Boost DC-DC Converter Feeding Constant Power Loads in Parallel with Conventional Loads in Vehicular Systems," in *IEEE Industrial Electronics, IECON 2006 - 32nd Annual Conference on*, 2006, pp. 2799-2804.

[21] A. Khaligh, A. M. Rahimi, M. Khaligh, and A. Emadi, "Sensitivity Analyses of Pulse Adjustment Control Technique of a Buck-Boost Converter Operating in Discontinuous Conduction Mode and Driving Constant Power Loads," in *Vehicle Power and Propulsion Conference, 2006. VPPC '06. IEEE*, 2006, pp. 1-5.

[22] A. Khaligh, "Realization of Parasitics in Stability of DC-DC Converters Loaded by Constant Power Loads in Advanced Multiconverter Automotive Systems," *Industrial Electronics, IEEE Transactions on,* vol. 55, pp. 2295-2305, 2008.

[23] W. Jiabin and D. Howe, "A Power Shaping Stabilizing Control Strategy for DC Power Systems With Constant Power Loads," *Power Electronics, IEEE Transactions on,* vol. 23, pp. 2982-2989, 2008.

[24] A. M. Rahimi and A. Emadi, "Active Damping in DC/DC Power Electronic Converters: A Novel Method to Overcome the Problems of Constant Power Loads," *Industrial Electronics, IEEE Transactions on,* vol. 56, pp. 1428-1439, 2009.

[25] A. M. Rahimi and A. Emadi, "Discontinuous-Conduction Mode DC/DC Converters Feeding Constant-Power Loads," *Industrial Electronics, IEEE Transactions on,* vol. 57, pp. 1318-1329, 2010.

[26] A. M. Rahimi, G. A. Williamson, and A. Emadi, "Loop-Cancellation Technique: A Novel Nonlinear Feedback to Overcome the Destabilizing Effect of Constant-Power Loads," *Vehicular Technology, IEEE Transactions on,* vol. 59, pp. 650-661, 2010.

[27] P. Liutanakul, A. B. Awan, S. Pierfederici, B. Nahid-Mobarakeh, and F. Meibody-Tabar, "Linear Stabilization of a DC Bus Supplying a Constant Power Load: A General Design Approach," *Power Electronics, IEEE Transactions on,* vol. 25, pp. 475-488, 2010.

## References


[28] Z. Fanghua and Y. Yangguang, "Start-Up Process and Step Response of a DC–DC Converter Loaded by Constant Power Loads," *Industrial Electronics, IEEE Transactions on,* vol. 58, pp. 298-304, 2011.

[29] C. N. Onwuchekwa and A. Kwasinski, "Analysis of Boundary Control for Buck Converters With Instantaneous Constant-Power Loads," *Power Electronics, IEEE Transactions on,* vol. 25, pp. 2018-2032, 2010.

[30] L. Yushan, K. R. Vannorsdel, A. J. Zirger, M. Norris, and D. Maksimovic, "Current Mode Control for Boost Converters With Constant Power Loads," *Circuits and Systems I: Regular Papers, IEEE Transactions on,* vol. 59, pp. 198-206, 2012.

[31] A. Kwasinski and C. N. Onwuchekwa, "Dynamic Behavior and Stabilization of DC Microgrids With Instantaneous Constant-Power Loads," *Power Electronics, IEEE Transactions on,* vol. 26, pp. 822-834, 2011.

[32] S. R. Huddy and J. D. Skufca, "Amplitude Death Solutions for Stabilization of DC Microgrids With Instantaneous Constant-Power Loads," *Power Electronics, IEEE Transactions on,* vol. 28, pp. 247-253, 2013.

[33] P. Magne, D. Marx, B. Nahid-Mobarakeh, and S. Pierfederici, "Large-Signal Stabilization of a DC-Link Supplying a Constant Power Load Using a Virtual Capacitor: Impact on the Domain of Attraction," *Industry Applications, IEEE Transactions on,* vol. 48, pp. 878-887, 2012.

[34] D. Marx, P. Magne, B. Nahid-Mobarakeh, S. Pierfederici, and B. Davat, "Large Signal Stability Analysis Tools in DC Power Systems With Constant Power Loads and Variable Power Loads;A Review," *Power Electronics, IEEE Transactions on,* vol. 27, pp. 1773-1787, 2012.

[35] L. Xinyun, A. J. Forsyth, and A. M. Cross, "Negative Input-Resistance Compensator for a Constant Power Load," *Industrial Electronics, IEEE Transactions on,* vol. 54, pp. 3188-3196, 2007.

[36] M. Belkhayat, R. Cooley, and A. Witulski, "Large signal stability criteria for distributed systems with constant power loads," in *Power Electronics Specialists Conference, 1995. PESC '95 Record., 26th Annual IEEE*, 1995, pp. 1333-1338 vol.2.

[37] M. Belkhayat, "Stability Criteria for AC Power Systems with Regulated Loads," Thesis for the Degree of Doctor of Philosophy, Purdue University, December 1997.

[38] A. Emadi, "Modeling of power electronic loads in AC distribution systems using the generalized State-space averaging method," *Industrial Electronics, IEEE Transactions on,* vol. 51, pp. 992-1000, 2004.

[39] A. Emadi, A. Khaligh, C. H. Rivetta, and G. A. Williamson, "Constant power loads and negative impedance instability in automotive systems: definition, modeling, stability, and control of power electronic converters and motor drives," *Vehicular Technology, IEEE Transactions on,* vol. 55, pp. 1112-1125, 2006.

[40] L. Xinbo, Z. Yuanjun, Z. Wei, and M. Shuohan, "Stability Criteria for Constant Power Loads With Multistage Filters," *Vehicular Technology, IEEE Transactions on,* vol. 60, pp. 2042-2049, 2011.

[41] A. Griffo and W. Jiabin, "Large Signal Stability Analysis of 'More Electric 'Aircraft Power Systems with Constant Power Loads," *Aerospace and Electronic Systems, IEEE Transactions on,* vol. 48, pp. 477-489, 2012.

## References


[42] Z. Xinan, D. M. Vilathgamuwa, T. King-Jet, B. S. Bhangu, and C. J. Gajanayake, "Power Buffer With Model Predictive Control for Stability of Vehicular Power Systems With Constant Power Loads," *Power Electronics, IEEE Transactions on,* vol. 28, pp. 5804-5812, 2013.

[43] F. Jiyuan and S. Borlase, "The evolution of distribution," *Power and Energy Magazine, IEEE,* vol. 7, pp. 63-68, 2009.

[44] R. H. Lasseter, "Smart Distribution: Coupled Microgrids," *Proceedings of the IEEE,* vol. 99, pp. 1074-1082, 2011.

[45] A. Bracale, P. Caramiaa, G. Carpinelli, F. Mottola, and D. Proto, "A hybrid AC/DC Smart Grid to improve power quality and reliability," in *Energy Conference and Exhibition (ENERGYCON), 2012 IEEE International*, 2012, pp. 507-514.

[46] R. F. Arritt and R. C. Dugan, "Distribution System Analysis and the Future Smart Grid," *Industry Applications, IEEE Transactions on,* vol. 47, pp. 2343-2350, 2011.

[47] H. Morais, T. Sousa, P. Faria, and Z. Vale, "Reactive power management strategies in future smart grids," in *Power and Energy Society General Meeting (PES), 2013 IEEE*, 2013, pp. 1-5.

[48] "IEEE Guide for Monitoring, Information Exchange, and Control of Distributed Resources Interconnected With Electric Power Systems," *IEEE Std 1547.3-2007,* pp. 1-158, 2007.

[49] M. Liserre, T. Sauter, and J. Y. Hung, "Future Energy Systems: Integrating Renewable Energy Sources into the Smart Power Grid Through Industrial Electronics," *Industrial Electronics Magazine, IEEE,* vol. 4, pp. 18-37, 2010.

[50] A. Bracale, C. Di Pema, M. Mangoni, and D. Proto, "Dispersed generators providing ancillary services through power electronic interfaces: A hybrid system," in *Universities Power Engineering Conference, 2008. UPEC 2008. 43rd International*, 2008, pp. 1-5.

[51] R. Angelino, G. Carpinelli, D. Proto, and A. Bracale, "Dispersed generation and storage systems for providing ancillary services in distribution systems," in *Power Electronics Electrical Drives Automation and Motion (SPEEDAM), 2010 International Symposium on*, 2010, pp. 343-351.

[52] F. Delfino, G. B. Denegri, M. Invernizzi, and R. Procopio, "Performance and control of PhotoVoltaic systems supplying both primary and ancillary services," in *Universities Power Engineering Conference, 2008. UPEC 2008. 43rd International*, 2008, pp. 1-5.

[53] F. Delfino, R. Procopio, M. Rossi, and G. Ronda, "Integration of large-size photovoltaic systems into the distribution grids: a p-q chart approach to assess reactive support capability," *Renewable Power Generation, IET,* vol. 4, pp. 329-340, 2010.

[54] R. Goic, D. Jakus, and J. Krstulovic, "Wind power plant as ancillary service provider," in *Energy Market (EEM), 2011 8th International Conference on the European*, 2011, pp. 562-567.

[55] F. Blaabjerg and M. Ke, "Future on Power Electronics for Wind Turbine Systems," *Emerging and Selected Topics in Power Electronics, IEEE Journal of,* vol. 1, pp. 139-152, 2013.

[56] S. Muller, M. Deicke, and R. W. De Doncker, "Doubly fed induction generator systems for wind turbines," *Industry Applications Magazine, IEEE,* vol. 8, pp. 26-33, 2002.

[57] M. Liserre, R. Cardenas, M. Molinas, and J. Rodriguez, "Overview of Multi-MW Wind Turbines and Wind Parks," *Industrial Electronics, IEEE Transactions on,* vol. 58, pp. 1081-1095, 2011.

## References


[58] M. Yilmaz and P. T. Krein, "Review of the Impact of Vehicle-to-Grid Technologies on Distribution Systems and Utility Interfaces," *Power Electronics, IEEE Transactions on,* vol. 28, pp. 5673-5689, 2013.

[59] J. R. Pillai and B. Bak-Jensen, "Integration of Vehicle-to-Grid in the Western Danish Power System," *Sustainable Energy, IEEE Transactions on,* vol. 2, pp. 12-19, 2011.

[60] S. Shafiee, M. Fotuhi-Firuzabad, and M. Rastegar, "Investigating the Impacts of Plug-in Hybrid Electric Vehicles on Power Distribution Systems," *Smart Grid, IEEE Transactions on,* vol. 4, pp. 1351-1360, 2013.

[61] J. Dixon, L. Moran, J. Rodriguez, and R. Domke, "Reactive Power Compensation Technologies: State-of-the-Art Review," *Proceedings of the IEEE,* vol. 93, pp. 2144-2164, 2005.

[62] A. F. Zobaa and M. Jovanovic, "A Comprehensive Overview on Reactive Power Compensation Technologies for Wind Power Applications," in *Power Electronics and Motion Control Conference, 2006. EPE-PEMC 2006. 12th International*, 2006, pp. 1848-1852.

[63] M. Elnashar, M. Kazerani, R. El-Shatshat, and M. M. A. Salama, "Comparative evaluation of reactive power compensation methods for a stand-alone wind energy conversion system," in *Power Electronics Specialists Conference, 2008. PESC 2008. IEEE*, 2008, pp. 4539-4544.

[64] B. Singh, S. S. Murthy, and S. Gupta, "Analysis and design of STATCOM-based voltage regulator for self-excited induction generators," *Energy Conversion, IEEE Transactions on,* vol. 19, pp. 783-790, 2004.

[65] N. Jelani, M. Molinas, and S. Bolognani, "Reactive Power Ancillary Service by Constant Power Loads in Distributed AC Systems," *Power Delivery, IEEE Transactions on,* vol. 28, pp. 920-927, 2013.

[66] N. Jelani and M. Molinas, "Optimal use of power electronic interfaces for loads in distributed systems," in *Industrial Electronics (ISIE), 2010 IEEE International Symposium on*, 2010, pp. 2449-2454.

[67] N. Jelani and M. Molinas, "Loss Minimization in AC Distribution System with High Share of Power Electronic Loads Providing Ancillary Reactive Power," in *PowerTech, 2011 IEEE Trondheim*, 2011, pp. 1-6.

[68] N. Jelani and M. Molinas, "Stability investigation of control system for power electronic converter acting as load interface in AC distribution system," in *Industrial Electronics (ISIE), 2011 IEEE International Symposium on*, 2011, pp. 408-413.

[69] N. Jelani and M. Molinas, "Mitigation of Asymmetrical Grid Faults in Induction Generator-Based Wind Turbines Using Constant Power Load," *Energies, MDPI,* vol. 6, pp. 1700-1717, 2013.

[70] N. Jelani and M. Molinas, "Asymmetrical Fault Ride Through as Ancillary Service by Constant Power Loads in Grid-Connected Wind Farm," *Power Electronics, IEEE Transactions on,* vol. PP, pp. 1-1, 2014.

[71] N. Jelani and M. Molinas, "Reactive Power Ancillary Service and Harmonic Alleviation with Constant Power Load under Non-Ideal Voltage Conditions in AC Distribution System," *IET, Power Electronics (Under Review)*.

## References


[72] N. Jelani and M. Molinas, "Shunt Active Filtering by Constant Power Load in Microgrid Based on IRP p-q and CPC Reference Signal Generation Schemes," in *Power System Technology (POWERCON), 2012 IEEE International Conference on*, 2012, pp. 1-6.

[73] M. Zadeh, N. Jelani, and M. Molinas, "Seamless Control of Distributed Multi-Converter System with High Power Quality," presented at the CIRED, 22nd International Conference on Electricity Distribution, Stockholm, 2013.

[74] M. Shahbaz, N. Jelani, and M. Molinas, "Alleviating Harmonic and Reactive Power Issues in Smart Grid Based on the Implementation of the Instantaneous p-q Power Theory under Unbalanced and Distorted Supply Voltages," presented at the International Conference on Power Systems Transients, IPST, Vancouver, Canada, 2013.

[75] M. Molinas, D. Moltoni, G. Fascendini, J. A. Suul, and T. Undeland, "Constant power loads in AC distribution systems: An investigation of stability," in *Industrial Electronics, 2008. ISIE 2008. IEEE International Symposium on*, 2008, pp. 1531-1536.

[76] C. Concordia and S. Ihara, "Load Representation in Power System Stability Studies," *Power Apparatus and Systems, IEEE Transactions on,* vol. PAS-101, pp. 969-977, 1982.

[77] Jan Machowski, Janusz Bialek , and J. Bumby, *Power System Dynamics, Stability and Control*, 2nd ed.: Wiley, 2008.

[78] Z. Saad-Saoud and N. Jenkins, "Models for predicting flicker induced by large wind turbines," *Energy Conversion, IEEE Transactions on,* vol. 14, pp. 743-748, 1999.

[79] A. B. Jusoh, "The instability effect of constant power loads," in *Power and Energy Conference, 2004. PECon 2004. Proceedings. National*, 2004, pp. 175-179.

[80] A. Khaligh, "Realization of Parasitics in Stability of DC Converters Loaded by Constant Power Loads in Advanced Multiconverter Automotive Systems," *Industrial Electronics, IEEE Transactions on,* vol. 55, pp. 2295-2305, 2008.

[81] D. Weijing, Z. Junming, Z. Yang, Q. Zhaoming, and P. Fangzheng, "Large signal stability analysis based on gyrator model with constant power load," in *Power and Energy Society General Meeting, 2011 IEEE*, 2011, pp. 1-8.

[82] P. J. M. Heskes, J. M. A. Myrzik, and W. L. Kling, "Power electronic loads with negative differential impedance in a low voltage distribution system," in *Electricity Distribution - Part 1, 2009. CIRED 2009. 20th International Conference and Exhibition on*, 2009, pp. 1-4.

[83] G. M. S. Azevedo, P. Rodriguez, M. C. Cavalcanti, G. Vazquez, and F. A. S. Neves, "New control strategy to allow the photovoltaic systems operation under grid faults," in *Power Electronics Conference, 2009. COBEP '09. Brazilian*, 2009, pp. 196-201.

[84] M. Molinas and J. Kondoh, "Power electronic loads as providers of reactive power ancillary service to the grid: Analytical and experimental study," in *Power Electronics and Applications, 2009. EPE '09. 13th European Conference on*, 2009, pp. 1-10.

[85] S. K. Chung, "Phase-locked loop for grid-connected three-phase power conversion systems," *Electric Power Applications, IEE Proceedings -,* vol. 147, pp. 213-219, 2000.

[86] W. Liying and N. Ertugrul, "Selection of PI compensator parameters for VSC-HVDC system using decoupled control strategy," in *Universities Power Engineering Conference (AUPEC), 2010 20th Australasian*, 2010, pp. 1-7.

## References


[87] C. Bajracharya., "Control of HVDC Light for Wind Power," Master Thesis, Norwegian University of Science and Technology, June 2008.

[88] Ned Mohan, Tore M. Undeland , and W. P. Robbins, *Power Electronics: Converters, Applications, and Design*, 3rd ed.: WILEY, November 2002.

[89] K. Ogata, *Modern Control Engineering*, 5th ed.: Prentice Hall, 2010.

[90] I. E. Davidson and N. M. Ijumba, "Optimization model for loss minimization in a deregulated power distribution network," in *Africon Conference in Africa, 2002. IEEE AFRICON. 6th*, 2002, pp. 887-894 vol.2.

[91] M. A. Kashem, A. D. T. Le, M. Negnevitsky, and G. Ledwich, "Distributed generation for minimization of power losses in distribution systems," in *Power Engineering Society General Meeting, 2006. IEEE*, 2006, p. 8 pp.

[92] I. Erlich, W. Winter, and A. Dittrich, "Advanced grid requirements for the integration of wind turbines into the German transmission system," in *Power Engineering Society General Meeting, 2006. IEEE*, 2006, p. 7 pp.

[93] P. Rodriguez, A. Luna, G. Medeiros, R. Tedorescu, and F. Blaabjerg, "Control of STATCOM in wind power plants based on induction generators during asymmetrical grid faults," in *Power Electronics Conference (IPEC), 2010 International*, 2010, pp. 2066-2073.

[94] M. J. Hossain, H. R. Pota, V. Ugrinovskii, and R. A. Ramos, "Robust STATCOM control for the enhancement of fault ride-through capability of fixed speed wind generators," in *Control Applications, (CCA) & Intelligent Control, (ISIC), 2009 IEEE*, 2009, pp. 1505-1510.

[95] D. BARRY, "Increasing Renewable Accessibility in Ireland," in *In Proceedings of 9th World Energy Congress*, 2004, pp. 1–10.

[96] Energinet, "Regulation TF 3.2.6 Wind Turbines Connected to Grids With Voltages Below 100 kV," Denmark, May 19, 2010.

[97] Energinet, "Regulation TF 3.2.5 Wind Turbines Connected to Grids With Voltages Above 100 kV," Denmark, Dec. 3, 2010.

[98] L. Chia-Tse, H. Che-Wei, and C. Po-Tai, "A Low-Voltage Ride-Through Technique for Grid-Connected Converters of Distributed Energy Resources," *Industry Applications, IEEE Transactions on,* vol. 47, pp. 1821-1832, 2011.

[99] C. Shih-Feng, L. Chia-Tse, C. Po-Tai, and F. Blaabjerg, "A reactive current injection technique for renewable energy converters in low voltage ride-through operations," in *Power and Energy Society General Meeting, 2011 IEEE*, 2011, pp. 1-7.

[100] O. A. Giddani, G. P. Adam, O. Anaya-Lara, G. Burt, and K. L. Lo, "Control strategies of VSC-HVDC transmission system for wind power integration to meet GB grid code requirements," in *Power Electronics Electrical Drives Automation and Motion (SPEEDAM), 2010 International Symposium on*, 2010, pp. 385-390.

[101] S. Deshmukh, B. Natarajan, and A. Pahwa, "Voltage/VAR Control in Distribution Networks via Reactive Power Injection Through Distributed Generators," *Smart Grid, IEEE Transactions on,* vol. 3, pp. 1226-1234, 2012.

## References


[102] C. Wessels, S. Grunau, and F. Fuchs, "Current injection targets for a statcom under unbalanced grid voltage condition and the impact on the pcc voltage," presented at the IEEE Energy Conversion Congress and Exposition (ECCE), April 2011.

[103] P. Rodriguez, G. Medeiros, A. Luna, M. C. Cavalcanti, and R. Teodorescu, "Safe current injection strategies for a STATCOM under asymmetrical grid faults," in *Energy Conversion Congress and Exposition (ECCE), 2010 IEEE*, 2010, pp. 3929-3935.

[104] M. Molinas, J. A. Suul, and T. Undeland, "Low Voltage Ride Through of Wind Farms With Cage Generators: STATCOM Versus SVC," *Power Electronics, IEEE Transactions on,* vol. 23, pp. 1104-1117, 2008.

[105] J. A. Suul, M. Molinas, and T. Undeland, "STATCOM-Based Indirect Torque Control of Induction Machines During Voltage Recovery After Grid Faults," *Power Electronics, IEEE Transactions on,* vol. 25, pp. 1240-1250, 2010.

[106] Y. Wang, L. Xu, and B. W. Williams, "Compensation of network voltage unbalance using doubly fed induction generator-based wind farms," *Renewable Power Generation, IET,* vol. 3, pp. 12-22, 2009.

[107] P. Rodriguez, A. Luna, M. Ciobotaru, R. Teodorescu, and F. Blaabjerg, "Advanced Grid Synchronization System for Power Converters under Unbalanced and Distorted Operating Conditions," in *IEEE Industrial Electronics, IECON 2006 - 32nd Annual Conference on*, 2006, pp. 5173-5178.

[108] P. Rodriguez, R. Teodorescu, I. Candela, A. V. Timbus, M. Liserre, and F. Blaabjerg, "New Positive-sequence Voltage Detector for Grid Synchronization of Power Converters under Faulty Grid Conditions," in *Power Electronics Specialists Conference, 2006. PESC '06. 37th IEEE*, 2006, pp. 1-7.

[109] M. Ciobotaru, R. Teodorescu, and F. Blaabjerg, "A New Single-Phase PLL Structure Based on Second Order Generalized Integrator," in *Power Electronics Specialists Conference, 2006. PESC '06. 37th IEEE*, 2006, pp. 1-6.

[110] J. A. Suul, "Control of Grid Integrated Voltage Source Converters under Unbalanced Conditions," Thesis for the degree of Philosophiae Doctor, Norwegian University of Science and Technology, Trondheim, March 2012.

[111] O. Noureldeen, "Low Voltage Ride Through Strategies for SCIG Wind Turbines Interconnected Grid," *International Journal of Electrical & Computer Sciences, IJECS,* vol. 11 No: 02, 2011.

[112] Olimpo Anaya-Lara, Nick Jenkins, Janaka Ekanayake, Phill Cartwright, and M. Hughes, *Wind Energy Generation: Modelling and Control*: John Wiley and sons, 2009.

[113] V. Khadkikar, A. Chandra, and B. N. Singh, "Generalised single-phase p-q theory for active power filtering: simulation and DSP-based experimental investigation," *Power Electronics, IET,* vol. 2, pp. 67-78, 2009.

[114] L. Dayi and T. Jun, "A novel active power filter for the voltage-source type harmonic source," in *Electrical Machines and Systems, 2008. ICEMS 2008. International Conference on*, 2008, pp. 2077-2080.

[115] F. Carastro, M. Sumner, and P. Zanchetta, "An Enhanced Shunt Active Filter with Energy Storage for Microgrids," in *Industry Applications Society Annual Meeting, 2008. IAS '08. IEEE*, 2008, pp. 1-7.

## References


[116] R. Gupta, A. Ghosh, and A. Joshi, "Performance Comparison of VSC-Based Shunt and Series Compensators Used for Load Voltage Control in Distribution Systems," *Power Delivery, IEEE Transactions on,* vol. 26, pp. 268-278, 2011.

[117] C. ChangQing, W. Liping, and Y. Guohui, "A three-phase active power filter based on park transformation," in *Computer Science & Education, 2009. ICCSE '09. 4th International Conference on*, 2009, pp. 1221-1224.

[118] H. Akagi, "New trends in active filters for power conditioning," *Industry Applications, IEEE Transactions on,* vol. 32, pp. 1312-1322, 1996.

[119] H. Akagi, Y. Kanazawa, and A. Nabae, "Instantaneous Reactive Power Compensators Comprising Switching Devices without Energy Storage Components," *Industry Applications, IEEE Transactions on,* vol. IA-20, pp. 625-630, 1984.

[120] H. Akagi, A. Nabae, and S. Atoh, "Control Strategy of Active Power Filters Using Multiple Voltage-Source PWM Converters," *Industry Applications, IEEE Transactions on,* vol. IA-22, pp. 460-465, 1986.

[121] H. Akagi, E.H. Watanabe, and M. Aredes, *Instantaneous power theory and applications to power conditioning. Electrical Engineering*: Electrical Engineering, Wiley-IEEE Press, 2007.

[122] L. S. Czarnecki, "Current's Physical Components (CPC) concept: A fundamental of power theory," in *Nonsinusoidal Currents and Compensation, 2008. ISNCC 2008. International School on*, 2008, pp. 1-11.

[123] L. S. Czarnecki and S. E. Pearce, "Compensation objectives and currents' physical components-based generation of reference signals for shunt switching compensator control," *Power Electronics, IET,* vol. 2, pp. 33-41, 2009.

[124] L. S. Czarnecki, "Effect of Supply Voltage Harmonics on IRP-Based Switching Compensator Control," *Power Electronics, IEEE Transactions on,* vol. 24, pp. 483-488, 2009.

[125] L. S. Czarnecki, "Physical interpretation of the reactive power in terms of the CPC power theory," *Electrical Power Quality and Utilisation, Journal,* vol. 13, 2007.

[126] L. S. Czarnecki, "Misinterpretations of some power properties of electric circuits," *Power Delivery, IEEE Transactions on,* vol. 9, pp. 1760-1769, 1994.

[127] L. S. Czarnecki, "Currents Physical Components (CPC) in Circuits with Nonsinusoidal Voltages and Currents," *Electrical Power Quality and Utilisation, Journal,* vol. 11, 2005.

[128] L. S. CZARNECKI, "Currents Physical Components (CPC) in Circuits with Nonsinusoidal Voltages and Currents," *Electrical Power Quality and Utilisation, Journal,* vol. 12, 2006.

[129] L. S. Czarnecki and S. S. Pearce, "CPC-based comparison of compensation goals in systems with nonsinusoidal voltages and currents," in *Nonsinusoidal Currents and Compensation (ISNCC), 2010 International School on*, 2010, pp. 27-36.

[130] L. S. Czarnecki, "Power related phenomena in three-phase unbalanced systems," *Power Delivery, IEEE Transactions on,* vol. 10, pp. 1168-1176, 1995.

[131] EWEA, "Large scale integration of wind energy in the european power supply: analysis, issues and recommendations," European Wind Energy Association (EWEA),Tech. Rep2005.

## References

[132] P. Tenti, A. Costabeber, P. Mattavelli, and D. Trombetti, "Distribution Loss Minimization by Token Ring Control of Power Electronic Interfaces in Residential Microgrids," *Industrial Electronics, IEEE Transactions on,* vol. 59, pp. 3817-3826, 2012.